Renewable and Sustainable Energy Reviews 28 (2013) 848–880

Contents lists available at ScienceDirect

Renewable and Sustainable Energy Reviews

journal homepage: www.elsevier.com/locate/rser

Characteristics of heat transfer and fluid flow in microtube and microchannel using conventional fluids and nanofluids: A review

B.H. Salman [a,*], H.A. Mohammed [b,*], K.M. Munisamy [a], A. Sh. Kherbeet [a]

[a] Mechanical Engineering Department, College of Engineering, Universiti Tenaga Nasional, Jalan IKRAM-UNITEN, 43000 Kajang, Selangor, Malaysia
[b] Department of Thermofluids, Faculty of Mechanical Engineering, Universiti Teknologi Malaysia, 81310 UTM Skudai, Johor Bahru, Malaysia

ARTICLE INFO

Article history:
Received 7 September 2012
Received in revised form
25 July 2013
Accepted 11 August 2013
Available online 13 September 2013

Keywords:
Microtube
Microchannel
Heat transfer
Nanofluids
Nanoparticles

ABSTRACT

Research on convective heat transfer on internal microtube and microchannel has been extensively conducted in the past decade. This review summarizes numerous researches on two topics; the first section focuses on studying the fluid flow and heat transfer behavior of different types of microtubes (MT) and microchannel (MC) at different orientations. The second section concentrates on nanofluids; its preparation, properties, behavior, and many others. The purpose of this article is to get a clear view and detailed summary of the influence of several parameters such as the geometrical specifications, boundary conditions, and type of fluids. The maximum Nusselt number is the main target of such research where correlation equations were developed in experimental and numerical studies are reported. The heat transfer enhancement of nanofluids along with the nanofluids preparation technique, types and shapes of nanoparticles, base fluids and additives, transport mechanisms, and stability of the suspension are also discussed.

Contents

* Corresponding authors. Tel.: +60 755 34716; fax: +60 755 66 159.
E-mail addresses: Eng.bassam2007@yahoo.com (B.H. Salman), Hussein.dash@yahoo.com (H.A. Mohammed).

1364-0321/$ - see front matter © 2013 Elsevier Ltd. All rights reserved.
http://dx.doi.org/10.1016/j.rser.2013.08.012

1. Introduction

The characteristics of flow and heat transfer in microchannels and microtubes have attracted much attention of researchers because of the rapid developments of micro-electromechanical systems (MEMS) and micrototal analysis system. These developments have great impacts on the microelectronic cooling techniques, the microheat exchanger, bioengineering, human genome project, medicine engineering, etc. It is evident that the understanding of the microscale phenomena is very important for designing efficient micro-devices. To explore the fundamental physical mechanisms of fluid flow and heat transfer in microchannels, many effects, including the size effect, rarefaction effect, surface roughness, viscous effect, electrostatic force effect, axial heat conduction in the channel wall, surface geometry, the measurement errors, etc. should be taken into account [1]. A large number of experimental and numerical studies focus on flow and heat transfer behavior in microtube and microchannel have been reported. These vast results and information have dealt with different conditions, parameters, geometry dimensions, and instrumentation, which indeed used for comparison purposes to indicate more accurate methodology for solving the case studies.

The purpose of this paper is threefold. The primary purpose is to review the available results of the flow and heat transfer presented in previously published data for microtubes and microchannels. The results of massive number of different parameters affect the fluid flow and heat transfer characteristics are summarized and presented to predict the peaks of the flow and heat transfer. The second purpose is to understand the characteristics and functions of nanofluids, to expect their effects and heat transfer enhancement in such geometries. The third purpose is to open a gate for new researches and propose suggestions that could lead to improve the ability to enhance the heat transfer in MT and MC using nanofluids. The review starts with an extensive review on the flow and heat transfer in microtube and microchannel. Then finish with a comprehensive review for nanofluids and its characteristics.

2. Microtube (MT)

2.1. Experimental studies on MT

In last few years, large number of researchers intend to study the heat transfer and fluid flow in MT. Zhou et al. [1] investigated experimentally and numerically the flow and heat transfer characteristics of liquid laminar flow in MT. They used the smooth fused silica and rough stainless steel microtubes with the hydraulic diameters of 50–100 μm and 373–1570 μm, respectively. Deionized water was used as the working fluid. The dimensions and surface roughness for the fused silica tubes and stainless steel are ranged 50 μm, 75 μm and 100 μm. The Reynolds numbers was ranged from 20 to 2400. The friction factors for smooth fused silica tubes are in good agreement with the prediction of the conventional theory. For the rough stainless steel tubes, the friction factor was higher than the prediction of the conventional theory. The results indicated that the conventional friction prediction is valid for water flow through MT with a relative surface roughness less than 1.5%. The experimental results show that the Nusselt number along the axial direction do not accord with the conventional results especially when the Reynolds number is low and the relative tube wall thickness is high.

Lelea et al. [2] investigated experimentally and numerically the heat transfer and fluid flow characteristics in a microchannel. The diameters of the microchannel used were 0.1 mm, 0.3 mm and 0.5 mm, the flow regime was laminar and the Reynolds number range was up to 800. The tube material was stainless steel SUS 304. The distilled water was used as a working fluid. They found that the results confirm that the conventional or classical theories are applicable for water flow through microchannel of above sizes.

Ding et al. [3] investigated experimentally the heat transfer behavior of aqueous suspensions of multi-walled carbon nanotubes (CNT nanofluids) flowing through a horizontal tube. A straight copper tube with 970 mm length, 4.5 mm inner diameter, and 6.35 mm outer diameter was used as the test section. Distilled water and multi-walled carbon nanotubes were used to produce nanofluids. Fig. 1 shows a SEM image of the dispersed sample. Significant enhancement was observed of the convective heat transfer in compared with pure water as the working fluid. They found this enhancement depends on the flow condition, CNT concentration and the pH level. The axial position of the maximum enhancement increases with the CNT concentration and the Reynolds number. The results indicate that the Reynolds number causes a significant increase in the convective heat transfer coefficient.

Yang and Lin [4] investigated experimentally the forced convective heat transfer performance of water flow through six micro stainless steel tubes with inner diameters ranging from 123 μm to 962 μm. The results indicate that the conventional heat transfer correlations for laminar and turbulent flows can be well applied for predicting the fully developed heat transfer performance in the MT. The transition occurs at Reynolds number from 2300 to 3000. The surface temperature fluctuation in transition regime is much larger than that in laminar and turbulent flow regimes. They observed that the heat loss is less than 4% and 1% of the total heat input for 123 μm and 962 μm tubes, respectively. At the lowest Reynolds number in the 123 μm tube, a 4% heat loss cause 25% heat transfer coefficient overestimate.

Celata et al. [5] investigated experimentally the influence of channel wall roughness and the channel wall hydrophobicity on adiabatic flow in circular microchannels. Different diameters of MT ranges from 70 μm to 326 μm were used with Reynolds number less than 300 for all diameters. The experiments were carried out on sooth glass/fused silica and a Teflon capillary tubes used with water. The results indicate that, with degassed water, there was no effect of slip flow noted due to hydrophobic channel walls even at 70 μm inner diameter. For roughened glass channels, an increased in friction factor above $64/Re$ was observed only at the smallest

Nomenclature

Al_2O_3	Aluminum oxide
C_p	Specific heat of the fluid (J/kg K)
CuO	Copper oxide
d_f	Diameter of base fluid molecule
d_p	Nanoparticle diameter (m)
g	Gravitational acceleration (m/s^2)
k	Thermal conductivity (W/m K)
k_{eff}	Effective thermal conductivity
k_{sf}	wall-to-fluid thermal conductivity ratio
L	Length of the tube (m)
M	Molecular weight of base fluid
N	Avogadro number ($N=6.022\times10^{23}$ mol^{-1})
Nu	Nusselt number ($Nu=hD/K$)
P	Pressure of fluid (Pa)
Pr	Prandtl number ($Pr=Cp\mu_0/k$)
q_x	Heat flux (W/m^2)
Re	Reynolds number ($Re=\rho_0V_0D/\mu_0$)
R_{np}	Nanoparticle radius (m)
SiO_2	Silicon oxide
T	Temperature of fluid (K)
T	Bulk temperature (K)
T_0	Reference temperature
U', V'	Velocities in x' and y' directions (m/s)
U, V	Dimensionless velocities in x and y directions
U_0	Average jet velocity at the entrance (m/s)
V	Axial velocity (m/s)
ZnO	Zinc oxide

Greek symbols

μ_{eff}	Effective viscosity
α	Thermal diffusivity (m^2/s)
μ	Dynamic viscosity of fluid (kg/ms)
υ	Kinematic viscosity of fluid (m^2/s)
θ	Inclination of tilted wall
ρ	Fluid density (kg/m^3)
ρ_1	Nanofluid density (kg/m^3)
ϕ	Volume fraction of nanoparticles
δ	Non-dimensional wall thickness
ε	Relative roughness height

Subscript

b_f	base-fluid
n_f	nanofluids
n_p	nanoparticle
eff	effective

diameter of 126 μm. The higher factor was caused by actual deformation of channel circularity rather than increased friction at the rougher wall, and similar behavior was observed in a Teflon tube.

Peng et al. [6] investigated water flow in a fused glass microtube with inner diameter of 230 μm and the outer diameter is about 500 μm. The Reynolds number was ranged from 1540 to 2960. The results indicates that, the flow transition from laminar to turbulent occurs at Reynolds number 1700 to 1900, and the turbulence becomes fully developed at $Re>2500$. The details of the flow structure such as stream wise streaks and transverse vortices were observed in the transitional flow fields for $1800<Re<2100$. The instantaneous velocity which observed by micro-PIV reveal large scale coherent structures in the turbulent flow in MT.

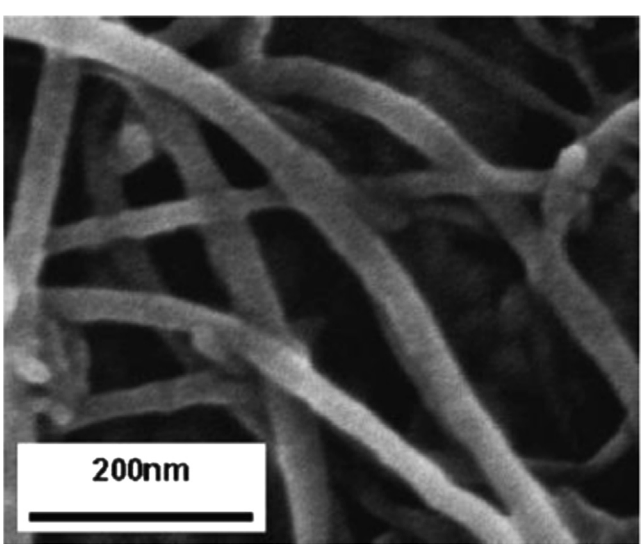


Fig. 1. SEM image of a dispersed sample of carbon nanotubes [3].

Celata et al. [7] investigated experimentally the characteristics of the adiabatic behavior of single-phase laminar flow in circular micro-tube. The diameters were used from 528 down to 120 μm. The experiments were carried out using water, which was degassed by passing through a very small and continuous of helium. The result indicates that, the Nusselt number decreased with decreasing the diameter. The smaller MT shows progressively less evidence of flow in the course of thermal development. The decreased in heat transfer performance with respect to the conventional value of Nusselt number ($Nu=4.36$) was more marked for decreasing the Reynolds number.

Sara et al. [8] investigated experimentally the laminar convective mass transfer and friction factor in MT with diameter of 0.20 mm and L/D in the range of 100 to 500. The Reynolds number was ranged from 40 to 1400. The distilled water was used as a working fluid. The results reveal that the friction factor was in a very good agreement with the Hagen–Poiseuille theory in the laminar regime and the conventional correlations can be used to determine the friction factor for MT with ID ≥ 0.20 mm. For mass transfer, the Sherwood number for MT was smaller than those obtained from the correlations developed for macrotubes.

Zhang and Fu [9] investigated experimentally the characteristics of two-phase flow of liquid nitrogen in vertically upward micro-tubes with inner diameters 0.531 and 1.042 mm. The results indicate that, the main two-phase flow patterns of liquid nitrogen in MT were bubbly flow, slug flow, churn flow and annular flow. The confined bubble flow was observed in 0.531 mm and 1.042 mm MT. The dry-out easily happened in 0.531 mm diameter tube and led to high vapor quality and mist flow appeared. The flow regime transition lines moved to lower superficial vapor velocity as the diameter of MT decreased. In addition, there was quite large divergence between the experimental results and the existed theoretical models, and it seemed that there was not yet a theoretical model which can predict the flow regime transition well for the two-phase flow. The slip ratio between two phases became larger as the inner diameter of the MT decreased.

Liu et al. [10] investigated experimentally the forced convective heat transfer characteristics in quartz microtubes with inner

diameters of 242 μm, 315 μm and 520 μm. The de-ionized water was used as the working fluid. The Reynolds number was ranged from 100 to 7000. The results indicate that, the experimental Nusselt number is a good agreement with that of the laminar correlations when the flow state was laminar. The Reynolds number of the laminar to turbulent transition region may be about 1500–4000, 1600–4500 and 1900–5500 for MT with inner diameters of 242 μm, 315 μm and 520 μm, respectively.

Celata et al. [11] investigated experimentally the effects of compressibility for helium flow through fused silica micro-tubes. The MT diameter was ranged from 30 μm to 254 μm. Reynolds number was ranged from 0.8 to 500. Two hydrodynamic models for compressible flow (isothermal and adiabatic) were confronted at normal conditions. Local friction factor was devised to compare with the global friction factor to quantify the effect of compressibility. The results reveal that, the friction factor has remarkably accurate prediction by the reference curve of Hagen–Poiseuille and a very close agreement between the incompressible and quasi-compressible correlations was obtained. The effect of density-change-induced acceleration was extremely limited on the particle scale and that an incompressible characterization of flow.

Qi et al. [12,13] investigated experimentally the flow boiling of liquid nitrogen in the MT with the diameter range from 0.531 mm to 1.931 mm. They investigated the heat transfer characteristics and the critical heat flux (CHF). The results reveal that, the wall increased in the single-phase flow region, drops abruptly at ONB and then decreased monotonically in the two-phase flow region and this decreased was a result of large two-phase flow pressure drop. For low mass quality region, heat transfer was governed by nucleate boiling and heat transfer coefficient was dependent on heat flux and pressure. In addition, the heat transfer coefficient increases with mass quality at low and medium heat fluxes. CHF increased with the mass flux whereas the critical mass quality decreased with mass flux. The CHF was governed by the liquid film near the inner wall.

Wen and Ding [14] investigated experimentally the effects of convective heat transfer of nanofluids at the entrance region of the copper tube with 970 mm length. The de-ionized water with Al_2O_3 nanoparticles were used as working fluids. Reynolds number was ranged from 500 to 2100. The results indicate that, the use of Al_2O_3 nanoparticles as the dispersed phase in water significantly enhanced the convective heat transfer in the laminar flow regime and this enhancement increased with Reynolds number and the particle concentration. The enhancement was particularly significant in the entrance region and decreased with the axial distance. The thermal developing length of nanofluids was greater than that of pure base liquid and increased with an increase in particle concentration.

2.2. Numerical studies on MT

Xiong and Chung [15] proposed a novel bottom-up approach to generate a three-dimensional random roughness on a MT surface. They used Gaussian random number generator to generate the corner points in the space with random heights and the bi-cubic Coons patch to create the boundary curves and surface based on the corner points. Many tiny generated surfaces were used to form the random rough of MT. Computational fluid dynamics (CFD) solver was used to isolate the roughness effect and to solve the three dimensional equations for the water flow through generated the rough MT with 50 μm diameter and 100 μm length. They assumed N points in space, and it is connected one by one using straight lines to form the bones of the rough surface in step two. At the third step, they created the curve surface and in the last step, they created two more surfaces for the inlet and outlet and then they used it to form a volume as shown in Fig. 2. Reynolds numbers ranged from 40 to 2000 and the viscous dissipation is not considered. They observed that the temperature has large values at the peaks and small values at the valleys of the MT surface. The roughness has a negligible on the averaged Nusselt number because the effects of peaks and valleys counteract each other for the whole MT surface. The local Nusselt numbers does not have a large fluctuation away from the theoretical value and it randomly distributes along the MT. For the hydraulic diameter they noticed, the improper use of the hydraulic diameter can result in increasing or decreasing the friction factor and *Nu* number.

Zhang et al. [16] investigated numerically the effects of wall axial heat conduction and fluid axial conduction for simultaneously developing the laminar flow and heat transfer in the wall of MT with constant outside wall temperature. The results indicated that the heat transfer process is most sensitive to wall-to-fluid conductivity ration k_{sf}, and in condition when $30 \le RePr \le 11{,}560$ and $k_{sf} > 25$; But when the conditions were used $30 \le RePr \le 11{,}560$ and $k_{sf} \le 25$, the increasing tube thickness and the decreasing k_{sf} could make the inner wall surface approaching the uniform heat flux condition. The maximum Nusselt number they obtained is about 4.3. It turns out that the basic function of the wall axial heat conduction is to unify the inner wall surface heat flux.

Giulio and Paola [17] investigated numerically the roughness effects on the heat transfer and pressure loss performances of microscale tubes and channels. The finite element was used based on the fractional step or projection approach. The surface roughness was modeled through a number of peaks and valleys along the ideal smooth surface. Different peak shapes and distribution was considered to arrive to the real roughness. The relative roughness height (ε) ranged from 0.0% to 5.3% was used and the geometrical parameter which representative of the tubes is the diameter ranged from 50 μm to 150 μm. The results indicated that for both configurations, a significant increase in Poiseuille number was detected. While the influence of roughness on the heat transfer is smaller and more sensitive to the geometry of both duct and roughness obstruction and it is highly dependent on the tube shape.

Kamali and Binesh [18] investigated numerically the effects of heat transfer for multi-wall carbon nanotube (MWCNT) based nanofluids in a straight tube under constant wall heat flux condition. The tube length was 914.4 mm and the tube diameter was 1.55 mm. Both water base fluid and aqueous 1% CNT nanofluid were used as fluids in simulations. The single phase model was used of two dimensional axisymmetric steady, forced laminar convection flows of nanofluids inside a straight circular tube. The results indicate that the heat transfer coefficient is dominated by the wall region due to non-Newtonian behavior of CNT nanofluid.

Hong and Asako [19] investigated the heat transfer characteristics of gaseous flows in a MT with constant heat flux whose value is positive or negative on 2D compressible laminar flow for no-slip regime. The tube diameter range was from 10 μm to 100 μm and the length to diameter ratio was 200. The constant heat flux range was from 10^{-4} W/m^2 to 10^4 W/m^2. The numerical methodology was based on the Arbitrary–Lagranging–Eulerian (ALE) method. They selected stagnation pressure in such a way that the Mach number at exit ranged from 0.1 to 0.7 and the outlet pressure was fixed at the atmosphere pressure. The results indicated that, in the case of slow flow, the wall and bulk temperatures normalized by heat fluxes increase for both positive and negative heat flux. A correlation for the prediction of the wall temperature of the gaseous flow in the MT was proposed. Supplementary runs with slip boundary conditions for the case of $D = 10$ μm were conducted and rarefaction effect was discussed. With increased *Ma* number, the compressibility effects are more dominant and the rarefaction effect is relatively insignificant where *Kn* number is less than 0.0096.

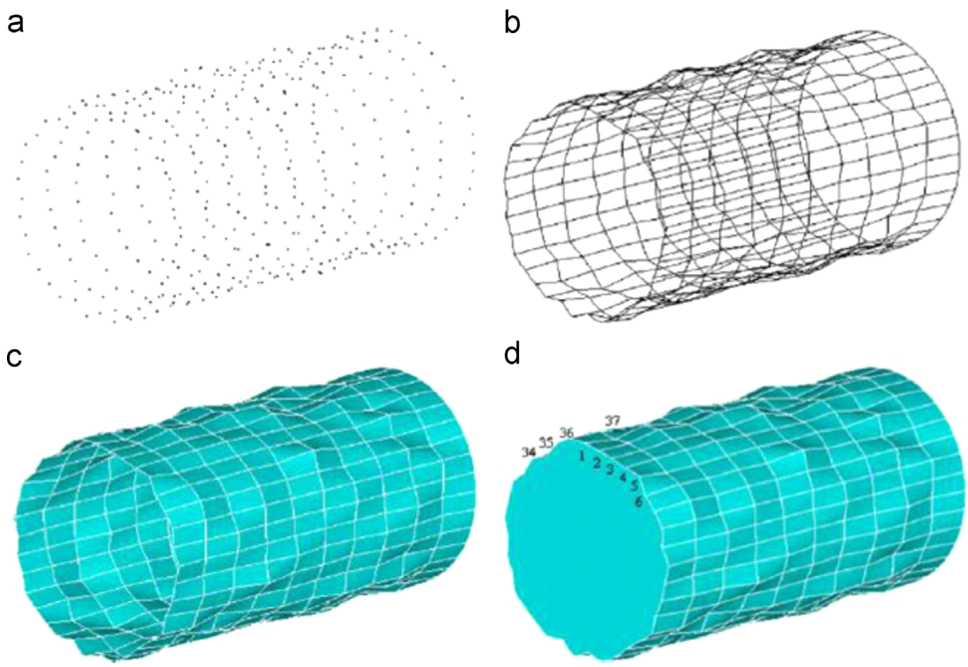


Fig. 2. Four steps to form the rough microtube: (a) points (b) lines (c) surfaces and (d) volume [15].

Bianco et al. [20] investigated numerically the development of laminar forced convection flow of a water–Al_2O_3 nanofluid in a circular tube with a constant heat flux at the wall. Single and two-phase model were employed with either constant or temperature-dependent properties. The *Re* number was ranged from 250 to 1050. The heat flux was ranged from 5000 W/m^2 to 10,000 W/m^2 and, ∅ (the nanoparticle volume fraction) was ranged from 1% to 4% for both constant and temperature-dependent properties. In all cases the size for the spherical particles was considered to equal 100 nm. The results indicate that the inclusion of nanoparticles produced a considerable increase of the heat transfer with respect to that of the base liquid. The heat transfer enhancement was increased with the concentration of particle volume and this increase was accompanied by increase wall shear stress values. The results of single and two-phase models were quite similar, the maximum difference detected was 11% for the average heat transfer coefficient especially for $\varnothing = 4\%$.

Xiao et al. [21] investigated numerically the effects of gas flow in microtube. The results indicate that, the heat transfer effects associated with rarefied flow were reduced for the second-order model and the effects of the second order terms was most significant at the upper of the slip regime. For the airflow at standard conditions, the maximum second-order changes of Nusselt number was on the order of 15%. Nusselt number was increased relative to the values of no-slip when the temperature jump effect was small.

Koo and Kleinstreuer [22] investigated the effects of viscous dissipation on the temperature field and the friction factor in microtube (MT) and microchannel (MC). Three working fluids were used, water, methanol and iso-propanol. The results indicate that, the viscous dissipation effect on the friction factor was increased as the system size decreases. For water flow in a tube with $D < 50$ μm, viscous dissipation becomes significant and should be considered for all experimental and computational analyses. In addition, the aspect ratio of a channel plays an important role in viscous dissipation, as the aspect ratio deviates from unity, the viscous dissipation effects increase. Ignoring the viscous dissipation effects could ultimately affect the friction factor measurements for flow in MT.

Lelea and Cioabla [23,24] investigated numerically the effects of viscous dissipation on heat transfer and fluid flow in micro-tubes. Three different fluids, water and two dielectric fluids, HFE-7600 and FC-70 with temperature dependent fluid properties were used. The diameter ratio of the MT was D_i/D_0=(0.1/0.33)mm with a tube length L=100 mm. Two different heat transfer conditions, cooling and heating and three different Brinkman number 0.01, 0.1 and 0.5 was used. Non-dimensional parameters were obtained, for water ($Re = 258-1684$, $Pr = 6.4-6.9$), HFE-7600 ($Re = 186-1130$, $Pr = 29.3-32.2$) and FC-70 ($Re = 7.2-43.2$, $Pr = 189.8-317.4$). The results reveal that, the friction factor and Poiseuille constant P_o are affected at $Br = 0.5$ for water and start with $Br = 0.1$ for highly viscous fluids HFE-7600 and FC-70. The Nusselt number for the cooling case for $Br = 0.5$ was about three times higher than for heating case, regardless the fluid type.

Satapathy [25] investigated forced convection for gaseous slip flow in an infinite microtube with mixed boundary conditions. The results indicate that for both the hot and cold wall situation in the thermal entrance region, the local bulk-mean temperature increased as Peclet number or Knudsen number increases and vice-versa. The local Nusselt number increased with the increase in Peclet number and decreased with the increase in Knudsen number. The fully-developed Nusselt number decreased with the increase in Knudsen number. For a fixed value of Knudsen number, it reaches to constant value for all Peclet numbers.

Wang and Wang [26] investigated numerically the influences of three-dimensional wall roughness on the laminar flow in micro-tube. The relative roughness was ranged from 0 to 0.05 and the wave number from 0 to 30. Reynolds number was ranged from 1 to 500. The results reveal that if the wave number of rough function or Reynolds number decreased, the disturbed areas of flow field becomes larger. The variation of disturbed area was independent of the variation of relative roughness if the relative roughness is a small quantity. In addition, the dimensionless pressure drop increased with the increases of relative roughness, Reynolds number or wave number of wall function. The influence of wall roughness on the flow pattern was different from those on the pressure drop.

Aziz and Niedbalski [27] investigated numerically the first and second order slip flow effects on the thermal development of dilute gas flow in a micro-tube with axial conduction and viscous dissipation. The results indicate that for the fully developed

Table 1
Summary of experimental and numerical studies for MT.

Researchers	Diameter/flow nature	Reynolds number	Fluid/gas	Findings
Zhou et al. [1]	50–1570 μm/laminar	20–2400	Deionized water	The Nusselt number along the axial direction did not accord with the conventional results
Lelea et al. [2]	0.1–0.5 mm/laminar	Up to 800	Distilled water	Results confirm that the conventional or classical theories are applicable for water flow through microchannel of above sizes
Ding et al. [3]	6.35 mm/laminar	700–1300	Distilled water /0.5 wt% CNT	At $Re=80$ Reynolds number causes a significant increase 350% in the convective heat transfer coefficient
Yang and Lin [4]	123–962 μm/laminar and turbulent	100–10,000	Water	Heat loss of the total heat input depends on the inner diameter and the Reynolds number values
Celata et al. [5]	70–326 μm/laminar	Less than 300	Demineralized water	No effect of slip flow noted due to hydrophobic channel walls even at 70 μm inner diameter. For roughened glass channels, an increased in friction factor above $64/Re$ was observed only at the smallest diameter of 126 μm
Peng et al. [6]	230 μm/laminar and turbulent	1540–2960	Deionized water	The flow transition from laminar to turbulent occurs at Reynolds number 1700–1900
Celata et al. [7]	50–528 μm/laminar and turbulent	50–3138	Demineralized water	The Nusselt number decreased with decreasing the diameter
Sara et al. [8]	0.20 mm/laminar	40–1400	Distilled water	Friction factor was in a very good agreement with the Hagen–Poiseuille theory. The Sherwood number for MT was smaller than those obtained from the correlations developed for macrotubes
Zhang and Fu [9]	0.531 and 1.042 mm	–	Nitrogen liquid	There was not yet a theoretical model which can predict the flow regime transition well for the two-phase flow
Liu et al. [10]	242, 315 and 520 μm/ laminar and turbulent	100–7000	Deionized water	Nusselt number is rough agreement with that of the laminar correlations
Celata et al. [11]	30–254 μm/laminar	0.8–500	Helium	Friction factor has remarkably accurate prediction by Hagen–Poiseuille and effect of density-change–induced acceleration was extremely limited on the particle scale and that an incompressible characterization of flow
Qi et al. [12,13]	0.531–1.931 mm	–	Hydrogen liquid	Heat transfer coefficient increased with mass quality at low and medium heat fluxes
Wen and Ding [14]	4.5 mm/laminar	500–2100	Al_2O_3/water	Significant enhancement the convective heat transfer in the laminar flow regime and this enhancement increased with Reynolds number and the particle concentration
Xiong and Chung [15]	50 μm/laminar	40–2000	Water	The hydraulic diameter can result in increasing or decreasing the friction factor and *Nu* number
Zhang et al. [16]	120–528 μm/laminar	10–2280	Water	Heat transfer process is most sensitive to wall-to-fluid conductivity ration k_{sf}.
Giulio and Paola [17]	50–150 μm/laminar	100–1700	–	The influence of roughness on the heat transfer is smaller and more sensitive to the geometry of both duct and roughness obstruction and it is highly dependent on the tube shape
Kamali and Binesh [18]	1.55 mm/laminar	600–1200	Water/aqueous 1% CNT	Heat transfer coefficient was dominated by the wall region due to non-Newtonian behavior of CNT nanofluid
Hong and Asako [19]	10–100 μm/laminar	14–1829	Gas	A correlation for the prediction of the wall temperature of the gaseous flow in the MT was proposed
Bianco et al. [20]	0.01 m/laminar	250–1050	Al_2O_3/water	Maximum difference detected was 11% for the average heat transfer coefficient especially for $\varnothing=4\%$
Xiao et al. [21]	–	–	Gas	The maximum second-order changes of Nusselt number was on the order of 15%
Koo and Kleinstreuer [22]	50 μm/laminar	20–2000	Water, methanol and iso-propanol	Viscous dissipation effects could ultimately affect the friction factor measurements for flow in MT
Lelea and Cioabla [23,24]	0.1 mm/laminar	7.2–1684	Water, HFE-7600 and FC-70	Friction factor and Poiseuille constant P_o affected on *Nu* at different values of *Br*
Satapathy [25]	–	–	Gas	The dimensionless pressure drop increased with the increases of relative roughness, Reynolds number or wave number of wall function
Wang and Wang [26]	–	1–500	–	The influence of wall roughness on the flow pattern was different from those on the pressure drop
Aziz and Niedbalski [27]	–	–	Gas	As the viscous dissipation gathers strength, the Nusselt number reaches a minimum and then increases again as the effect of viscous dissipation continues to prevail over the cooling effect
Salman et al. [28]	50 μm/laminar	10–1500	Al_2O_3/EG CuO/EG SiO_2/EG ZnO/EG	SiO_2–EG nanofluid has the highest Nusselt number, followed by ZnO–EG, CuO–EG, Al_2O_3–EG, and lastly pure EG. The Nusselt number for all cases increases with the volume fraction but it decreases with the rise in the diameter of nanoparticles. In all configurations, the Nusselt number increases with Reynolds number

hydrodynamic condition, the analytical solution for the velocity with the second-order slip model predicts higher velocities in the central region of the flow but the trend was reversed near the wall region. In addition, the local Nusselt number decreased as the fluid flows through the cooled section of the tube. However, as the viscous dissipation gathers strength, the Nusselt number reaches a minimum and then increases again as the effect of viscous dissipation continues to prevail over the cooling effect. Salman et al. [28] investigated numerically laminar convective heat transfer in a microtube (MT) with 50 μm diameter and 250 μm length with constant heat flux using finite volume method (FVM). Different types of nanofluids Al2O3, CuO, SiO2 and ZnO, with different nanoparticle sizes 25, 45, 65 and 80nm, and different volume fractions ranged from 1% to 4% using ethylene glycol as base fluids were used. This investigation covers Reynolds number in the range of 10 to 1500. The results have shown that SiO2-EG nanofluid has the highest Nusselt number, followed by ZnO-EG, CuO-EG, Al2O3-EG, and lastly pure EG. The Nusselt number for all cases increases with the volume fraction but it decreases with the rise in the diameter of nanoparticles. In all configurations, the Nusselt number increases with Reynolds number. A summary for the experimental and numerical studies in MT is shown in Table 1.

3. Microchannel (MC)

3.1. Experimental studies on MC

Jung et al. [29] measured experimentally the heat transfer coefficient and friction factor of nanofluids in rectangular microchannel (MC). Aluminum dioxide (Al_2O_3) with diameter of 170 nm nanofluids with various particle volume fractions of 0.6%, 1.2% and 1.8% were used as working fluids. The Reynolds number was tasted in the range of 5 and 300. The results indicated that the convective heat transfer coefficient of Al_2O_3 nanofluid in laminar flow regime was increased up to 32% compared to the distilled water at a volume fraction of 1.8% without major friction loss. The Nusselt number increases with increasing the Reynolds number in laminar flow regime. The Nusselt number was successfully correlated with Reynolds number and Prandtl number based on the thermal conductivity of nanofluids.

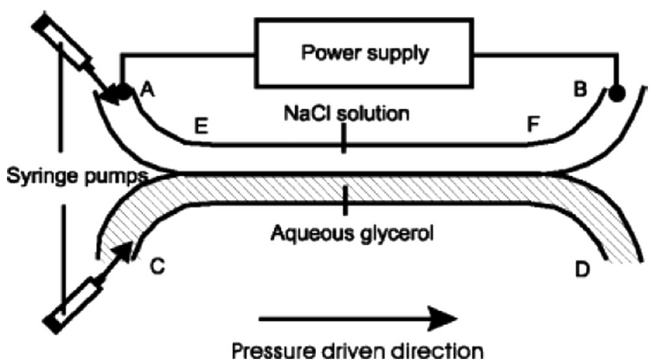


Fig. 3. Schematic of an H-shaped microfluidic device [30].

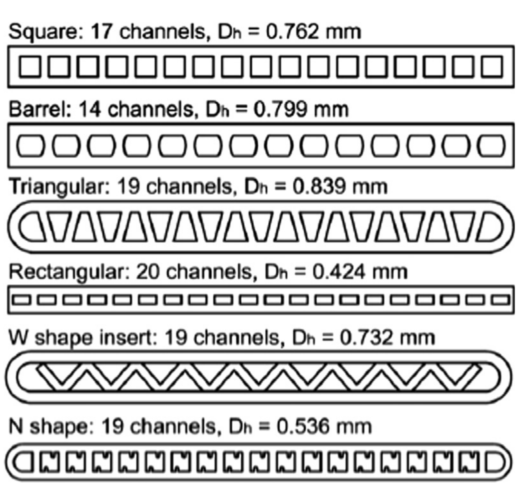


Fig. 4. Tube shapes [31].

Cheng et al. [30] reported a novel concept to control the interface location of the pressure driven multi-phase flow in microchannel. An H-shape microfluidic device was used to demonstrate the concept of interface control as shown in Fig. 3. Two fluids, aqueous NaCl solution and diluted glycerol were introduced through the inlets by a syringe pump. The flow rates for NaCl solution and diluted glycerol was maintained at the same value. For a purely pressure driven two-fluid flow, the aqueous NaCl solution with a lower viscosity flows faster and occupied a smaller width of the microchannel. The results show that this method is effective for low flow rates, and small viscosity ratio close to 1. The experimental results demonstrate a new method to solve the unmatched viscosity problem of the two-fluid flow in microchannel.

Agarwal et al. [31] investigated experimentally the heat transfer coefficients in six non-circular horizontal MC with diameters ranged from 0.424 mm to 0.939 mm of different shapes during condensation of refrigerant R134a over the mass flux in the range of 150 kg/m^2/s to 750 kg/m^2/s. The channels included barrel-shape, N-shape, rectangular, square, and triangular extruded tubes as shown in Fig. 4. The results reveal that the models developed for larger tubes result in significant deviations from the measured data, because the models were not intended for and could not account the flow phenomena and interfacial shear behavior specific to MC. For square, rectangular, and barrel-shaped channels an annular-film flow based model was developed. For triangular, N-shaped, and W-insert channels, it was assumed that the liquid fraction was retained at the corners, with the flow at the rest of the wall and in the core being approximated as mist flow. The annular-flow-based model recommended to be used for the square, barrel-shaped and rectangular channels, while the mist-flow correlation should be used for channels with sharp corners.

Roland et al. [32] investigated experimentally and numerically the hydrodynamics in two-dimensional MC having 700 μm and 200 μm height. Reynolds number used was ranged from 200 to 8000. The tested fluids were demineralized water with an electrical conductivity of 300 μS/cm. In addition, two-dimensional numerical model corresponding to the symmetry plane of the test section was developed. The model accounted for free convection heat transfer with surrounding air at the outside walls of the test section. The results indicate that a reduction in the Nusselt number for laminar flow at the microscale is occurred. In the laminar regime, the validity of the conventional transport phenomena theory may be extended to the small scales (200 μm). Transition to turbulence was observed both in the global pressure losses measurements and in the *Nu* with *Re* evolutions. In addition, the critical Reynolds numbers were found to vary from 3500 to 4500 which are consistent with the values observed at the larger scales. The experimental corrected data matched both with the Blasius hydrodynamic law and the Dittus and Boelter heat transfer correlation.

Wu and Cheng [33] investigated experimentally laminar heat transfer and pressure drop of water through 13 different trapezoidal silicon micro-channels with different geometry, surface roughness and surface hydrophilic properties. The results indicate that the bottom to top width ratio, the height to top width ratio and the length to diameter ratio have a great effect on the laminar Nusselt number and apparent friction constant of the trapezoidal MCs. The laminar Nusselt number and apparent friction constant of the trapezoidal MCs increased with the increase of surface roughness and this increase is more obvious at large Reynolds

numbers. The Nusselt Number and apparent friction constant are higher when using strong hydrophilic surfaces than those with weak hydrophilic surfaces (silicon surfaces). In addition, the laminar convective heat transfer shows two different characteristics at low and high Reynolds number ranges. For very low Reynolds number flow ($0 < Re < 100$), the Nusselt number increased almost linearly with the rise of Reynolds number. However, the increased of the Nusselt number after $Re = 100$ was gentle with the rice of Reynolds number.

Park and Punch [34] investigated experimentally the friction factor and heat transfer in multiple MCs with hydraulic diameters from 106 μm to 307 μm for single phase liquid flow. The Reynolds number used was ranged from 69 to 800. Deionized water was used as a working fluid. The results indicate that the friction factors obtained by experiments on the MC prove that the conventional theory for fully-developed flow was applicable within the range of the values of parameters they used. In order to predict heat transfer rate accurately, they proposed an empirical correlation in terms of $Nu/(Re^{0.62}Pr^{0.33})$and Brinkman number confined to the experimental range. The correlation was expected to be useful to design the MC devices related to heat transfer.

Quan et al. [35] investigated experimentally in determination annular condensation heat transfer coefficient of steam in two silicon microchannels with hydraulic diameters of 127 μm and 173 μm with trapezoidal cross sections. The air was used as the coolant for the steam flowing in the MC. The results indicate that the annular condensation heat transfer coefficient in MC increased with mass flux and quality and decreased with the hydraulic diameter. The annular condensation heat transfer coefficient based on a semi-analytical approach of turbulent liquid film with correlations for two-phase pressure drop and void fraction are valid in MC.

Lee et al. [36] investigated experimentally and numerically the behavior in single-phase flow through rectangular microchannels with width range from 194 μm to 534 μm. Deionized water was used as a working fluid. Reynolds number was ranged from 300 to 3500. The result indicates that the heat transfer coefficient increased with the decrease of the channel size depending on the flow rate. The experimental results were compared against conventional correlations to evaluate their applicability in predicting MC heat transfer. The wide disparities revealed that the mismatch in the boundary and inlet conditions between the MC experiments and the conventional correlations precluded their use for predictions. The numerical results agreed with the experimental data, suggesting that such approaches when coupled with carefully matched entrance and boundary conditions can be employed with confidence for predicting heat transfer behavior in MC. The results also confirm that the simplified thin wall analysis can be used as a computationally economical alternative to a full 3D conjugate analysis.

Harirchian and Garimella [37] investigated experimentally the local flow boiling heat transfer of a dielectric fluid (Fluorinert FC-77) in microchannel heat sinks as shown in Fig. 5. The mass flux used was ranged from 250 kg/m^2/s to 1600 kg/m^2/s. Seven different test pieces made from silicon and consisting of parallel MCs with nominal width ranged from 100 μm to 5850 μm with a nominal depth of 400 μm were obtained. The results indicate that for MCs of width 400 μm and greater, the heat transfer coefficients corresponded to a fixed wall heat flux as well as the boiling curves was independent of channel size. The heat transfer coefficients and boiling curves was independent of mass flux in the nucleate boiling region for a fixed channel size, but affected by mass flux as convective boiling dominates. In addition, a strong dependence of pressure drop on both channel size and mass flux was observed.

Ergu et al. [38] investigated experimentally the pressure drop and point mass transfer in a rectangular microchannel with a width of 3.70 mm, height of 0.107 mm and length of 35 mm. Distilled water was used as a working fluid. Reynolds number used was ranged from 100 to 845. The results indicate that the friction factor values were slightly higher than those calculated by theoretical correlation and these values increased with increasing Reynolds number. The classical laminar flow equations can be used for the calculation of the friction factor in MCs.

Owhaib et al. [39] investigated experimentally saturated flow boiling in MCs. Heat transfer coefficients were measured for saturated boiling of working fluid (R 134a) in vertical circular tubes with internal diameters ranged from 0.862 mm to 1.7 mm, with a uniform heating length of 220 mm. Heat transfer coefficients were obtained for a heat flux ranged from 3 kW/m^2 to 34 kW/m^2 and a mass flux was ranged from 50 kW/m^2/s to 400 kW/m^2/s and vapor qualities up to 0.6. The results reveal that the saturated flow boiling heat transfer coefficient was more or less independent of vapor quality and mass flux, but it is highly dependent on the heat flux for vapor fraction $x < 0.6$. The contribution of forced convection heat transfer to the overall transfer rate was small and that heat transfer by a mechanism similar to that in nucleate boiling was dominant. In addition, flow boiling heat transfer coefficients was higher for smaller diameter tubes. Also, an increase in the system pressure improves the heat transfer performance.

Chiu et al. [40] investigated experimentally and numerically the heat transfer performance and characteristics of liquid cooling heat sink microchnnels. The height of MCs was constant. The aspect ratio was set from 1.67 to 14.29 and the porosity was from 25% to 85%. The imposed pressure drop used was ranged from 490 Pa and 2940 Pa. The result indicate that the overall averaged Reynolds number in MCs decreased with both increasing the aspect ratio and cross-sectional porosity under same pressure drop. The aspect ratio for the lowest effective thermal resistance was dependent on the pressure drop between the inlet and the outlet of heatsink. In addition, the heat transfer enhancement due to raising pressure drop was more significant on MCs with high aspect ratio hence thinner channels are more advantageous under high pressure drop. The local Nusselt number in a channel decreased with increasing the aspect ratio. The value of Nu monotonically decreased along the channel for high aspect ratio.

Shen et al. [41] investigated experimentally the single phase heat transfer in a compact heat sink consisting of 2 rectangular MCs of 300 μm width and 800 μm depths. The relative roughness was ranged from 4% to 6%. Deinonized water was used as the working fluid. The Reynolds number used was ranged from 162 to 1257. The inlet liquid temperature used was ranged from 30 °C to 70 °C and the heating powers were used from 140 W to 450 W. The results indicate that the surface roughness has a great effect on the laminar flow in rough MCs. For developed flow, the Poiseuille number in the regime of high Reynolds numbers was higher than the conventional theory predictions and increase with increasing the Reynolds number, rather than remaining constant. In addition, the average Nusselt number increased with the increase of Reynolds number and Prandtl number. Both the local and the average Nusselt numbers were significantly lower than the conventional theory predictions for all flow rates and this was attributed to two main factors, the cross-sectional aspect ratio and the surface roughness.

Barber et al. [42] investigated experimentally the effects of hydrodynamics and heat transfer during flow boiling instabilities in a single MC with a hydraulic diameter of 727 μm. The uniform heat flux used was 4.26 kW/m^2 and the inlet liquid mass flow rate held constant at 1.13×10^{-5} kg/s. The results reveal that the flow, pressure and temperature conditions leading to nucleate boiling, flow instabilities and transition regimes during flow boiling in a MC. A quantify and characterize the timescales of various observed instabilities during flow boiling in a MC. High speed imaging revealed some of the controlling physical mechanisms responsible for the observed instabilities.

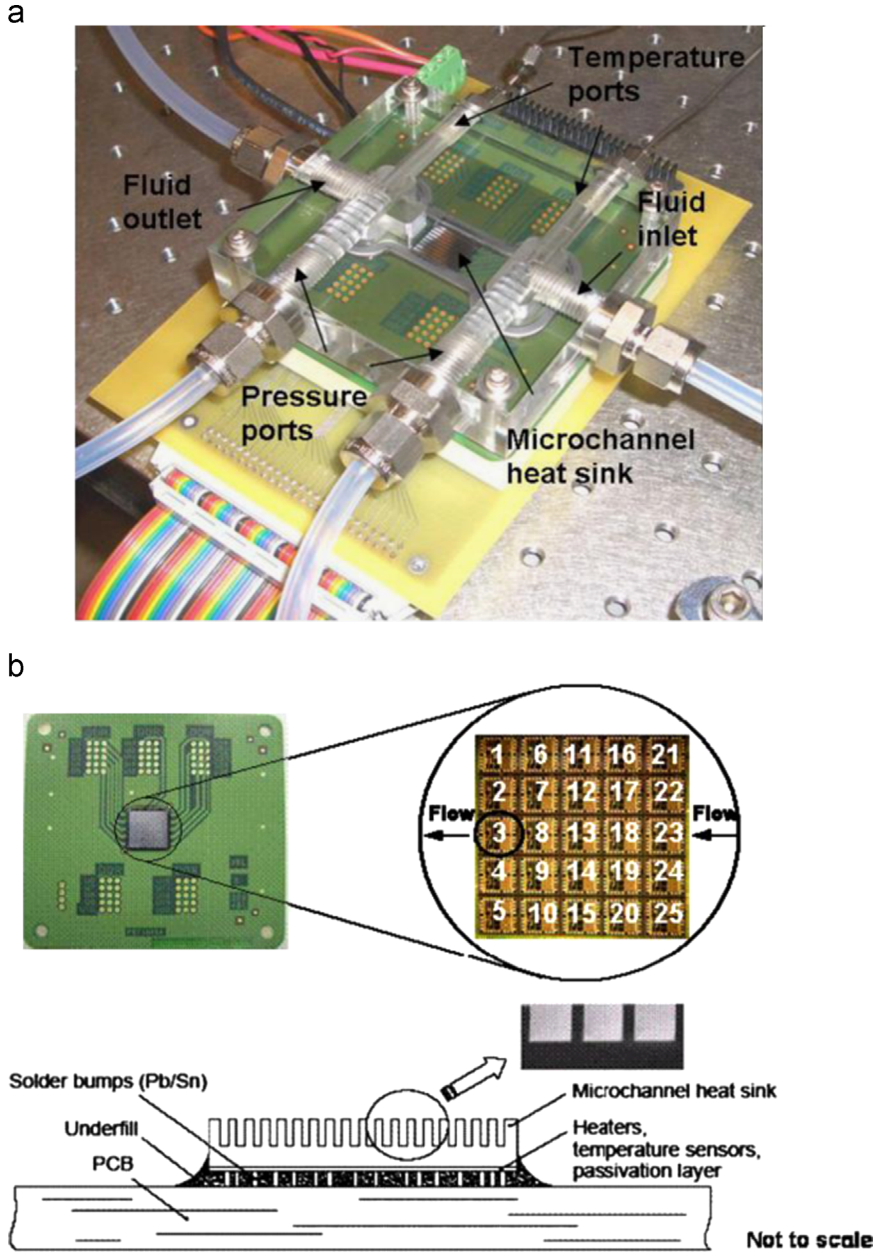


Fig. 5. (a) Microchannel test section and (b) integrated heaters and temperature sensors in the microchannel test piece [37].

Lee and Garimella [43] investigated experimentally the flow boiling in arrays of parallel MCs by using a silicon test piece with imbedded discrete heat sources and integrated local temperature sensors. The MCs width used was ranged from 102 μm to 997 μm and the width was 400 μm. Deionized water was used as a working fluid. The results reveal that the pressure drop across the MCs increased rapidly with the heat flux when the incipience heat flux (for the onset of nucleate boiling) was exceeded. At low to medium heat fluxes, the local heat coefficient increased almost linearly with heat flux. While, at higher heat fluxes, the saturated heat transfer coefficient becomes largely insensitive to heat flux for the range tested.

Celata et al. [44] investigated experimentally heat transfer characteristics of subcooled flow boiling of FC-72 in a single horizontal circular cross section MC with 480 μm inner diameter, 800 μm outer diameter and 102 mm long. Different flow patterns, both in the stable and unstable flow boiling regimes were considered. The results indicate that the stable flow boiling with alternating bubbly/slug flow, slug/annular flow and annular/mist flow was observed for heat flux of 150 kW/m^2 or higher and mass flux of 1500 kg/m^2 s or higher. Back and forth oscillations with flow instabilities were observed in cases of lower heat and mass fluxes. No complete reverse flow was observed in upstream direction. In addition, the heat transfer coefficient increased with the increases of vapor quality at higher vapor quality, and at lower vapor quality, the heat transfer coefficient was rather independent of heat flux.

Megahed [45] investigated experimentally flow boiling characteristics in a cross-linked MC heat sink at low mass fluxes and high heat fluxes. The heat sink used consists of 45 straight MCs with a hydraulic diameter of 248 μm and heated length of 16 mm. The dielectric coolant FC-72 was used as a working fluid. The heat flux used was ranged from 7.2 kW/m^2 to104.2 kW/m^2, mass flux from 99 kg/m^2/s to 290 kg/m^2/s, and exit quality from 0.01 to 0.71. The results indicate that the instability increased with decreasing the mass flux. The inlet pressure and outlet saturation temperature oscillate with higher amplitudes as the mass flux decreases. The two-phase pressure drop through MC heat sinks with cross-links was much higher compared to the straight MC heat sinks due to the

cross-link effect. The two-phase heat transfer coefficient was strongly increased with the exit quality because of the domination of the nucleation boiling mechanism in the cross-link region.

Diaz and Schmidt [46] investigated experimentally flow boiling heat transfer in a single rectangular MC made of the nickel alloy Inconel 600 with 0.3 mm height, 12.7 mm width and 200 mm length. Water and ethanol were used as test fluids. The mass fluxes used ranged between 50 kg/m^2/s and 500 kg/m^2/s and heat fluxes up to 400 kW/m^2 at an outlet pressure of 0.1 MPa. The results reveal that, high amplitude oscillations for water were found in the region of subcooled boiling at qualities slightly below zero. The amplitude decreased as quality increases and no characteristic frequency was observed. Flow boiling of ethanol yielded low amplitude oscillations of the wall temperature, even within the subcooled boiling region. Increase in quality resulted in increasing oscillation amplitude. In addition, the heat transfer coefficient decreased with increasing quality for water. Different observed for ethanol after the low quality region. The heat transfer coefficient increased with increasing quality at low heat fluxes. With increasing heat flux, the heat transfer coefficient decreased with quality.

Chen et al. [47] investigated experimentally the condensation of steam in a series of triangular silicon MCs with hydraulic diameters ranged from 100 to 250 μm. The number of channels in each silicon chip was 10 and the length for each channel was 56.7 mm. The results indicate that the droplet, annular, injection and slug–bubbly flow are the dominant flow patterns in triangular silicon MCs. The flow of condensation instability was higher with increased inlet vapor Reynolds number, condensate Weber number and the prolongation of the injection location, or with a decrease in the hydraulic diameter of the channel. In addition, the wall temperature of the channel decreased along the condensation stream. The total pressure drop, the average condensation heat transfer coefficient and the average Nusselt number were observed to be larger with increased inlet vapor Reynolds number. Moreover, it was found that the condensation heat transfer was enhanced by a reduction in the channel scale.

Betz and Attinger [48] investigated experimentally heat transfer enhancement in MC heat sink with the introduction of segment flow. The segmented flow pattern was created by the periodic injection of air bubbles into water-filled channels. Reynolds number used was ranged from 160 to 1580. The results reveal that the segmented flow would provide an intermediate step between single-phase and boiling flow for the purpose of electronic cooling. The segmented flow increases the Nusselt number of laminar flow by more than 100%. The heat transfer enhancement only occurs for a specific range of flow rates and capillary numbers. At lower or higher capillary numbers, there was no significant heat transfer enhancement observed because segmented flow was replaced by bubbly or churn flow, respectively.

Wojtan et al. [49] investigated experimentally the saturated critical heat flux (CHF) in 0.5 mm and 0.8 mm internal diameter MC tubes as a function of refrigerant mass velocity, heated length, saturation temperature and inlet liquid subcooling. The tested refrigerants were R-134a and R-245fa and the heated length of MC was varied between 20 mm and 70 mm. The results reveal that a strong dependence of CHF on mass velocity, heated length and MC diameter but no influence of liquid subcooling (2–15 °C) was observed. A new MC version of the Katto–Ohno correlation was developed to predict the CHF in circular, uniformly heated MCs.

Asthana et al. [50] investigated experimentally convective heat transfer in serpentine MCs cross section 100 μm with a segmented flow of two immiscible liquids for flow rates up to 130 μl/min. The results reveal that for slug flow, the movement of the oil slugs induces intensive fluid recirculation in the carrier water phase between the slugs, which disrupts the formation of a boundary layer and improves mixing, more so for increasing oil volume fractions. In addition, the local temperature of the water region separating the droplets was higher than in the case of pure water flow. For segmented flow, up to a four-fold increased the Nusselt number compared to pure water flow was observed. Increased heat removal increased the pressure drop, which was strongly affected by the fluid temperature.

Wang and Cheng [51] investigated experimentally stable and unstable flow boiling phenomena of deionized water in a single MC with hydraulic diameter of 155 μm. The results reveal that stable flow boiling occurred in a single MC if exit vapor quality $x_e < 0.013$, where vapor bubbles generated and pushed away by the incoming subcooled liquid. Single-phase liquid flow, bubbly flow and elongated bubbly/slug flow were observed sequentially in the stable flow boiling mode. In addition, unstable flow boiling occurred in a single MC if $x_e > 0.013$, where vapor plug expanded upstream resulting in oscillations of temperature and pressure. In this unstable flow boiling mode, bubbly flow, elongated bubbly/slug flow, semiannular flow and annular/mist flow were observed at different times near the outlet depending on the mass flux.

Wu et al. [52] investigated experimentally steam condensation flow in wide rectangular silicon MCs with the hydraulic diameter of 90.6 μm, 483.4 μm width and 50 μm depth. The results reveal that droplet-annular compound flow, injection flow, and vapor slug–bubbly flow were observed along the channel, which differ from that in other cross-sectional shape MCs. In the droplet-annular compound flow region, the vertical walls (short side) of the channel were completely covered by the condensate, while droplet condensation still exists on the horizontal wall (long side) of the channel. The location of the injection flow postponed with the increasing inlet vapor Reynolds number. The injection frequency increased with increasing the inlet vapor Reynolds number and condensate Weber number. In addition, the frequency in the wide rectangular MCs was lower than that in triangular MCs with the same hydraulic diameter. It is confirmed that the cross-sectional shape of the MC plays a significant role on the instability of condensation flow. The correlation of Nusselt number was also obtained.

Steinke and Kandlikar [53] investigated experimentally the different components of the total pressure drop measurement for adiabatic and single-phase degassed water in MC with a width of 200 μm, a depth of 250 μm and a length of 10 mm. An in-depth comparison of previous experimental data was performed to identify the discrepancies in reported literature. The Reynolds number used was ranged from 14 to 789. The results reveal that, the procedure for correcting the measured pressure drop, the data was corrected for inlet and exit losses and then it was corrected for developing flows. The corrected data shows good preliminary agreement in value and trend with the conventional theory for laminar fluid flow. The conventional Stokes and Poiseuille flow theories apply for single-phase liquid flow in MC flows.

Wu et al. [54] investigated experimentally static and dynamic flow instability of a parallel MC heat sink consisting of 26 rectangular MCs with 300 μm width, 800 μm depth, at high heat fluxes. Water and methanol were used as a working fluid with mass fluxes of 20–1200 kg/m^2/s. The inlet temperature used was ranged from 300 °C to 70 °C. The results indicate that the onset of flow instability occurs at the outlet fluid temperature of 93–96 °C, which were several degrees lower than the saturated temperature corresponding to the exit pressure of the MCs. In addition, the outlet temperature and inlet pressure were always in phase, but they were out of phase with the pressure drop across the MCs. The wall temperatures generally match the oscillation trends of the inlet pressure and the outlet temperature, but a time delay occurs due to the thermal inertia of the copper block.

Zhang et al. [55] investigated experimentally the control of pressure-drop flow instabilities in boiling microchannel systems with

61 μm width, 272 μm height and 15 mm length. Deionized water was used as a working fluid. The results reveal that the predictions from the flow oscillation model were agreed well with the experimental pressure-drop observations across a flow meter and a MCHS. In addition, a family of state and dynamic output-feedback active flow controllers was developed and evaluated for the dynamic pressure-drop instability suppression. The flow oscillation amplitude can be regulated to whatever level is desired under certain conditions.

Kohl et al. [56] investigated experimentally the flow with internal pressure measurements in straight microchannel test section with hydraulic diameters ranged from 25 μm to 100 μm. The Reynolds number used was ranged from 4.9 to 18,814. The results suggest that friction factors for MCs can be accurately determined from data for standard large channels.

Rosengarten et al. [57] investigated experimentally the effect of contract angle (surface wettability) on the convective heat transfer coefficient in microchannels using thin film coating technology. Distilled water was used as a working fluid. The results reveal that, the pressure drop decreases relative to that expected with non-slip theory above a critical shear rate and this decrease was dependent on the contact angle. Associated with the decrease in pressure drop was a concurrent decrease in the convective heat transfer coefficient which again was more pronounced for hydrophobic surfaces. Slip flow was an extremely important for micro and in particular nano heat exchanger designs as heat transfer rates may decrease more than 10% at high shear rates.

Tang et al. [58] investigated experimentally compressibility, roughness and rarefaction influences for nitrogen and helium in stainless steel MTs with diameters ranged from 119 μm to 300 μm, fused silica MTs with hydraulic diameter ranged from 52 μm to 201 μm and fused silica square MCs with diameters ranged from 52 μm to 100 μm. The Reynolds number used was ranged from 3 to 6300. The tested outlet Knudsen number used was ranged from 1.4×10^{-4} to 4×10^{-3}, and the tested outlet Mach number was ranged from 0.01 to 0.6. The results indicate that the gaseous flow friction factor in stainless steel tube (SST) was observed to be much higher than the theoretical prediction for conventional size tubes. The friction factor in the fused silica tubes and fused silica channels (FST, FSC) agreed well with the theoretical prediction. In addition, the increase in friction factor was attributed to the dense roughness distribution in the inner surface of the stainless steel tubes. Surface roughness in MCs was found to affect the friction factor. It is suggested that for gaseous flow in MCs with a relative surface roughness less than 1%, the conventional laminar prediction should still be applied.

Huh et al. [59] investigated experimentally the unique characteristics of flow boiling in a polydimethylsiloxane (PDMS) rectangular single microchannel with a hydraulic diameter of 103.5 μm and length of 40 mm. Deionized water was used as a working fluid. The mass fluxes used were 170 kg/m^2 and 360 kg/m^2 and the heat fluxes were ranged from 200 kW/m^2 to 530 kW/m^2. The results indicate that flow boiling fluctuations with a very long period and large amplitude were observed. Both the pressure drop and mass flux had these fluctuations, but a phase shift occurred between them that controlled the flow patterns. The fluctuation of wall temperature and heat flux had the same period as that of the mass flux. In addition, the variation in temperatures, pressure, and mass flux exactly matched the flow pattern transitions between bubbly/slug flow and elongated slug/semiannular flow. The flow pattern transition instabilities in the single MC caused the cyclic behavior of the wall temperature, pressure drop, and mass flux. As the supplied heat flux and vapor quality increased, the period of the unstable fluctuations lengthened and the amplitude also increased.

Mokrani et al. [60] investigated experimentally the fluid flow and convective heat transfer in flat microchannels with constant width, height ranged between 50 μm and 500 μm and the hydraulic diameter was varying between 1 μm and 100 μm. The tap water was used as working fluid with flow rate ranged from 0.04 ml/min to 240 ml/min. Reynolds number used was ranged from 100 to 5000. The results reveal that the conventional laws and correlations describing the flow and convective heat transfer in ducts of large dimension were directly applicable to the MCs of heights between 500 μm and 50 μm. In addition, the transition from the laminar to turbulent regime occurred in a range of Reynolds numbers similar to that observed in ducts of large sizes.

Bertsch et al. [61] investigated experimentally the flow boiling heat transfer with the refrigerants R-134a and R-245fa in copper microchannel cold plate evaporators. Array of MCs were used with hydraulic diameter 1.09 mm and 0.54 mm. The aspect ratio of the rectangular cross section of the channels in both test section was 2.5. The saturation temperatures used were ranged from 8 °C to 30 °C, mass flux from 20 kg/m^2/s to 350 kg/m^2/s and the heat flux was ranged from 0 W/cm^2 to 22 W/cm^2. The results indicate that the heat transfer coefficient for R-245fa in comparison with R-134a in single-phase flow was higher. The pool boiling heat transfer for R-245fa was lower as a result of its higher molecular mass and surface tension. In addition, the flow boiling heat transfer coefficient strongly increased with the increase of the heat flux and was dominated by nucleate boiling. It also shows a strong dependence on thermodynamic vapor quality with a rapid decrease at qualities above 0.5. The maximum heat transfer coefficient occurs at vapor qualities between 0.1 and 0.5 depending on fluid, geometry and flow conditions. The heat transfer coefficient increased weakly with increases mass flux and was almost constant. However, a comparison of the measurements against predictions from several correlations showed reasonable agreement only with a very few correlations except of a pool boiling equation that were developed specifically for small channels did not predict the heat transfer coefficient better.

Ngo et al. [62] investigated experimentally the thermal-hydraulic characteristics of microchannel heat exchangers (MCHEs) with S-shaped and zigzag fins by varying Prandtl number widely from 0.75 to 2.2. The results indicate that the pressure-drop factor of the MCHE with S-shaped fins was 4–5 times less than that of MCHE with zigzag fins, although *Nu* was 24–34% less, depending on the Reynolds number within its range. However, the *Nu* correlation of the MCHE with S-shaped fins reproduces the experimental data of overall heat transfer coefficients with a standard deviation of $\pm 2.3\%$, although it is $\pm 3.0\%$ for the MCHE with zigzag fins. The calculated pressure drops obtained from pressure-drop factor correlations agreed with the experimental data within a standard deviation of $\pm 16.6\%$ and $\pm 13.5\%$ for the MCHEs with S-shaped and zigzag fins, respectively.

Wei and Joshi [63] investigated experimentally and numerically the sidewall profile effects on flow and heat transfer inside microchannels with diameter ranged from 53 μm to 112 μm. Numerical modeling was conducted for conjugate heat transfer inside MCs. To simulate the practical application conditions such as those in electronic cooling, uniform heat flux condition was applied at the bottom region while the interface of the channel was assumed adiabatic. Three different cases were considered in which the channel profiles were rectangular, positively tapered and re-entrant respectively. The results reveal that the location of the maximum velocity deviates from the mid-plane along the depth direction due to the wall taper. In addition, for constant heat flux condition, serious degradation in overall heat transfer occurs for channel with 5° slope. For conjugate heat transfer, the degradation in heat transfer was much less and re-entrant channel has better heat transfer performance than positively tapered channel. It was concluded that for MCs with large aspect ratio the transport characteristics very sensitive to the channel profiles, therefore, careful design and control of the micro-fabrication process were crucial to the performance of the micro-scale devices.

Fang et al. [64] investigated experimentally the influences of film thickness and cross-sectional geometry on hydrophilic microchannel condensation, with aspect ratios ranged from 1 to 5 and hydraulic diameters ranged from 100 μm through 300 μm. The results reveal that the experimental measurement qualitatively matches the prediction of previous theoretical models accounting for the surface tension effect, which highlights the importance of surface tension force and channel geometry in the MC condensation. In addition, the pressure drop increased linearly with both inlet vapor mass flux and inlet vapor mass flowrate. Under the same vapor flow rate and aspect ratio, the channel with the smaller hydraulic diameter exhibits the higher pressure drop. While the pressure drop reduced with increases the hydraulic diameters so does the mean heat flux. Therefore, the optimization of hydrophilic channel geometry for film condensation enhancement lies in the trade-off between these two factors. If the pumping power of the compact heat exchanger is primary concern, a larger channel was more desirable considering its small pressure drop. In contrast, if heat exchanger size or channel length is the primary limit, a smaller channel was more favorable due to its high mean heat flux.

Bogojevic et al. [65] investigated experimentally the effects of non-uniform heating on flow boiling instabilities in microchannel-based heat sink using water as the cooling liquid. The results indicate that the onset of boiling caused metastable non-uniform flow distribution, with boiling in some channels and single-phase flow in others, leading to transverse variations in temperature that were less severe when the hotspot was at the downstream position. The non-uniformity was attributed to statistical variations in the small numbers of stable bubble nucleation sites per channel. In addition, the oscillations were superimposed on the non-uniform flow distributions. At low hotspot heat flux, there were high amplitude oscillations at a dominant low frequency (HALF). With increasing heat flux, this changed progressively to lower amplitude oscillations at higher frequency (LAHF). In the HALF regime, synchronized fluctuations in the wall temperature occurred in channels with and without boiling, indicating that the oscillations were not driven by the growth of confined bubbles in individual channels.

Wang et al. [66] investigated experimentally the effects of inlet/outlet configurations on flow boiling instability in parallel microchannels have a 30 mm length and a hydraulic diameter of 186 μm. Three types of inlet/outlet configurations were obtained. In Type-A connection, inlet and outlet conduits were perpendicular to the parallel MCs in the test section. In Type-B connection, fluid could flow into and exit from the parallel MCs without any restriction, and in Type-C connection, fluid entered each of the MCs through an inlet restriction. The results indicate that the amplitudes of temperature and pressure oscillations in Type-B connection was much smaller than those in Type-A connection under the same heat flux and mass flux conditions. Nearly steady flow boiling exists in the parallel MCs with Type-C connection under the experimental conditions as shown in Fig. 6. Therefore, this configuration was recommended for high-heat flux MC applications. The experimental data of pressure drop was higher and heat transfer coefficients was lower for boiling flow at high vapor quality in MCs than those predicted from correlation equations for boiling flow in MCs, due to local dryout.

Hernando et al. [67] investigated experimentally fluid flow and heat transfer in a single-phase liquid flow micro-heat exchanger, characterized by MCs of $100 \times 100\,\mu m$ and $200 \times 200\,\mu m$ square cross section. The deionized water was used as a working fluid. The results show good agreement with the general theory and no special effect related to the small dimension of the channels was observed. In addition, no heat transfer increment appeared as a result of the small channel dimensions. For very low Reynolds numbers, the results show discrepancies with the available models and correlations, which

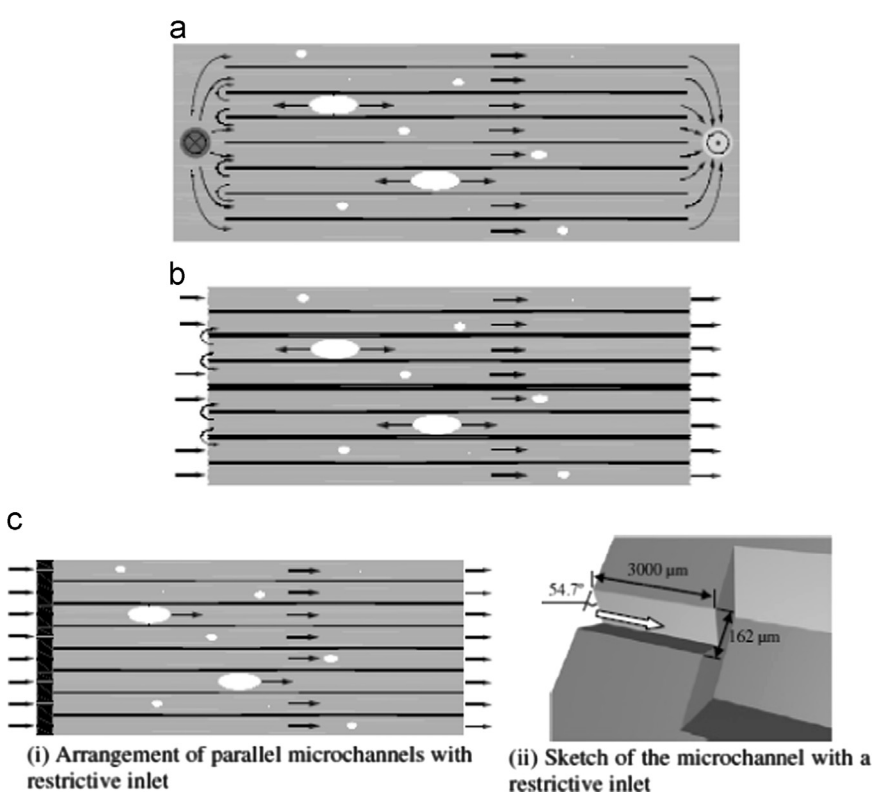


Fig. 6. Parallel microchannels with three different inlet/outlet connections [66]. (a) Type-A connections: flow entering and exiting from paral microchannels with restrications because inlet/outlet conduit perpendicular to microchannels, (b) Type-B connection: flow entering to and exiting from microchannels freely withuot restriction and (c) Type-C connection: flow entering with restriction and exiting without restriction in microchannels.

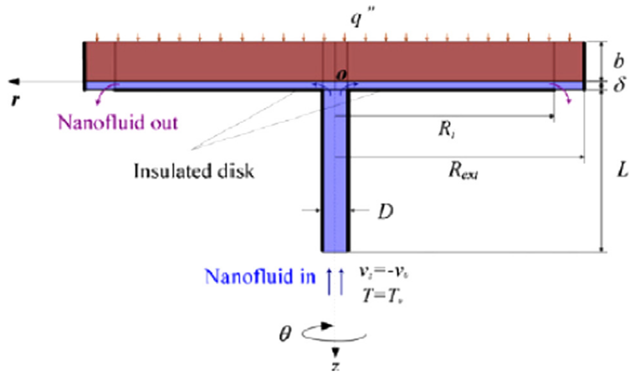


Fig. 7. geometrical configuration [68].

overestimate the convection coefficients which related with the adequacy of the boundary conditions. On the other hand, the plate conduction thermal resistance was a major restriction for micro-heat exchanger performance. The plate thickness and plate material were critical in the design of micro-heat exchangers.

3.2. Numerical studies on MC

Yang and Lai [68] investigated numerically the effects of forced convection flow of Al_2O_3–water nanofluids in the radial flow cooling system using a single-phase approach. The geometrical configuration of the confined radial flow was used shown in Fig. 7. The two plates separated by a gap were parallel and stationary. The lower disk (with nozzle) acts as the insulated confinement plate, while the upper one (wafer) was subjected to a constant heat flux. The numerical simulations were performed based on the following conditions: volume concentration of 47 nm Al_2O_3 nanoparticle suspended within water is from 0% to 10%, flow Reynolds number range from 300 to 900 with the heat flux 2438 W/m^2 and 3900 W/m^2. The inlet fluid temperature $T_o = 296$ K. The results indicate that the heat transfer coefficient increased with the increases of Reynolds number and particle volume fraction.

Wu et al. [69] proposed a new correlation for the saturated-flow boiling critical heat flux (CHF) in microchannel for both multi and single channel configurations. The saturated CHF correlation was proposed by using the boiling number, length to diameter ratio and the exit quality. The results reveal that the boiling number at CHF decreased greatly with a small increase in length to diameter ratio L_h/d_{he} when this ratio ≤ 50. The transition was appeared in the range of $50 < L_h/d_{he} \leq 150$. This correlation can predict the overall MC database accurately. This method almost predicts 97% of the non-aqueous data and 94% of the water data within the $\pm 30\%$ error band.

Shevade and Rahman [70] investigated numerically the convective heat transfer in rectangular and square cross sections MCs for volumetric heat generation. Gadolinium was used as the substrate material and water as the working fluid. The results reveal that the Nusselt number decreased along the x or y-axis from the mid-section of the channel to the corner due to smaller fluid velocity which caused by larger frictional resistance at the corner. In rectangular channels, the heat transfer coefficient values are higher on the longer side than on the shorter side. At a smaller flow rate, the local Nusselt number decreased and the outlet temperature increased as the low velocity fluid remains in contact with the solid for a longer period of time. The pressure drop in the channel increased as the Reynolds number increased. Nusselt number increased as the channel dimensions increased. For the same channel, Nusselt number increased with Reynolds number.

Gamrat et al. [71] investigated numerically the roughness effects on heat transfer in thermally fully-developed laminar flows through microchannels. The models considered parallelepipedic elements periodically distributed on the plane walls of a micro-channel of infinite span. Three-dimensional numerical simulations were first conducted in a computational domain extending over one wavelength in streamwise and spanwise directions. The numerical results reveal that the Poiseuille number P_o and the Nusselt number (Nu) increased with the relative roughness and nearly independent of Reynolds number in the laminar regime ($Re < 2000$). In addition, the roughness increase the friction factor more than the heat transfer coefficient for a relative roughness height expected in the fabrication of MCs.

Mlcak et al. [72] investigated numerically the heat transfer and laminar fluid flow in an array of parallel microchannels etched on a silicon substrate with water as the circulating fluid. The hydraulic diameter used was 85.6 μm and aspect rations ranged from 0.10 to 1.0. Reynolds number used was ranged from 50 to 400. The results reveal that the linearly increasing friction coefficient that was observed between Reynolds numbers 50 and 400 as a result of increased hydraulic entrance length. Friction coefficient values were found to monotonically increase for aspect ratios approaching 0.10. The values of inlet and outlet thermal resistance decreased for aspect ratios approaching 0.10, for the same hydraulic diameter the inlet and outlet thermal resistance and friction coefficient values changed very little for aspect ratios larger than 0.50.

Chen et al. [73] investigated numerically the heat transfer and fluid flow in noncircular microchannel heat sink. The cooling fluid in the channel used was deionized water. The geometries for the triangular, rectangular and trapezoidal channel were used, 129.6 μm, 40 μm and 158 μm, respectively. The results reveal that, the circumferential average Nusselt number has a much higher value at the inlet region but it quickly approaches the constant fully developed value. The liquid and solid temperature increased along the flow direction. In addition, the Poiseuille number in MCs with a certain cross section remained almost constant and independent with the Reynolds number for fully developed laminar flow which was similar to fluid flow in MCs. Triangular MC heat sink has the highest thermal efficiency among the three heat sinks, the trapezoidal MC was inferior to triangular but superior to rectangular.

Zhu and Liao [74] investigated theoretically the laminar forced heat transfer for a gas flow through a microchannel of arbitrary cross section with axial constant heat flux and circumferential varied wall temperature boundary condition in the slip flow and temperature-jump regime. The influences of Knudsen number, the channel aspect ratio, and the thermal boundary condition on heat transfer behavior were estimated. The results indicate that for a rectangular and triangular microchannel, the average Nusselt numbers were smaller than those of a macrochannel with the same thermal boundary conditions and it decreases with increasing Knudsen number. Knudsen number has more significant influences on the average Nusselt number of the rectangular microchannel with a smaller channel aspect ratio. The varying trends of the average Nusselt number with the channel aspect ratio were similar at various Kn numbers. The channel aspect ratio has few effects on the average Nusselt number ratio at a fixed Knudsen number within a moderate range of channel aspect ratio.

Ji et al. [75] investigated numerically the wall roughness on gaseous flow and heat transfer in a microchannel with length range from 1 μm to 100 μm. The effect was examined for gas flows under inlet Mach number ranged from 0.0055 to 0.202. The Reynolds number used was ranged from 0.001 to 100. The results indicated that the rough elements restrict the upstream gas flow and cause more pressure drop and increase the Poiseuille number due to the obstruction effect and formation of recirculation regions. Rarefied flow was sensitive to the shape of roughness

elements. The average Poiseuille number increased not only as the roughness height increases but also as the spacing distance between the roughness elements was decreased. However, this effect was much stronger on the gas flow with a lower Knudsen number. In addition, for a highly compressible flow, the average Nusselt number does not change much or increases slightly. The existence of wall roughness enhances the heat transfer.

Sui et al. [76] investigated numerically laminar liquid water flow and heat transfer in three-dimensional wavy MCs with rectangular cross section under constant wall heat flux. In the conjugate simulation, a uniform heat flux was applied at the bottom wall of the silicon substrate and on the upper surface adiabatic boundary condition was employed. The results reveal that when liquid coolant flows through the wavy MCs, secondary flow (Dean vortices) was generated. The quantity and the location of the vortices may change along the flow direction, leading to chaotic advection, which can greatly enhance the convective fluid mixing, and thus the heat transfer performance of the wavy MCs was much better than that of straight MCs with the same cross section. In addition, the pressure drop penalty of the wavy MCs was much smaller than the heat transfer enhancement.

Muhammad et al. [77] investigated numerically the convective heat transfer in a composite trapezoidal microchannel with length 23 mm during magnetic heating. The channel was formed by etching a silicon 100 μm wafer and bonding it with a slab of gadolinium with height varied between 1.5 mm and 5 mm. Reynolds number used was ranged from 1000 to 3000. The roughness height used was 0.35 nm for silicon MC surface and 1 nm for gadolinium. Magnetic field used was ranged from 2.5 T to 10 T. The results reveal that for a smaller flow rate, the outlet temperature increased as a lower velocity fluid remains in contact with the solid for a longer period of time. The peripheral average heat transfer coefficient and Nusselt number decreased along the length of the channel due to the development of thermal boundary layer. Increasing the channel spacing slightly increased the local Nusselt number all along the length of the channel. The Nusselt number increased with decrease of channel hydraulic diameter at any given Reynolds number due to higher fluid velocity. Compared to helium and FC-72, water provides better thermal performance with higher values of Nusselt number.

Liu et al. [78] investigated numerically fluid flow and heat transfer in MC cooling passages. Two-dimensional simulation was performed for low Reynolds number flow of liquid water with diameter $D=100$ μm of single channel subjected to localized heat flux boundary conditions. The results reveal that the heat transfer enhancement due to viscosity-variation was pronounced, though the axial conduction introduced by thermal-conductivity-variation was insignificant unless for the cases with very low Reynolds numbers.

Renksizbulut et al. [79] investigated numerically rarefied gas flow and heat transfer in the entrance region of rectangular MC in the slip-flow regime. The Reynolds number used was ranged from 0.1 to 10, channel aspect ratio ranged from 0 to 1 and the Knudsen number was $Kn \le 0.1$. The results indicate that the slip-flow regime was associated with very large reductions in wall friction and heat transfer in the entrance region. Fully developed values of friction coefficient and heat transfer rates were more influenced with rarefaction effects in a flat channel than a square duct due to the major influence of channel corners where rarefaction effects largely vanish.

Niazmand et al. [80] investigated numerically the velocity and temperature fields in the slip-flow regime in trapezoidal MCs with constant wall temperatures. The range of channel aspect ratio used was from 0.25 to 2, side angles from 30° to 90° and the Reynolds number ranged from 0.1 to 10. The prandtl Number used was $Pr=1$. The results reveal that the major reductions in the friction and heat transfer coefficients were observed in the entrance region due to large amounts of velocity-slip and temperature-jump. The friction coefficient decreased strongly both with increasing the Knudsen number and aspect ratio but has a weaker dependence on the side angle.

Khadem et al. [81] investigated numerically fluid flow and heat transfer characteristics in MCs at slip flow regime with consideration of slip and temperature-jump. The results reveal that the rough elements restrict the upstream gas flow and cause more pressure drop and increases in the Poiseuille number due to the obstruction effect. Roughness has more significant effect on higher Knudsen number flows with higher relative roughness. The changing in roughness shape leads to extremely different flow patterns except for small relative roughness.

Zade et al. [82] investigated numerically the effects of variable physical properties on the flow and heat transfer characteristics of simultaneously developing slip-flow in rectangular MCs with constant wall temperature. The Reynolds number used was set equal to 0.1. The inlet gas temperature in all simulations was specified to be $T_{in}=300$ K, and the wall temperature was $T_w=350$ K. The results indicate that in the entrance region, Nusselt number was only affected by the change in the Knudsen number and was higher in variable-density slip-flow cases. The Nusselt number was generally higher in the variable-property simulations. In the fully-developed region, since the effect of density change diminishes, friction coefficient and Nusselt number predictions of the variable-property simulations were higher in comparison to those of the constant-property cases.

Shokouhmand and Bigham [83] investigated numerically the effects of Knudsen number and geometry on thermal and hydrodynamic characteristics of flow in the wavy microchannel at constant Reynolds number. The results reveal that the Nusselt number and C_f. Re decreased with Knudsen number. In the divergent parts, Nusselt number experiences a rapid decrease. The very high heat transfer rate and C_f. Re at the entrance declines rapidly as the thermally-hydraulically developing flow approaches fully developed flow. In addition, the effect of viscous dissipation has a considerable effect in MCs and this effect can be more significant by increasing Knudsen number.

Mohammed et al. [84,85] investigated numerically the influence of channel shapes (zigzag, curvy, wavy) on the thermal and hydraulic performance of microchannel heat sink (MCHS). The Reynolds number used was ranged from 100 to 1000 for all channel flow shapes. Water was used as a working fluid. The inlet temperature of water used was 293 K and the heat flux at the top plate of MCHS was 100 W/m^2. The results reveal that, the temperature and the heat transfer coefficient of the zigzag MCHS was the least and greatest, respectively, comparing to other channel shapes. The second best thermal performance was provided by curvy channels after the wavy channels. The zigzag MCHS was the best channel for the best thermal performance, while the step MCHS was the best channel for the hydraulic performance with moderate degradation of heat transfer compared to conventional straight MCHS

Kosar [86] investigated numerically the effect of substrate thickness and material on heat transfer in microchannels heat sink. The size of the MCs used (200 μm × 200 μm, 5 cm long). The substrate thickness was ranged from 100 μm to 1000 μm and the MEMS materials used (polyimide, Silica Glass, Quartz, steel, silicon and copper). Temperature, pressure and velocity distributions across a MC heat sink were found under a broad range of Reynolds number and heat transfer using water as a working fluid. The results reveal that a very good agreement

between the model results and the theoretical prediction corresponding to constant heat flux boundary condition for Reynolds number $Re < 976$ was observed, beyond $Re = 1000$ Nusselt number results were greater than the theoretical value of Nusselt number for developed flows due to developing effects. The Nusselt number was lower for low thermal conductivity materials than the Nusselt number obtained from high conductivity materials. The weaker dependence of substrate thickness on Nusselt number compared to the effect of thermal conductivity was because of the existing constraint in the ratio of substrate thickness to the MC size.

Mohammed et al. [87,88] investigated numerically the influences of nanofluids on parallel flow square and rectangular microchannel heat exchanger (MCHE) performance. Four different nanofluids (aluminum oxide (Al_2O_3), silicon dioxide (SiO_2), silver (Ag) and titanium dioxide (TiO_2) with three nanoparticle volume fraction of 2%, 5% and 10% were used with water as base fluid. Reynolds number used was ranged from 100 to 800. The results reveal that as the nanoparticle volume fraction increased, the bulk average temperature of the cold fluid increased and the heat transfer rate decreased. On the other hand, as the Reynolds number increased, the average bulk temperature of the cold fluid decreased and the heat transfer rate increased. In addition, aluminum oxide nanofluid has the highest heat transfer coefficient among all the nanofluids tested. The presence of nanoparticles increase the pressure drop slightly with silver nanofluid has the lowest pressure drop, while the highest difference of pressure drop from water was lower than 5%.

Revillin and Thome [89] reported a theoretical model for the prediction of the critical heat flux (CHF) of refrigerants flowing in heated microchannel. The prediction was based on the local dryout of the liquid film in annular flow occurring when the film thickness becomes equal to the interfacial wave height during evaporation. The model was based on the conservation of mass, momentum and energy, the Laplace–Young equation and a semi-empirical expression for the height of interfacial waves. The results reveal that more than 96% of the data was predicted within a $\pm 20\%$ error band and a mean absolute error of 8%. It is possible to predict CHF data from a third laboratory for water and R-113 flowing in rectangular (using the width of the channel as the characteristic dimension) and circular MCHS with multiple channels.

Revellin et al. [90] reported status of prediction methods for critical heat flux in mini and microchannel. 2996 data point collected from 19 different laboratories includes nine different fluids (R-134a, R-245fa, R-236fa, R-123, R-32, R-113, nitrogen, CO_2 and water) for a wide range of experimental conditions were compared to 6 different correlations and 1 theoretically based model to provide the best CHF prediction method. It predicts almost 86% of the CHF data for non-aqueous fluids within a 30% error band. This method predicts almost 83% of the CHF data for water within a 30% error band.

Rosa et al. [91] reviewed an experimental and numerical result from different references about the importance of scaling effects (entrance effects, conjugate heat transfer, viscous heating, electric double layer (EDL) effects, temperature dependent properties, surface roughness, rarefaction and compressibility Effects) in the single-phase heat transfer in microchannels. Their review concludes with a concise set of recommendations for purposes of performance and design. For single channels, available correlations for macro-channels can also give reliable predictions at the micro-scale, but only if all the scaling effects can be considered negligible. Otherwise, when scaling effects cannot be neglected or for the case of heat exchangers with parallel channels, suitable numerical simulations may be the sole alternative to carefully designed experiments to evaluate the heat transfer rates. A summary for the numerical and experimental studies in MC is shown in Table 2.

4. Nanofluids

4.1. Preparation of nanofulids

The powder form nanoparticles which disperse in host liquids are called nanofluids. Nanofluids can be produced by two techniques; the two-step (double-step) method, and one-step (single-step) method. These methods have been utilized using different types of chemical and physical techniques to make sure that the solid–liquid mixture is stable to avoid agglomeration, additional flow resistance, possible erosion and clogging, poor thermal conductivity, and poor heat transfer. The two-step method is done by producing the nanoparticles powder initially as introduced in the previous section, and then disperses them into a host liquid. However, in one-step method the nanoparticles are simultaneously made and directly dispersed into the base fluid [92]. It is noticed in the literature that nanofluids with oxide nanoparticles and carbon nanotubes are produced well by the two-step method, while it is not suitable for nanofluids with metallic nanoparticles.

Chopkar et al. [93] presented a simple method of preparing nanofluids comprising a small amount (<1 vol%) of nanocrystalline metallic particles ($Al_{70}Cu_{30}$) as a stable colloidal dispersion in ethylene glycol. The size/microstructure of the nanoparticles was characterized by X-ray diffraction and transmission electron microscopy, and the thermal conductivity of the nanofluid was measured by using a modified thermal comparator. The results showed that the thermal conductivity measurements, using a purpose-built thermal comparator device, revealed to that the conductivity of this nanofluid is significantly greater (1.2–2 times) than that of the base fluid. Moreover, the increase in conductivity is a function of volume fraction, size and thermal property of the solid suspension. The results also demonstrated that the heat removal rate or efficiency of the nanofluid is better than that of the base fluid, especially at lower temperatures. The results revealed to that the nanofluid could be useful in microthermal heat transfer applications including in MEMS and automobiles.

4.2. Experimental studies on nanofluids

4.2.1. Thermal conductivity

It is reported that many experimental studies have been done on thermal conductivity of nanofluids because it is a primary assessment of the heat transfer performance of nanofluids. The physical mechanism for thermal conductivity enhancement of nanofluids is not well understood up to date. Li et al. [94] presented investigation of the effective thermal conductivity of Al_2O_3/water nanofluids with normal diameters of 47 nm at different volume fractions (0.5%, 2%, 4%, and 6%). In this investigation two different methodologies were utilized: a transient hot-wire method and a steady-state cut-bar method. The comparison of the measured data obtained by using two different experimental systems at room temperature was conducted and the experimental data at higher temperatures were obtained with steady-state cut-bar method and compared with previously reported data obtained using a transient hot-wire method. The results showed that at room temperature, both the steady-state cut-bar and transient hot-wire methods result in closely identical values for the effective thermal conductivity of the nanofluids tested. Furthermore, at higher temperatures, the onset of natural convection results in larger measured effective thermal conductivities for the hot-wire method than those obtained using the steady-state cut-bar method. The results also confirmed

Table 2
Summary of experimental and numerical studies for MC.

Researchers	Diameter/flow nature	Reynolds number	Fluid/gas	Findings
Jung et al. [29]	50–100 μm/laminar	5–300	Water Water+EG/Al_2O_3	The convective heat transfer coefficient of the Al_2O_3 was increased up to 32% compared to the distilled water
Cheng Wang et al. [30]	25 mm/laminar	–	NaCl and diluted glycerol	Demonstrated a new method to solve the unmatched viscosity problem of the two-fluid flow in MC
Agarwal et al. [31]	0.424–0.939 mm/Laminar	–	R134a	Developed a correlation for heat transfer during condensation of refrigerant R134a in horizontal non-circular MC
Roland et al. [32]	700–*200 μm/laminar and turbulent	200–8000	Demineralized water	A reduction in the Nusselt number for laminar flow at the microscale is occurred
Wu and Cheng [33]	L/D=285.41–451.40/laminar	0–100	Water	Nusselt number increased almost linearly with the rise of Reynolds number
Park and Punch [34]	106–307 μm/laminar	69–800	Deionized water	The conventional theory for fully-developed flow was applicable within the range of the values of parameters they use
Quan et al. [35]	127–173 μm/laminar	240	Water	Heat transfer coefficient in MC increased with mass flux and quality and decreased with the hydraulic diameter
Lee et al. [36]	194–534 μm	300–3500	Deionized water	Heat transfer coefficient increased with the decrease of the channel size depending on the flow rate
Harirchian and Garimella [37]	Width 100–5850 μm with depth 400 μm/laminar	–	Fluorinert FC-77	A strong dependence of pressure drop on both channel size and mass flux was observed
Ergu et al. [38]	Width=3.70 mm, height=0.107 mm, length=35 mm/laminar	100–845	Distilled water	The classical laminar flow equations can be used for the calculation of the friction factor in MCs
Owhaib et al. [39]	0.862–1.7 mm/laminar	–	R134a	Heat transfer coefficient was higher for smaller diameter tubes. An increase in the system pressure improves the heat transfer performance
Chiu et al. [40]	W/H=1.67–14.29/laminar	50–1000	Water	Heat transfer enhancement was more significant on MCs with high aspect ratio
Shen et al. [41]	Width=300 μm, Height=800 μm/laminar	162–1257	Deinonized water	Nusselt numbers were significantly lower than the conventional theory predictions for two main factors, the cross-sectional aspect ratio and the surface roughness
Barber et al. [42]	727 μm/laminar to turbulent	–	Not given	Flow, pressure and temperature conditions leading to nucleate boiling, flow instabilities and transition regimes during flow boiling in a MC
Seng Lee and Garimella [43]	Width=102–997 μm, depth=400 μm	–	Deionized water	The saturated heat transfer coefficient becomes largely insensitive to heat flux
Celata et al. [44]	480 μm/laminar	–	FC-72	Heat transfer coefficient was rather independent of heat flux
Megahed [45]	248 μm/laminar	–	FC-72	The instability increased with decreasing the mass flux
Diaz and Schmidt [46]	Height=0.3 mm, width=12.7 mm/laminar	–	Water/ethanol	Heat transfer coefficient increased with increasing quality at low heat fluxes
Chen et al. [47]	100–250 μm/laminar	200–1700	Water	The condensation heat transfer was enhanced by a reduction in the channel scale
Betz and Attinger [48]	2 mm/laminar	160–1580	Water	The segmented flow increases the Nusselt number of laminar flow by more than 100%
Wojtan et al. [49]	0.5 and 0.8 mm/laminar	–	R-134a and R-245fa	A strong dependence of CHF on mass velocity, heated length and MC diameter
Asthana et al. [50]	100 μm/laminar	–	Water/oil	Increased heat removal increased the pressure drop, which is strongly affected by the fluid temperature
Wang and Cheng [51]	155 μm/laminar	–	Deionized water	The stable flow boiling occurred in a single MC depending on the vapor quality
Wu et al. [52]	90.6 μm/laminar	300–900	Water	Cross-sectional shape of the MC plays a significant role on the instability of condensation flow
Steinke and Kandlikar [53]	Width=200 μm, depth=250 μm and a length=10 mm	14–789	Water	The conventional Stokes and Poiseuille flow theories apply for single-phase liquid flow in MC flows
Wu et al. [54]	Width=300 μm, depth=800 μm/laminar	–	Water/methanol	The wall temperatures generally match the oscillation trends of the inlet pressure and the outlet temperature, but a time delay occurs due to the thermal inertia of the copper block
Zhang et al. [55]	Width=61 μm, height=272 μm, length=15 mm/laminar	–	Deionized water	The predictions from the flow oscillation model were agreed well with the experimental pressure-drop observations across a flow meter and a MCHS
Kohl et al. [56]	25–100 μm/laminar and turbulent	4.9–18,814	Water and air	The results suggest that friction factors for MCs can be accurately determined from data for standard large channel
Rosengarten et al. [57]	100 mm/laminar	0–70	Distilled water	Slip flow was an extremely important for micro and in particular nano heat exchanger designs as heat transfer rates may decrease more than 10% at high shear rates
Tang et al. [58]	52–300 μm/laminar	3–6300	Nitrogen and helium	Surface roughness in MCs affected on the friction factor
Huh et al. [59]	103.5 μm/laminar	19.2–38.3	Deionized water	As the supplied heat flux and vapor quality increased, the period of the unstable fluctuations lengthened and the amplitude also increased

Table 2 (*continued*)

Researchers	Diameter/flow nature	Reynolds number	Fluid/gas	Findings
Mokrani et al. [60]	1 and 100 μm/laminar and turbulent	100–5000	Water	Conventional laws and correlations were directly applicable to the MCs of heights between 500 μm and 50 μm
Bertsch et al. [61]	1.09 and 0.54 mm	–	R-134a and R-245fa	Heat transfer coefficient for R-245fa in comparison with R-134a in single-phase flow was higher
Ngo et al. [62]	1.09 mm/laminar	250–2500	CO_2	Pressure-drop factor of the MCHE with S-shaped fins was 4–5 times less than that of MCHE with zigzag fins
Wei and Joshi [63]	53–112 μm/laminar	–	Water	Careful design and control of the micro-fabrication process were crucial to the performance of the micro-scale devices
Fang et al. [64]	100–300 μm/laminar	–	Degassed water	Smaller channel was more favorable due to its high mean heat flux
Bogojevic et al. [65]	194 μm/laminar	82	Water	The onset of boiling caused metastable non-uniform flow distribution
Wang et al. [66]	186 μm/laminar	–	Deionized water	Pressure drop was higher and heat transfer coefficients was lower for boiling flow at high vapor quality in MCs than those predicted from correlation equations for boiling flow in MCs
Hernando et al. [67]	100–200 μm/laminar	10–5000	Deionized water	Plate conduction thermal resistance was a major restriction for micro-heat exchanger performance. The plate thickness and plate material were critical in the design of micro-heat exchangers
Yang and Lai [68]	15 mm/laminar	300–900	Al_2O_3/water	Heat transfer coefficient increased with the increases of Reynolds number and particle volume fraction
Wu et al. [69]	$L/D=50$–150/laminar	–	R134a, R123, R245fa, R236fa, nitrogen and water	This proposed method almost predicts 97% of the non-aqueous data and 94% of the water data within the $\pm 30\%$ error band
Shevade and Rahman [70]	0.06–0.2 cm/turbulent	1600–3000	Water	The pressure drop in the channel increased as the Reynolds number increases. Nusselt number increased as the channel dimensions increase
Mlcak et al. [72]	85.6 μm/laminar	50–400	Water	Friction coefficient linearly increased as the hydraulic entrance length increase
Chen et al. [73]	40–158 μm/laminar	30–500	Deionized water	Triangular MC heat sink has the highest thermal efficiency among the three heat sinks, the trapezoidal MC was inferior to triangular but superior to rectangular
Zhu and Liao [74]	–/laminar	–	Gas	For a rectangular and triangular microchannel, the average Nusselt numbers were smaller than those of a macrochannel with the same thermal boundary conditions and it decreases with increasing Knudsen number.
Ji et al. [75]	Length 1–100 μm/laminar	0.001–100	Gas	Average Poiseuille number increased not only as the roughness height increases but also as the spacing distance between the roughness elements was decreased
Sui et al. [76]	1.5×10^{-4} m	100–800	Water	The quantity and the location of the vortices may change along the flow direction, leading to chaotic advection, which can greatly enhance the convective fluid mixing, and thus the heat transfer performance of the wavy MCs was much better than that of straight MCs with the same cross section
Muhammad et al. [77]	Height=300 μm. Depth=100–250 μm	1000 to 3000	FC-72, helium and water	Compared to helium and FC-72, water provides better thermal performance with higher values of Nusselt number
Liu et al. [78]	100 μm/laminar	10–200	Water	Heat transfer enhancement due to viscosity-variation was pronounced, though the axial conduction introduced by thermal-conductivity-variation was insignificant unless for the cases with very low Reynolds numbers
Renksizbulut et al. [79]	Width/height=0–1/laminar	0.1–10	Gas	Slip-flow regime was associated with very large reductions in wall friction and heat transfer in the entrance region
Niazmand et al. [80]	Width/height=0.25–2/laminar	0.1–10	Gas	Major reductions in the friction and heat transfer coefficients were observed in the entrance region due to large amounts of velocity-slip and temperature-jump
Khadem et al. [81]	$L/H=20$ laminar	–	Gas	Roughness has more significant effect on higher Knudsen number flows with higher relative roughness.
Zade et al. [82]	10 μm/laminar	0.1	Gas	In the entrance region, Nusselt number was only affected by the change in the Knudsen number and was higher in variable-density slip-flow cases.
Shokouhmand and Bigham [83]	–	2	Gas	Nusselt number and $C_f.$ *Re* decreased with increaseing Knudsen number
Mohammed et al. [84,85]	339.15 μm/laminar	100–1000	Water	Temperature and the heat transfer coefficient of the zigzag MCHS was the least and greatest comparing to other channel shapes. The second best thermal performance was provided by curvy channels after the wavy channels
Kosar [86]	Height=200 μm Width=200 μm/Laminar	50–2000	Water	The Nusselt number was lower for low thermal conductivity and vice versa
Mohammed et al. [87,88]	–	100 to 800	Al_2O_3/water SiO_2/water Ag/ water TiO_2/water	Al_2O_3 nanofluid has the highest heat transfer coefficient

that the observed enhancement of the thermal conductivity of Al_2O_3/water nanofluids exists and is independent of the measurement technique.

Zhang et al. [95] reported measurements of the effective thermal conductivity and thermal diffusivity of Al_2O_3/water, ZrO_2/water, TiO_2/water, and CuO/water nanofluids for various volume fractions and temperature by using the transient short-hot-wire technique. The average diameters of Al_2O_3, ZrO_2, TiO_2, and CuO particles were 20 nm, 20 nm, 40 nm and 33 nm, respectively. The results demonstrated that the effective thermal diffusivity and thermal conductivity increase with an increase in the particle concentration and in the thermal conductivity of nanoparticles. However, the effective thermal conductivity did not show any anomalous enhancement.

Murshed at al. [96] presented investigation of enhancing the thermal conductivity of TiO_2–water based nanofluids. The nanofluids were prepared by dispersing TiO_2 nanoparticles in rod-shapes of $\phi = 10$ nm × 40 nm (diameter by length) and in spherical shapes of $\phi = 15$ nm in deionized water. The thermal conductivities of these nanofluids were measured by using the transient hot-wire apparatus with an integrated correlation model. The viscosity and pH value of the nanofluids were also characterized. The experimental results showed that the thermal conductivity increases with an increase of particle volume fraction and the nanofluids containing a small amount of nanoparticles have much higher thermal conductivities than normal base fluids. The particle size and shape also have influence of the thermal conductivity enhancement of nanofluids. The results of TiO_2 particles of ϕ10 nm × 40 nm and ϕ15 nm dimensions with maximum 5% volume fraction showed that the enhancement was nearly 33% and close to 30%, respectively over the base fluid.

Murshed et al. [97] conducted an experimental and theoretical analyzing on the effective thermal conductivity and viscosity of nanofluids. Two static mechanisms-based models were presented to predict the enhanced thermal conductivity of nanofluids having spherical and cylindrical nanoparticles. The transient hot-wire technique was utilized to measure the thermal conductivity of nanofluids at different temperatures ranging from 20 °C to 60 °C. The results of this investigation showed that the thermal conductivity and viscosity of nanofluids were found to be substantially higher than the values of the base fluids. Both the thermal conductivity and viscosity of nanofluids increase with increases the nanoparticle volume fraction. The results also presented that the thermal conductivity of nanofluids observed to be strongly dependent on temperature and increases linearly with the increases of temperature. The results of the proposed models which consider particle size, interfacial layer, and volume fraction showed reasonably good agreement with the experimental results and give better predictions for the effective thermal conductivity of nanofluids compared to existing classical models.

Oh et al. [98] presented experimental data of the thermal conductivity enhancement in Al_2O_3 nanofluids with DI water and ethylene glycol as base fluids by using the modified 3ω method. The results revealed that the thermal conductivity of the nanofluid continuously increase with time. The effect of gravitational on the nanoparticle aggregates is believed to be the reason behind this observation. The increscent of thermal conductivity due to sedimentation effect was also measured quantitatively. In comparison with the conventional thermal conductivity measurement methods, the proposed 3ω measurement technique offered several advantages and it can be used with only a small sample volume to show whether homogeneous mixing is achieved for the stationary nanofluid.

Petal et al. [99] presented comprehensive experimental investigation of thermal conductivity of nanofluids with variation in nanoparticle material, base liquid, particle size, particle volume fraction and suspension temperature. Transient hot wire (THW) equipment as well as temperature oscillation equipment were developed for the measurement of thermal conductivity of liquids. The results showed that, in general, thermal conductivity values of all the nanofluids are higher than that of the equivalent macro-particle suspensions. A very significant effect of particle size and suspension temperature was observed for the thermal conductivity of nanoparticle suspensions. The results also revealed to that the metallic nanofluids were found to give higher enhancements than that of oxide nanofluids. The investigation results also presented that the increasing in the temperature significantly increase the thermal conductivity of nanofluid. It was also found that the thermal conductivity of nanoparticle suspensions is relatively higher at lower volume fractions, thereby giving a non-linear dependence on the particle volume fraction. However, the enhancement in thermal conductivity of suspensions increases with the decrease in the base fluid conductivity. This is due to the fact that the relative contribution of particles in the total heat conduction increases with reduced contribution from the lower conductivity base fluids.

Xie et al. [100] investigated the thermal conductivity behavior of SiC dilute nanoparticle-fluid mixtures. The transient hot-wire method was utilized to measure the thermal conductivities of four series suspensions. The experimental results showed that the thermal conductivities of SiC suspensions, containing a small amount of solid particles, are significantly higher than those of the base liquids. For low volume fraction range, the thermal conductivity enhancing ratios increasing almost linearly with the increase of the volume fraction of solid particles. The results of different systems containing the same kind of particles showed that the thermal conductivity ratios were independent of the base fluids, but the absolute value of the thermal conductivity of the suspension is proportional to that of the base liquids.

Sharma et al. [101] presented nanofluids synthesized using silver nitrate (precursor), ethylene glycol (reducing agent), and polyacrylamide-*co*-acrylicacid (dispersion stabilizer) in order to enhance the thermal conductivity. The different concentrations of silver nanofluid (1000–10,000 ppm) were synthesized. The thermal conductivity as well as stability of these nanofluids were determined with a transient hot-wire apparatus. Typically, 10,000 ppm silver nanofluid exhibited rapid increase in the particle size with the passage of time. The results presented that the thermal conductivity of silver nanofluids increased with increases the amount of silver particles in nanofluid. The results showed that after 30 days of preparation, the thermal conductivity of 1000 ppm and 5000 ppm silver nanofluids slightly decreased from 10%, and 15% to 9%, and 14%, respectively. While, the thermal conductivity of 10,000 ppm nanofluid decreased after 30 days of preparation from 18% to 14%. It was observed also that the silver particles were aggregated in early stage of preparation (upto 15 days), which leads to increase in the size of silver particles. However, the stability of silver nanofluid was strongly affected by the characteristics of the suspended particle and base fluid such as the particle morphology, the chemical structure of the particles and base fluid.

Wong and Kurma [102] presented study of three transport properties, namely thermal conductivity, electrical conductivity and viscosity, for Alumina nanoparticles with a mean diameter of 36 nm dispersed in water. Experiments were performed both as a function of volumetric concentration (3–8%) and temperature (2–50 °C). The results illustrated that the thermal conductivity of alumina nanofluid increased with both increase in temperature and concentration. A maximum thermal conductivity of 0.7351 W/m K^{-1} was observed for an 8.47% volume concentration of alumina nanoparticles at 46.6 °C. The effective thermal conductivity at this concentration and temperature was 1.1501, which lead to an increase in thermal conductivity by 22% when compared to water at room temperature. In order to determine the kinematic viscosity of alumina nanofluid, a

standard kinematic viscometer with constant temperature bath was used. The results revealed to an increase of 35.5% in the kinematic viscosity for an 8.47% volumetric concentration of alumina nanoparticles in water. The maximum kinematic viscosity of alumina nanofluid was 2.901 42 mm^2/ s, obtained at 0 °C for an 8.47% volumetric concentration of alumina nanoparticles.

Turgut et al. [103] presented investigation of the thermal conductivity and viscosity of TiO_2 nanoparticles in deionized water for volume fraction from 0.2% to 3% of particles. The mean diameter of TiO_2 nanoparticles was 21 nm. While, the measurement of nanofluids thermal conductivity was done by using the 3ω method. The effective thermal conductivity of TiO_2 nanoparticles in deionized water was measured at temperatures of 13 °C, 23 °C, 40 °C, and 55 °C. The experimental results demonstrated that the thermal conductivity increases with an increase of particle volume fraction, and the enhancement was observed to be 7.4% over the base fluid for a nanofluid with 3% volume fraction of TiO_2 nanoparticles at 13 °C. The results also showed that there is no dependence related to temperature; the thermal conductivity increased by the same order of magnitude as the base fluid which is water. The effective viscosities of TiO_2–water nanofluids with concentrations from 0.2 vol% to 3.0 vol% were measured. The results revealed that for low volume concentration of nanoparticles for 0.2 vol%. fraction, the viscosity values follow quite well the viscosity values of pure water with a decrease in viscosity with increasing temperature. While, for higher additions of TiO_2 nanoparticles, the increase in the nanofluid viscosity was larger than the enhancement in the thermal conductivity.

Chandrasekar and Suresh [104] presented development of lower and upper limits for thermal conductivity of nanofluids. The upper limit is estimated by coupling heat transfer mechanisms like particle shape, nanolayer and Brownian motion. While the lower limit is based on Maxwell′s equation. Experimental data from a range of independent published sources is used for validation of the developed limits. The comparison with the published experimental data indicated that, the experimental data considered lie between the newly developed limits. Comparison also showed that the present limits are more rigorous in placing a narrow lower and upper limit. As most of the experimental data lies within the newly developed limits, it can be concluded that particle shape, nanolayer and Brownian motion are significant in enhancing the thermal conductivity of nanofluids.

Chen et al. [105] proposed a methodology for predicting the effective thermal conductivity of dilute suspensions of nanoparticles (nanofluids) based on rheology. The methodology utilizes the rheological data to infer microstructures of nanoparticles quantitatively, which is then included into the conventional Hamilton–Crosser equation to predict the effective thermal conductivity of nanofluids. The results showed that the conventional correlations failed to predict the thermal conductivity of nanofluids, while, by incorporating the microstructure parameters acquired from rheological measurements, the thermal conductivity can be predicted accurately. The results also presented the importance of the rheological characterization of nanofluids, which could provide structural information required for the prediction of the suspension thermal conductivity.

Hong et al. [106] proposed a mixture of nanoparticles and fluid, have enormous potential to improve the efficiency of heat transfer fluids. Fe nanofluids are prepared with ethylene glycol and Fe nanocrystalline powder synthesized by a chemical vapor condensation process. The results revealed to that the thermal conductivity of a Fe nanofluid is increased nonlinearly up to 18% as the volume fraction of particles is increased up to 0.55 vol%. In comparison with the Cu nanofluids dispersed with a little agglomeration, Fe nanofluids showed a more effective thermal transport property. Hence, the highly thermally conductive material is not always the best candidate for the suspension in improving thermal transport property of fluids.

Liu et al. [107] presented study of enhancement of the thermal conductivity of water in the presence of copper (Cu) using the chemical reduction method. Copper nanoparticles showed the characteristics of small particle sizes and uniform size distribution. The typical copper nanoparticles diameter were around 50–100 nm with square and spherical shapes. The volume fractions of Cu nanoparticle suspensions in water liquid were in the range from 0.05 vol% to 0.2 vol%. The results showed that without the addition of dispersant and surfactant, the thermal conductivity of the produced nanofluids reveals a time-dependent characteristic. The results revealed to that, Cu water nanofluids with low concentration of nanoparticles have noticeably higher thermal conductivities than the water base fluid without Cu. Furthermore, for Cu nanoparticles at a volume fraction of 0.1 vol%, thermal conductivity was enhanced by up to 23.8%.

Yu et al. [108] presented investigation of the thermal conductivity and viscosity of Ethylene glycol (EG) based nanofluids containing ZnO nanoparticles. The results showed that the thermal conductivity of ZnO–EG nanofluids is independent of setting time from 20 min to 360 min. However, the absolute thermal conductivity increases with the temperature range from 10 °C to 60 °C, while the enhanced ratios were almost constant. The thermal conductivity of ZnO–EG nanofluids was strongly depends on the particle concentration and it increases nonlinearly with the volume fraction of nanoparticles. The enhanced in thermal conductivity of ZnO–EG nanofluid was 26.5 vol% of 5.0 vol%. The rheological behaviors of the nanofluids showed that ZnO–EG nanofluids demonstrated Newtonian behaviors with low volume concentrations. While, the shear-shinning behavior observed for higher volume concentrations nanofluids and showing non-Newtonain behavior due to the effective volume fraction of aggregates is much higher than the actual solid volume fraction.

Xie et al. [109] presented a technical route for preparing homogeneous and stable nanofluids including diamond nanoparticles (DNPs) with the mixture of distilled water (DW) and ethylene glycol (EG) (DW–EG) as the base fluid. The results showed that the thermal conductivity enhancement of the DNP nanofluids increases with increase the volume fraction of DNPs. The thermal conductivity enhancement was more than 18.0% for a nanofluid at a DNP volume fraction of 0.02. The convective heat transfer coefficient increases with increasing volume fraction of DNPs, first, and then it decreases with a further increase in the volume fraction of DNPs.

Jimenez-Perez et al. [110] proposed a study of using thermal lens spectrometry (TLS) and photopyroelectric (PPE) techniques to obtain the thermal diffusivity and effusivity of three different solvents samples ethanol, water, and ethylene glycol (EG) with gold nanoparticles. The thermal effusivity of these samples was determined by the PPE technique in a front detection configuration. The experimental results revealed that the thermal diffusivity values of different solvents (water, ethanol, and ethylene glycol) were the presence of gold nanoparticles increases when compared with the pure solvents.

4.2.2. *Effects of thermal conductivity on heat transfer*

Many experimental studies have been done by different researchers for examining and improving the thermal conductivity enhancement of certain types of nanofluids using different methods and parameters. They calculated the thermal conductivity enhancement by using the ratio of the thermal conductivity of the nanofluid over its base fluid thermal conductivity. It is noticed that most of the studies did not concerned or noticed the particle size distribution. In addition, the effect of the particles agglomeration in the base fluid is also unknown. It is declared that the thermal conductivity of nanofluid is sensitive to certain parameters which are responsible for constant nanofluids such as particle size,

particle material, particle shape, base fluid material, temperature, additives and surfactants, and acidity. These parameters will be introduced in the following sections separately base on the previous experimental investigations and findings.

4.2.2.1. Effects of particle size on heat transfer. The size of particle plays a significant role in thermal conductivity and heat transfer enhancement in base fluids. As introduced before that different suspension sizes of millimeter and micrometer particles in host liquid have been used to increase the thermal conductivity, but the particles agglomerate quickly and settled out of the liquid. Nanoparticles are formed to decrease the size of the particles so that the time of sedimentation decreases to reach in some cases to more than few weeks or months.

Petal et al. [111] presented comprehensive experimental investigation of thermal conductivity of nanofluids with variation in nanoparticle material, base liquid, particle size, particle volume fraction and suspension temperature. Transient hot wire (THW) equipment as well as temperature oscillation equipment were developed for the measurement of thermal conductivity of liquids. The results showed that, in general, thermal conductivity values of all the nanofluids are higher than that of the equivalent macroparticle suspensions. A very significant effect of particle size and suspension temperature was observed for the thermal conductivity of nanoparticle suspensions. The results also revealed to that the metallic nanofluids were found to give higher enhancements than that of oxide nanofluids. The particle size was found to have a tremendous effect on the thermal conductivity of nanofluids with enhancement in the thermal conductivity increasing with the reduction in the particle size. The effect of particle size may be attributed mainly to two reasons which are the high specific surface area of the nanoparticles and Brownian motion.

Timofeeva et al. [112] investigated the effect of average particle sizes on basic macroscopic properties and heat transfer performance of water-based silicon carbide suspensions. The average particle sizes, calculated from the specific surface area of nanoparticles, were varied from 16 nm to 90 nm. The results revealed that the nanofluids of same material and volume concentration with larger particles provide higher thermal conductivity and lower viscosity increases than those with smaller particles due to the smaller solid/liquid interfacial area of larger particles.

Anoop et al. [113] presented an experimental investigation on the convective heat transfer characteristics in the developing region of tube flow with constant heat flux carried out with alumina–water nanofluids. In this study the effect of particle size on convective heat transfer in laminar developing region was evaluated. Two particle sizes were used, one with average particle size off 45 nm and the other with 150 nm. The results revealed that both nanofluids showed higher heat transfer characteristics than the base fluid. Nanofluids with of 45 nm particles showed higher heat transfer coefficient than that with 150 nm particles. The results also showed with increase in flow rate and particle concentration the average heat transfer coefficient value was increased.

Beck et al. [114] presented a new data for the thermal conductivity enhancement in seven nanofluids containing 8–282 nm diameter alumina nanoparticles in water or ethylene glycol. The results showed that the thermal conductivity enhancement in these nanofluids decreases as the particle size decreases below about 50 nm. This decrease in enhancement can be attributed to a decrease in the thermal conductivity of the nanoparticles themselves as the particle size becomes small enough to be affected by increased phonon scattering.

Chopkar et al. [115] presented experimental investigation of the impact of Al_2Cu and Ag_2Al nanoparticle size and volume fraction on the effective thermal conductivity of water and ethylene glycol based nanofluid prepared by a two-stage process. The thermal conductivity ratio of nanofluid, was measured by using an indigenously developed thermal comparator device. The results revealed that the thermal conductivity ratio, relative to that of base fluid, increases nonlinearly with the increase in volume fraction and the decrease in the size/diameter of nanoparticles. This increase was up to 100 pct with only 1.5 vol%/pct nanoparticles of 30- to 40-nm average diameter. Moreover, the analytical model denoted that the interfacial layer significantly influences the effective thermal conductivity ratio of nanofluid for the comparable amount of nanoparticles.

Ding and Wen [116] presented investigation of migration particle migration in pressure-driven laminar pipe flows of relatively dilute suspensions of nanoparticles (nanofluids). A theoretical model is formulated to predict particle concentration, and velocity field of nanofluids in the transverse plane of the pipe. The results showed that the particle concentration in the wall region can be much lower than that in the central core region. That indicates a highly nonuniform thermal conductivity profile across the transverse plane of the pipe, and thus has a significant implication to heat transfer intensification using nanofluids.

4.2.2.2. Effects of acidity (PH). Limited studies have been published on the effect of fluid acidity on the thermal conductivity enhancement of nanofluids, but the general trend is that acidity increases the thermal conductivity enhancement. Xian-Ju and Xian-Fang [117] investigated the viscosity and the thermal conductivity of Cu and Al_2O_3 nanoparticles dispersed in water under different pH values. The experimental results showed that the viscosity is closely related to the enhancement of thermal conductivity. Furthermore, there exists an optimal pH value can results in the highest thermal conductivity and the lowest viscosity of nanofluids.

Wang et al. [118] investigated the enhancement of heat transfer of Al_2O_3 and Cu nanoparticles dispersed in water as a base fluid under different pH values and different sodium dodecylbenzene sulfonate (SDBS) dispersant concentrations. The experimental results showed that the stability of nanofluids has a good corresponding relation with thermal conductivity and the better dispersion behavior, the higher thermal conductivity.

4.2.2.3. Effects of particles material. There are many types of materials have been utilized to produce nanofluids. It was found that metallic and allotrops of carbon nanoparticles (such as diamond) increase the thermal conductivity of a host fluid more than other types of nanoparticles having the same volume concentration. Nguyen et al. [119] investigated experimentally the behavior and heat transfer enhancement of a particular nanofluid, Al_2O_3 nanoparticle–water mixture, flowing inside a closed system that is destined for cooling of microprocessors or other electronic components. The heat transfer coefficient of a particular nanofluid with 6.8% particle volume concentration, was found to increase as much as 40% compared to that of the base fluid, and the results clearly revealed that the heat transfer coefficient was considerably increase with an increase of particle concentration. However, an increase of particle concentration produced a clear decrease of the heated component temperature.

4.2.2.4. Effects of temperature. The nature of the nanofluid thermal conductivity is sensitive to temperature. Many studies have been done for the effect of temperature on thermal conductivity. Minsta et al. [120] presented experimental determination of thermal conductivity values for three types of water-based nanofluids for various temperatures ranging between 20 °C and 40 °C. The considered nanofluids were composed of 29 nm CuO particles as well as 36 nm and 47 nm Al_2O_3 particles. For each nanofluid considered, three volume fractions of particles were investigated: 3%, 6% and 9%

between 20 °C and 40 °C. The thermal conductivity measurement technique utilized was based on the transient hot wire method. The results clearly demonstrated that the effective thermal conductivity of nanofluids increases with temperature. In the temperature range of 20 °C and 40 °C, the average an increase in thermal conductivity was approximately 16% for each type nanofluid.

Yu-Hua et al. [121] studied the temperature effects on the thermal conductivity of nanofluids. The mechanism of thermal conductivity of nanofluids was analyzed and calculated, including particle agglomeration, Brownian motion effects and viscosity, together influenced by temperature. The results showed that the higher temperature lead to decrease the of agglomeration of nanoparticles through the reduction of the particle surface area, and makes the Brownian motion more intensive due to the decreases of viscosity.

Nguyen et al. [122] investigated experimentally the influence of both the temperature and the particle size on the dynamic viscosities of two particular water-based nanofluids, namely water–Al_2O_3 and water–CuO mixtures. The results revealed that for particle volume fractions less than 4%, viscosities of 36 nm and 47 nm particle-size alumina–water nanofluids are approximately identical. However, the viscosities of 47 nm particle-size and higher particle fractions were clearly higher than those of 36 nm size. The results showed that for all the nanofluids tested, their viscosities were strongly dependent on both particle volume fraction and temperature.

Hosseini and Ahmadi [123] presented study of the structural changes of nanofluid as increasing the temperature which is very important for engineering designs. The results revealed that the nanoparticles increase the temperature of nanofluid when it is prepared in ultrasonic mixer than other impure fluids. The main reason of increasing the temperature of operating suspension than solution mainly due to sending out the waves from ultrasonic prop, collapsing between particles, and touching fraction between particles.

4.2.2.5. Effects of base fluids material. Many host liquids have been used to produce nanofluids such as aqueous and organic liquids (ethylene glycol, and oils) to enhance thermal conductivity. Xie et al. [124] analyzed the effect of the base fluid on the thermal conductivity of nanofluids. Nanofluids with Al_2O_3 nanoparticles were prepared by using different base fluids; deionized water, ethylene glycol, glycerol, and pump oil. In addition, glycerol–water and ethylene glycol–water mixtures with different volume fractions were also used as base fluids and the variation of the thermal conductivity ratio with thermal conductivity of the base fluid mixture was examined. The results revealed that, the thermal conductivity ratio decreased with increasing thermal conductivity of the base fluid.

Li and Peterson [125] presented investigation of analyzing, modeling for the mixing effect of the base fluid in the immediate vicinity of the nanoparticles caused by the Brownian. The results indicated that the micro convection/mixing induced by the Brownian motion of the nanoparticles could significantly affect the macro heat transfer capability of the nanofluids.

Xie et al. [126] investigated the thermal conductivities of various suspensions containing Al_2O_3 nanoparticles with specific surface areas prepared in a range of 5–124 m^2/g. The results illustrated that the nanoparticle suspensions, containing a small amount of Al_2O_3, have substantially higher thermal conductivity than the base fluid. The enhancement of thermal conductivity increases with the volume fraction of Al_2O_3. Whereas, the enhanced thermal conductivity increases with an increase in the difference between the pH value of aqueous suspension and the isoelectric point of Al_2O_3 particle.

Maïga et al. [127] presented a study of forced convection flow of water–γAl_2O_3 and ethylene glycol–γAl_2O_3 nanofluids inside a uniformly heated tube that is subjected to a constant and uniform heat flux at the wall. The results showed that the inclusion of nanoparticles has increased considerably the heat transfer at the tube wall for both the laminar and turbulent regimes. However, with increasing the particle concentration the improvement of heat transfer becomes more pronounced. The results also demonstrated that the ethylene glycol–γAl_2O_3 mixture gives a far better heat transfer enhancement than the water–γAl_2O_3 mixture.

4.2.2.6. Specific heat. Shin et al. [128] presented investigation of using Silica nanoparticles (1% by weight) dispersed in a eutectic of lithium carbonate and potassium carbonate (62:38 ratio) to obtain enhancement of specified heat. A differential scanning calorimeter instrument was used to measure the specific heat of the neat molten salt eutectic and after addition of nanoparticles. The results showed that the specific heat of the nanofluid was enhanced by 19–24%. The microscopy results revealed that the nanofluids were fairly stable with the minimal agglomeration of the nanoparticles after repeated thermocycling.

4.3. Viscosity

Lee et al. [129] experimentally investigated the effective viscosities and thermal conductivities of water-based nanofluids containing very low concentrations of Al_2O_3 nanoparticles. The results showed that the alumina nanoparticles can be best dispersed and stabilized in DI water with little evidence of aggregation at 5 or more hours of ultrasonic vibration. The results of viscosity measurements showed that the viscosity of the Al_2O_3–water nanofluids decreases significantly with increasing temperature. The results also showed that in contrast to viscosity, the measured thermal conductivities of the dilute Al_2O_3–water nanofluids increase closely linearly with the concentration.

Kole and Dey et al. [130] presented investigation of thermal conductivity and viscosity of the nanofluids as a function of volume fraction of Al_2O_3 nanoparticles as well as temperature between 10 °C and 80 °C. Many of the suspensions containing Al_2O_3 nanoparticles (<50 nm) in a car engine coolant prepared by using oleic acid as the surfactant and are tested to be stable for more than 80 days. The results indicated that the volume fraction of 0.035 of Al_2O_3 nanoparticles in the engine coolant enhanced the thermal conductivity of the fluid. This enhancement in thermal conductivity of the nanofluid varied linearly with the volume fraction of the nanoparticles and reaches a highest of 11.25% at 80 °C for the nanofluid of 0.035 vol% of Al_2O_3 nanoparticles. The results revealed that the viscosity of the nanofluids increases with alumina volume fraction and decreases with the rise in temperature.

Masoumi et al. [131] introduced a new equation for calculating the nanofluid viscosity by considering the Brownian motion of nanoparticles. The proposed equation calculates the nanofluid viscosity as a function of the temperature, the nanoparticle volume fraction, the mean nanoparticle diameter, the nanoparticle density and the base fluid physical properties. The results showed with the comparison with many experimental works that the presented model could well predict the effective viscosity of different nanofluids (CuO–H_2O, Al_2O_3–H_2O, CuO–EG, TiO_2–EG and CuO–EG–H_2O) at different nanoparticle mean diameters, volume fractions and also temperature variations.

Abu-Nada and Chamkha [132] presented study of natural convection heat transfer characteristics in a differentially heated enclosure filled with a CuO–EG–Water nanofluid for different published variable thermal conductivity and variable viscosity models. The results showed that for high Rayleigh numbers, the average Nusselt number decreased as the nanoparticles volume fraction increased.

Table 3
The thermal conductivity and viscosity correlations for nanofluids.

Researchers	Equation	Remarks
Koo and Kleinstreuer [140]	$K_{eff}=\frac{kp+2kBF+2(kp-kBF)\Phi}{kp+2kBF-(kp-kBF)\Phi}kBF+5\times10^4\beta\Phi\rho_p\,Cp\sqrt{\frac{K_BT}{\rho_pD}}f(T,\phi)$ $\beta=\frac{0.013}{(100\phi)^{-0.8229}}$ for $\phi<1\%$ $\beta=\frac{0.0011}{(100\phi)^{-0.7272}}$ for $\phi>1\%$ $f(T,\alpha_d)=(-6.04\alpha_d+0.4705)T+(1722.3\alpha_d-134.63)$	$1\%<\alpha_d<4\%$ $300<T<325$ K
Chon [178]	$\frac{knf}{kbf}=1+64.7\phi^{0.7640}\left(\frac{d_f}{d_p}\right)^{0.3690}\left(\frac{k_f}{k_p}\right)^{0.7476}Pr^{0.9955}\,Re^{1.2321}$	
Vajjha and Das [179]	$K_{eff}=\frac{kp+2kBF+2(kp-kBF)\Phi}{kp+2kBF-(kp-kBF)\Phi}kBF+5\times10^4\beta\Phi\rho_p\,Cp\sqrt{\frac{K_BT}{\rho_pD}}f(T,\phi)$ $f(T,\alpha_d)=(2.8217\times10^{-2}\phi+3.917\times10^{-3})\frac{(T+273.15)}{(T_0+273.15)}+(-3.0669\times10^{-2}\phi-3.91123\times10^{-3})$ $\beta=8.4407(100\phi)^{-1.07304}$	
Corcione [180]	$\frac{K_{eff}}{K_f}=1+4.4\,Re^{0.4}Pr^{0.66}(\frac{T}{T_{fr}})^{10}\,(\frac{Ks}{K_f})^{0.03}\,\phi^{0.66}$	$Re=(\frac{2\rho_f\,K_bT}{\pi\mu_f^2d_p})$
Seyf-Feizbakhshi [181]	$\bar{k}_{nf}=\frac{1}{v}\int k_{nf}\,dv$	Where V is the volume of computational domain
Nguyen et al. [122]	$\mu_{nf}=\mu_{bf}\times0.904\,e^{0.1482\phi}$ $\mu_{nf}=\mu_{bf}(1+0.025\phi+0.015\phi^2)$	
Masoumi et al. [131]	$\mu_{nf}=\mu_{bf}+\frac{\rho PV_Bd_p^2}{72C\delta}$ $V_B=\frac{1}{d_p}\sqrt{\frac{18K_bT}{\pi\rho PdP}}K_b$ $C=\mu_{bf}^{-1}[(C_1d_p+C_2)\phi+(C_3d_p+C_4)]$	C_1 C_2 C_3 and C_4 are constants
Abu-Nada [173]	$\mu_{Al_2O_3}=-0.155-\frac{19.582}{T}+0.794\phi+\frac{2094.47}{T^2}-0.192\phi^2-8.11\frac{\phi}{T}-\frac{27463.863}{T^3}+0.127\phi^3+1.6044\frac{\phi^2}{T}+2.1754\frac{\phi}{T^2}$	
Tseng and Lin [175]	$\mu_{nf}=\mu_{bf}\times13.47\,e^{35.98\phi}$	
Chen et al. [176]	$\mu_{nf}=\mu_{bf}\left(1-\left(\frac{\phi_a}{\phi_m}\right)\right)^{-2.5\phi_m}$ $\phi_a=\phi\left(\frac{a_a}{a}\right)^{3-D}$	
Chen et al. [177]	$\mu_{nf}=\mu_{bf}(1+10.6\phi+(10.6\phi)^2)$	
Koo and Klennstreuer [182]	$\mu_{eff}=\mu_{static}+\mu_{Brownian}\mu_{static}=\mu_{f/(1-\phi)^{2.5}}$ $\mu_{Brownian}=5x10^4\beta\phi\rho_f\sqrt{\frac{kT}{2\rho_{np}R_{np}}}f(T,\phi)$ $\beta=0.013(100\phi)^{-0.8229}$ for $\phi<1\%$ $\beta=0.0011(100\phi)^{-0.7272}$ for $\phi>1\%$ $f\,(T,\alpha_d)=(-6.04\alpha_d+0.4705)T+(1722.3\alpha_d-134.63)$	
Vajjha [183]	$\frac{\mu_{nf}}{\mu_{bf}}=A_1e^{(A_2\,\phi)}$	A_1 and A_2 depends on dp and ϕ
Mahbubul [184]	$\mu_{nf}=\mu_{bf}\times\exp\left[m+\alpha\left(\frac{T}{T_o}\right)+\beta(\varnothing_h)+\gamma\left(\frac{d}{1+r}\right)\right]$	
Tseng and Chen [185]	$\mu_{nf}=\mu_{bf}\times0.4513\,e^{0.6965\phi}$	
Cheng and Law [186]	$\mu_{nf}=\mu_{bf}(1+2.5\phi_e+(2.5\phi_e)^2+(2.5\phi_e)^3+(2.5\phi_e)^4+\cdots)$ $\phi_e=\phi\left(1+\frac{h}{r}\right)^3$	
Kulkarni et al. [187]	$\ln(\mu_{nf})=A\left(\frac{1}{T}\right)-B$	Here A and B are functions of volume percentage ϕ
Namburu et al. [188]	$Log\,(\mu_{nf})=Ae^{-BT}$ $A=1.8375(\phi)^2-29.643(\phi)+165.56$ with $R^2=0.9873$ $B=4\times10^{-6}(\phi)^2-0.001(\phi)+0.0186$ with $R^2=0.988$	A, B are functions of particle volume percentage ϕ
Masoud Hosseini et al. [189]	$\mu_{nf}=\mu_{bf}\times\exp\left[m+\alpha\left(\frac{T}{T_0}\right)+\beta(\phi_h)+\gamma\left(\frac{d}{1-r}\right)\right]$	

Nguyen et al. [133] presented experimental investigation of the effect due to temperature and particle volume concentration on the dynamic viscosity for the water–Al_2O_3 nanofluid. The viscosity data were collected using a 'piston-type' commercial viscometer for temperatures ranging from room condition up to 75 °C. Two different particle sizes were considered 36 nm and 47 nm and

particle volume fraction varying from 1 to nearly 13%. The results illustrated that the nanofluid dynamic viscosity increases significantly with particle volume fraction but it obviously decreases with a temperature increase. The results also showed that the Einstein′s formula and some other ones that were originated from the classical theory of linear fluid appeared to be limited to nanofluids with low particle volume fractions.

Jia et al. [134] presented investigation of the viscosity of silicon dioxide nanofluid at different particle sizes and pH values considering nanoparticle aggregation. The experimental and simulation results revealed that the nanoparticle diameter is of crucial importance for the viscosity of a nanofluid. The results showed that as the particle size is smaller, the viscosity is much larger and is much more dependent on the nanofluid volume fraction. The researcher′s correlations for thermal conductivity and viscosity of nanofluids are summarized in Table 3.

5. Numerical studies on nanofluids

Feng et al. [135] proposed a new model for the effective thermal conductivities by taking into account the nanolayer and nanoparticles aggregation. This model is expressed as a function of the thickness of the nanoparticle size, the nanolayer, the nanoparticle volume fraction, the thermal conductivities of suspended nanoparticles and base fluid. The model predictions of effective thermal conductivity showed a good agreement with the available experimental data.

Tillman and Hill [136] presented a survey of some of the attempts to model the enhanced thermal conductivity of such nanofluids, and address issues such as the nanoparticles themselves, cluster structure, the surrounding layer, the fluid environment, and different heat transport processes at the micro and nano-scales. The reported models showed that the effective thermal conductivity of nanofluids is a function of the thermal conductivities of base fluid and nanoparticles, nanoparticle size and shape, aggregation, particle clustering and fluid temperature. The essential limitations of conventional heat conduction models for solid/liquid suspensions, which were rooted in macroscopic transport laws, such as the Fourier law of heat conduction diffusion have been recognized. However, the ballistic/diffusive conduction has only briefly been introduced in solid/liquid system. The core–shell–medium, multi-component models reflect the nanofluid structure and incorporate the correct thermal conductivity of nanoparticles which presented to be less than that of bulk material.

Wang et al. [137] presented a method for modeling the effective thermal conductivity of nanofluid based on the effective medium approximation and the fractal theory for the description of nanoparticle cluster and its radial distribution. The surface adsorption and the size effect of nanoparticles were taken into considerations. The results revealed to that the proposed fractal model predicts well the trend for variation of the effective thermal conductivity with dilute suspension of nanoparticles, and fits successfully with the experimental data for 50 nm CuO particles suspension in deionized water when the volume concentration $<0.5\%$. However, the calculated result also showed that the predictive calculation of effective thermal conductivity is complicated. The effective thermal conductivity of nanoparticle suspension can be expressed as:

$$\frac{k_{\text{eff}}}{k_f}=\frac{(1-\varnothing)+3\varnothing\int_0^{\infty}(k_{cl}(r)n(r)/k_{cl}(r)+2k_f)dr}{(1-\varnothing)+3\varnothing\int_0^{\infty}(k_{cl}n(r)/k_{cl}(r)+2k_f)dr} \tag{1}$$

where k_{cl} is the effective thermal conductivity of clusters, $n(r)$ is the radius distribution function.

Xue and Xu [138] derived an expression for the effective thermal conductivity of nanofluids with interfacial shells. The expression is not only depended on the thermal conductivity of the liquid and solid and their relative volume fraction, but also depended on the interfacial properties and particle size. The theoretical results of the proposed model on the effective thermal conductivity of CuO/water and CuO/ethylene glycol nanofluids were in good agreement with the experimental data.

$$9\left(1-\frac{v}{\alpha}\right)\frac{k_e-k_m}{2k_e+k_m}+\frac{v}{\alpha}\frac{(k_e-k_2)(2k_2+k_1)-\alpha(k_1-k_2)(2k_2+k_e)}{(2k_e+k_2)(2k_2+k_1)+2\alpha(k_1-k_2)(k_2-k_e)}=0 \tag{2}$$

where k_e the effective thermal conductivity; v/α are the volume fraction of the complex nanoparticles; k_m and k_2 are the thermal conductivity of the base fluid and particle, respectively.

Leong et al. [139] proposed a model for predicting the effective thermal conductivity of nanofluids by considering the effect of the interfacial layer at the solid particle/liquid interface. It has been documented that the interfacial layer at the solid (particle)/liquid interface and particle size is one of the major mechanisms for enhancing the thermal conductivity of nanofluids. The proposed model takes into account some additional effects including thickness, volume fraction, particle size and thermal conductivity of the interfacial layer. The results of this model showed good predictions for the effective thermal conductivity of different types of nanofluids. The proposed model is found to be better than the existing models due to the predicted effective thermal conductivity of different types of nanofluids were closer to the experimental results.

$$k_{\text{eff}}=\frac{(k_p-k_{1r})\varnothing_1k_{1r}[2\beta_1^3-\beta^3+1]+(k_p+2k_{1r})\beta_1^3[\varnothing_1\beta^3(k_{1r}-k_f)+k_f]}{\beta_1^3(k_p+2k_{1r})-(k_p-k_{1r})\varnothing_1[\beta_1^3+\beta^3-1]} \tag{3}$$

where k_{1r} and k_f is interfacial layer at the particle/liquid interface; $\beta_1=\beta=1$.

Koo and Kleinstreuer [140] developed a new thermal conductivity model for nanofluids, which takes the effects of particle volume fraction and temperature dependence, particle size, as well as properties of base liquid and particle phase into consideration by considering surrounding liquid traveling with randomly moving nanoparticles. The nanoparticles in quiescent suspension move randomly and thereby carry relatively large volumes of surrounding liquid with them. This micro-scale interaction may occur between cold and hot regions, resulting in a lower local temperature gradient for a given heat flux compared with the pure liquid case. Therefore, the effective thermal conductivity, k_{eff}, as a result of Brownian motion, increases to result in a lower temperature gradient for a given heat flux.

$$k_{\text{Brownian}}=5\times10^4\beta\alpha_d\rho_lc_l\sqrt{\frac{kT}{\rho_dD}}f(T,\alpha_d) \tag{4}$$

$$f(T,\alpha_d)=(-6.04\alpha_d+0.4705)T+(1722.3\alpha_d-134.63) \tag{5}$$

Yu and Choi [141] developed a new model for the prediction of the thermal conductivities of three-phase suspensions of ellipsoidal particle-in-liquid suspensions by extending the Hamilton–Crosser model to include the particle–liquid interfacial layer. The solid/liquid interface is described as a confocal ellipsoid with a solid particle. The model was utilized to predict the thermal conductivities of nanotube-in-oil suspensions, in which both the nanotube-to-liquid thermal conductivity ratio and nanotube eccentricity are extreme values. The results of developed model were found to be in good agreement with the experimental data. However, this new model is not able to predict the nonlinear behavior of the nanofluid thermal conductivity.

$$\frac{k_e-k_1}{k_e+(n-1)k_1}=\frac{f_e}{3}\sum_{j=a,b,c}\frac{k_{pj}-k_1}{k_{pj}+(n-1)k_1} \tag{6}$$

where k_e effective thermal conductivity; k_1 is thermal conductivity of liquid medium; n is the empirical shape factor; f_e, equivalent volume concentration.

Moghadassi et al. [142] presented a novel model for the prediction of the effective thermal conductivity of nanofluids based on dimensionless groups. The model expresses the thermal conductivity of a nanofluid as a function of the thermal conductivity of the solid and liquid, their particle size, volume fractions and interfacial shell properties. The results of this model revealed that the thermal conductivity changes nonlinearly with nanoparticle loading as shown in this equation:

$$\frac{k_{\mathrm{eff}}}{k_m} = 1 + m\frac{(V_p)^{\alpha}}{(d_p)^{\beta}} \tag{7}$$

where m is a factor that depends on the properties of the solid particle and interfacial shell, while α and β are empirical constants.

Nan et al. [143] proposed a quite simple formula of thermal conductivity enhancement in carbon nanotube composites based on a conventional model. The theoretical results of this simple formula predicted much higher thermal conductivity enhancement even in the dilute case of the carbon nanotubes, due to ultrahigh thermal conductivity and aspect ratio of the carbon nanotubes. The large inconsistency between the predictions and current experiments could be attributed to interfacial thermal resistance between the matrix and nanotubes, and aggregation and twist of the nanotubes in the composites. The results also concluded that the reasonable conventional models were still valid for the carbon nanotube based composites.

Petal et al. [144] presented a simple theoretical model for predicting the thermal conductivity of carbon nanotube (CNT) nanofluids. The effects due to the high thermal conductivity of CNTs and the percolation of heat through it were considered to be the most important reasons for their anomalously high thermal conductivity enhancement. The new approach was taken for the modeling, the novelty of which lies in the prediction of the thermal behavior of water based as well as oil based CNT nanofluids, which are quite different from each other in thermal characteristics. The results of this model successfully match the experimental data, varying over two orders of magnitude in their thermal conductivity enhancement values. The effective thermal conductivity equation is shown as follow:

$$k_{\mathrm{eff}} = k_1\left[1 + \frac{k_s \varepsilon r_1}{k_1(1-\varepsilon) r_s}\right] \tag{8}$$

k_1 is thermal conductivity of liquid medium; k_s thermal conductivity of particle; ε, particle volume fraction; r, is the particle radius.

Xue [145] presented a novel model of the effective thermal conductivity for nanofluids by considering the interface effect between the solid particles and the base fluid in nanofluids. The formula of calculating the effective thermal conductivity of nanofluids given based on Maxwell theory and average polarization. The theoretical results revealed that the effective thermal conductivity of nanotube/oil nanofluid and Al_2O_3/water nanofluid were in good agreement with the experimental data.

$$9\left(1-\frac{v}{\lambda}\right)\frac{k_e-k_m}{2k_e+k_m} + \frac{v}{\lambda}\left[\frac{k_e-k_{c,x}}{K_e+B_2(k_{c,x}-k_e)} + 4\frac{k_e-k_{c,y}}{2K_e+(1-B_{2,x})(k_{c,y}-k_e)}\right] = 0 \tag{9}$$

where $k_{c,x}$ and $k_{c,y}$ are the thermal conductivity components of the complex elliptical particle along the x and y axes, respectively. v and v/λ are the volume fractions of nanoparticles and complex nanoparticles, respectively.

Xu and Yu [146] reported a new model for predicting the thermal conductivity of nanofluids by taking into account the fractal distribution of nanoparticle sizes and heat convection between nanoparticles and liquids due to the Brownian motion of nanoparticles in fluids. The proposed model is expressed as a function of the average size of nanoparticles, concentration of nanoparticles, fractal dimension, temperature and properties of fluids. The results of this model showed that the reasonable dependences of the thermal conductivity on the temperature of nanofluids, nanoparticle size and concentration. The predictions of this model were in good agreement with the available experimental data. The total effective thermal conductivity of nanofluids is written as:

$$\frac{k_{nf}}{k_f} = k_s^{+} + k_c^{+} = \frac{k_p+2k_f-2\varnothing(k_f-k_p)}{k_p+2k_f+2\varnothing(k_f-k_p)} + c\frac{Nu \times d_f(2-D_f)D_f[(\lambda_{\max}/\lambda_{\min})^{1-D_f}-1]^2}{pr\,(1-D_f)^2\,(\lambda_{\max}/\lambda_{\min})^{2-D_f}-1}\frac{1}{\lambda} \tag{10}$$

$$D_f = d - \frac{\ln \varnothing}{\ln(\lambda_{\max}/\lambda_{\min})} \tag{11}$$

Mirmasoumi and Behzadmehr [147] presented numerical study of fully developed mixed convection of a nanofluid (water/Al_2O_3). Two-phase mixture model was utilized to analyze the effects of nanoparticles mean diameter on the flow parameters. The results showed that the convection heat transfer coefficient significantly increases with decreasing the nanoparticles means diameter. However it does not significantly change the skin friction coefficient. The thermal conductivity correlation that used in this study as follow [178].

Behzadmehr et al. [148] presented numerical study of turbulent forced convection heat transfer in a circular tube with a nanofluid consisting of water and 1 vol% Cu. Two phase mixture model has been implemented to study such a flow field. The results showed that the mixture model is more accurate than the single phase model. However, the accuracy of mixture model it seems could improve by using suitable effective physical properties for nanofluid instead of volume weighted average of particle and fluid properties. The results demonstrated that, adding 1% nanoparticles (Cu) increases the Nusselt number more than 15% while it does not have any significant effect on the skin friction.

Ben-Abdullah [149] presented numerical simulation using the Landauer–Buttiker theory to calculate the thermal conductance associated to plasmons modes in one dimensional array of nanoparticles closely spaced in a host fluid. The results showed that the contribution of near-field interactions to the transport of heat in weakly concentrated nanofluids when the average separation distance between particles is small in front of plasmons wavelengths.

6. Theoretical studies on nanofluids

Perez-Madrid et al. [150] analyzed heat transfer between two nanoparticles separated by a distance lying in the near-field domain in which energy interchange is due to the Coulomb interactions. The thermal conductance was computed by assuming that the particles have charge distributions characterized by fluctuating multipole moments in equilibrium with heat baths at two different temperatures. This quantity follows from the fluctuation-dissipation theorem for the fluctuations of the multipolar moments. The results revealed that the analysis of the heat interchanged between two NPs separated by a few submicrons agrees with the explainations of the rapid growth of the conductance even when the NPs are in contact.

Putnam et al. [151] described an optical beam deflection technique for measurements of the thermal diffusivity of fluid mixtures and suspensions of nanoparticles with a precision of better than 1%. The proposed approach was tested by using the thermal conductivity of ethanol–water mixtures. The results revealed that there was no significant enhancement in the thermal conductivity of fluids

that are loaded by small volume fractions of nanoparticles and the largest increase in thermal conductivity observed is 1.3% $\pm$0.8% for 4 nm diameter Au particles suspended in ethanol.

Eapen et al. [152] presented an investigation of the conduction in nanofluids. The classical Maxwell theory has two limiting bounds that correspond to two geometrical nanoparticle configurations in the colloidal state. For the first bound, nanoparticles form the dispersed phase and the fluid medium acts as the continuous phase. Whereas, for the second the roles are reversed with the nanoparticles and the fluid medium constituting the continuous and dispersed phases, respectively. The results showed that almost all the reported thermal conductivity data are enveloped by the upper and lower Maxwell bounds. Moreover, for a homogeneous nanofluid system, these bounds organize the limits for thermal conductivity enhancements. The thermal conductivity for the upper bound is maximally biased toward the thermal conductivity of the nanoparticles and vice versa for the lower bound.

Moghaddami et al. [153] presented analytically the effects of adding nanoparticles on the entropy generation of water–Al_2O_3 and ethylene glycol$-Al_2O_3$ nanofluid flows through a circular pipe under uniform wall heat flux thermal boundary condition in both laminar and turbulent regimes. The results obtained for water–Al_2O_3 nanofluid illustrated that adding 1% to the nanoparticle volume concentration for laminar flows decreases the entropy generation about 3.6%. The entropy generation at the $Re=853$ minimized for each specified nanoparticles volume concentration. The results showed also, at the $Re=853$ and $\phi=5\%$, maximum reduction in the entropy generation occurs.

7. Single phase and two phase models

Liu et al. [154] presented an experimental investigation of single-phase forced convection of Al_2O_3–water nanofluid in a circular minichannel with a 1.09 mm inner diameter. The Reynolds number was varied from 600 to 4500, covering the laminar, transition, and early fully developed turbulent regions. The results revealed that in the laminar region, the nanofluids exhibit pronounced entrance region behaviors possibly due to the flattening of the velocity profile caused by the flow-induced particle migration. Furthermore, the convective heat transfer of nanofluids is enhanced in the laminar flow with the penalty of increased pressure drop. The increasing in both pressure drop and heat transfer were proportional to the nanoparticle volume concentration. The results revealed that the nanofluids should be used in either the laminar flow or the fully developed turbulent flow with sufficiently high Reynolds number in order to yield enhanced heat transfer performance for engineering applications.

Kumar et al. [155] presented numerical simulations for analysis of flow and thermal field in a thermally driven cavity using nanofluid. The controlling parameters considered for this investigation were Grashof number ($10^3 < Gr < 10^5$), solid volume fraction ($0 < \phi < 0.2$) and empirical shape factor ($0.5 < n < 6$). The results showed that the dispersed thermal conductivity is more in the region near the walls where the magnitude of velocity is more compared to the center of the domain. The results also revealed that maximum value of the dispersed thermal conductivity increases when the hydraulic diameter of the particles is increased.

8. Mechanism of heat conduction

Keblinski et al. [156] presented a critical analysis of the experimental data in terms of the potential mechanisms. The considerations of this investigation strongly suggest that the apparent disagreement between the experiment and the effective medium theory is simply an artifact of focusing on a particular effective medium theory, namely, Maxwell's theory of well-dispersed particles. The results illustrated that, by accounting for linear particle aggregation, the well established effective medium theories for composite materials are capable of explaining the vast majority of the reported data without resorting to novel mechanisms such as Brownian motion induced nanoconvection, liquid layering at the interface, or near-field radiation. The results also showed that the effective medium theories are competent of predicting thermal conductivity enhancements well beyond the Maxwell prediction. The results revealed to that the significant aggregation is required to obtain substantial increases in thermal transport has an important consequence on the potential application of such fluids in flow based cooling.

Keblinski [157] presented a study of potential mechanisms that were put forward in order to understand nanofluid thermal conductivity and demonstrate that particle aggregation is currently the only physically reasonable mechanism that can explain the majority of the experimental data. The results revealed that significant aggregation is required to obtain substantial increases in thermal transport has an important consequence for the potential application of such fluids in flow-based cooling, which is the most important benefit from the technological point of view.

8.1. Brownian motion

Brownian motion is one of the parameters that affect the flow and heat transfer of nanofluids. It is basically the random dynamic mode of particles in a liquid where the particles collide between each other. It was determined that the thermal conductivity increases with an increase in temperature, but also it was shown that nanofluids compose of smaller particles experienced greater enhancement than with larger particles. Since temperature represents the overall kinetic energy of the particles, an increase in temperature will cause increase in the particles motion. It is easier for smaller particles to move; therefore, smaller particles will display a higher level of Brownian motion than larger particles. Some researcher conducted studies in this motion, Xuan et al. [158] applied the theory of Brownian motion and the diffusion-limited aggregation model to simulate random motion and the aggregation process of the nanoparticles. By considering physical properties of both nanoparticles and the base liquid, as well as the structure of the nanoparticles, aggregates, a theoretical model has been developed to predict the thermal conductivity of nanofluids. The results obtained from this model were in satisfactory agreement with the experimental results especially when the effect of nanoparticle aggregation is taken into account. A theoretical model is developed to predict the thermal conductivity of nanofluids. Comparison between the theoretical and experimental results shows the validity and accuracy of the theoretical model. The results revealed to that, the thermal conductivity of a nanofluid increases when the fluid temperature increase.

Evans et al. [159] presented investigation of using simple kinetic theory based analysis of heat flow in fluid suspensions of solid nanoparticles (nanofluids) to demonstrate that the hydrodynamics effects associated with Brownian motion have a minor effect on the thermal conductivity of the nanofluid. The results of kinetic theory argument and the results of molecular dynamics simulations, revealed to that the thermal conductivity of a nanofluid with well dispersed nanoparticles is well described by the effective medium theory and did not show any significant enhancements due to effects associated with Brownian motion of nanoparticles.

Nie et al. [160] considered several mechanisms that might account for the high enhancement of thermal conductivity observed by many groups and presented the exact result of enhancement of

thermal conductivity due to the Brownian motion and estimated it is order of magnitude. The results revealed that the possibility of convection caused by Brownian particles was found to be unlikely. Analyzing the possibility of the micro convection in the nanofluid concluded that this phenomenon cannot happen because of the quick decay of the hydrodynamic field around the Brownian nanoparticles. The phonon mean free path and phonon transport speed in nanofluid due to the existence of suspending nanoparticles also discussed. The authors found that only a thin layer of one nanometer may form around the nanoparticle and most of the base fluid molecules will remain unperturbed; hence there is no improvement on the structure of the fluid phase. The exploring the compressibility of the nanofluid with single spherical nanoparticle or aggregates of nanoparticles suspended, revealed to negligible changes in compressibility, which indicates the speed of phonon transport found to be negligible due to the existence of nanoparticles in the low volume fraction limit.

8.2. Nature of heat transport in nanoparticles

Heat is transferred via conduction implies that heat is transferred internally, by vibrations of atoms and molecules. The vibrations of the atoms which are connected together as give rise to the vibrations of the whole crystal, that is, to lattice vibrations. The energy of the whole vibrating system is quantized, and the quantum of thermal energy absorbed or emitted by an atom is called a phonon. Therefore, a phonon is essentially a quantized mode of vibration occurring in rigid crystal lattice and plays a major role in material′s thermal conduction. Buongiorno [161] presented development of two-component four-equation nonhomogeneous equilibrium model for mass, momentum, and heat transport in nanofluids. Nondimensional analyses of the equations proposed that the energy transfer by nanoparticle dispersion is negligible, and thus cannot explain the abnormal heat transfer coefficient increases. Furthermore, a comparison of the nanoparticle and turbulent eddy time and length scales clearly indicates that the nanoparticles move homogeneously with the fluid in the presence of turbulent eddies, so an effect on turbulence intensity is doubtful. Thus, there was alternative explanation proposed for the abnormal heat transfer coefficient increases. For a heated fluid, these effects can result in a significant decrease of viscosity within the boundary layer, thus leading to heat transfer enhancement. The results showed that the Brownian diffusion and thermophoresis have been identified as the two most important nanoparticle/base-fluid slip mechanisms.

Keblinski et al. [162] presented investigation of development the fundamental understanding of heat transport in solid nanoparticles colloids under stationary conditions and evaluating the extent to which four specific mechanisms could contribute to the thermal conductivity. The four possible explanitions for this anomalous increase: Brownian motion of the particles, molecular-level layering of the liquid at the liquid/particle interface, the nature of heat transport in nanoparticles and the effects of nanoparticle clustering were explored. The results revealed that in a particle with a diameter smaller than 35 nm, the heat transport is not diffusive, but heat is transported ballistically. Although this fact prevents the application of conventional theories for the modeling of thermal conductivity of nanofluids, the results illustrated that the ballistic heat transport still cannot explain the anomalous thermal conductivity enhancements, and that′s attributed to the temperature inside the nanoparticles is closely constant and this fact does not depend on whether heat is transported by diffusion or ballistically.

8.3. Nanolayer thickness

There are some studies declared that there is a liquid layering on the nanoparticles, which improves the enhancement of nanofluid heat transfer properties. Yu and Choi [163] presented a modification of Maxwell model, which includes a nanolayer. The modified model showed the ability of measuring the increases of effective volume fraction and subsequently the thermal conductivity of nanofluids, especially when particle diameter is <10 nm. The results of this model revealed to, when the nanolayers are accounted for, there is potential for up to an eight-fold increase in the thermal conductivity of nanofluids over the enhancement predicted by the Maxwell model without the nanolayer.

Xie et al. [164] proposed a model including the consideration of the role of nanolayer at particle-fluid interface for predicting the effective thermal conductivities of nanoparticle-fluid mixtures. The results revealed that the nanolayer thickness, volume fraction, nanoparticle size and thermal conductivity ratio of particle to fluid have effects on the enhanced thermal conductivity ratios.

Xue et al. [165] examined the effect of nanolayer by using non-equilibrium molecular dynamics simulations in which a temperature gradient is imposed. The simulations results of a simple monoatomic liquid revealed that the layering of the liquid atoms at the liquid–solid interface does not have any significant effect on thermal transport properties.

Tillman and Hill [166] presented investigation of determine the nanolayer thickness and the thermal conductivity profile within the nanolayer. The nanolayer of a nanoparticle can be also considered as a monolayer from the adsorption of liquid molecules on the particle surface. The accuracy and robustness of the present method are verified by comparing the thermal conductance of the solid–fluid interface calculated from an inverse estimation of the nanolayer thickness obtained from observed experimental values. The results of molecular dynamic simulation showed that the thermal conduction in the nanolayer can vary greatly depending on the type of bonding between the liquid and the solid.

8.4. Effects of clustering

Clustering of particles is one of the major problems that affects of the enhancement of thermal conductivity by creating path of lower thermal resistance. It is noticed that as the particles agglomerate increases, the size increases and becomes denser where they clustered down, and end with low thermal conductivity enhancement. Karthikeyan et al. [167] presented investigation of the parameters influencing the thermal conductivity enhancement in water and ethylene glycol based nanofluids of CuO nanoparticles of average diameter 8 nm. The results illustrated that the thermal conductivity enhancement observed in water and ethylene glycol based nanofluids with 1 vol% CuO nanoparticles loading are 31.6% and 54%, respectively. The finer particle size and monodispersity of nanoparticles are the main reasons attribute to the large enhancement in thermal conductivity. The results revealed that the thermal conductivity of the nanofluid increases nonlinearly with the volume fraction of nanoparticles. The time-dependent thermal conductivity in water based CuO nanofluid showed that the thermal conductivity decreases with elapsed time due to clustering of nanoparticles with time, as confirmed microscopically.

Evans et al. [168] proposed investigation of analyzing the role of aggregation and interfacial thermal resistance on the effective thermal conductivity of nanofluids and nanocomposites. The results showed that the thermal conductivity of nanofluids and nanocomposites can be significantly enhanced by the aggregation of nanoparticles into clusters. Moreover, the results also revealed to that the conductivity enhancement due to aggregation is also a strong function of the chemical dimension of the aggregates and the radius of gyration of the aggregates.

9. Heat transfer enhancement

Sommers and Yerkes [169] investigated the thermal-hydraulic performance of dilute suspensions of 10 nm aluminum oxide nanoparticles in propanol (0.5 wt%, 1 wt%, and 3 wt%). The changes in thermal conductivity with particle concentration, density, specific heat were measured and found to be linear, whereas changes in viscosity were nonlinear and increased sharply with particle loading. Nanofluid heat transfer performance data were generally commensurate with that measured for the baseline. The results also showed that for the 1 wt% concentration, a small but pronounced enhancement in the heat transfer coefficient was recorded for $1800 < Re < 2800$, due to an earlier transition to turbulent flow. However, for the 1 wt% Al_2O_3/propanol nanofluid for $Re_D < 2100$, the pressure drop was found to increase from 400% to 600%. In the case of high particle loading (i.e. 3 wt%), the thermal performance was observed to deteriorate.

Mansour et al. [170] analyzed the effect of utilizing different correlations for the determination of the thermophysical properties of nanofluids on the results of the thermal performance analyses of nanofluids. For both laminar and turbulent flow cases, fully develop condition was examined and nanofluids were considered as single phase fluids. Different expression used for the determination of specific heat, dynamic viscosity and thermal conductivity were presented and the discrepancy between them was demonstrated. Two different sets of correlations utilized for performing the analyses of pressure drop and heat transfer of a simple configuration for the determination of the mentioned properties. The results showed that for a different particle volume fractions two cases provided different results. The results illustrated that for the laminar flow condition, the results were contradictory not only quantitatively and qualitatively.

Guo et al. [171] presented investigation of homogeneous and stable magnetic nanofluids containing γ-Fe_2O_3 nanoparticles which prepared by using a two-step method, and their thermal transport properties. The proposed technical route included preparing stable nanofluids composed of γ-Fe_2O_3 nanoparticles and the mixture of deionized water (DW) and ethylene glycol (EG) (DW–EG) as the base fluid. Sodium oleate was used as surfactant, and it was proved to be beneficial to the dispersion of the nanoparticles in the nanofluids. The results showed that the viscosity of the γ-Fe_2O_3 nanofluids fits Newtonian behavior and strongly depends on the temperature and the volume fraction. However, the viscosity measurements revealed to that the nanofluids illustrated Newtonian behavior and the viscosity of the nanofluids depended strongly on the tested temperatures and the nanoparticles loadings. The results demonstrated also that the thermal conductivities of the nanofluids were measured to be higher than that of base fluid, and the enhanced values increase with the volume fraction of the nanoparticles.

Mosavian et al. [172] studied in this investigation the heat transfer enhancement of laminar flow in circular tube utilizing different nanofluids including Al_2O_3 (20 nm), CuO (50 nm), and Cu (25 nm) nanoparticles in water. Constant wall temperature was adopted as thermal boundary condition. The results indicated that the heat transfer enhanced with increasing nanoparticle concentrations and Peclet number. The heat transfer coefficient enhancements for all nanofluids were higher than the prediction of single phase heat transfer correlation with nanofluids properties (homogeneous model). The results also demonstrated that the nanofluids that contain metal nanoparticles (Cu/water) exhibited more enhancement compared to oxide nanofluids (Al_2O_3/water and CuO/water). Furthermore, the CuO/water nanofluid showed less enhancement in heat transfer coefficient at the same nanoparticle concentration and Peclet number. However, that is attributed to the large particle size and high viscosity of CuO/water and high thermal conductivity of Cu/water nanofluid.

Abu-Nada [173] presented an investigation of Heat transfer enhancement in horizontal annuli using variable properties of Al_2O_3–water nanofluid. Different viscosity and thermal conductivity models are used to evaluate heat transfer enhancement in the annulus. The base case uses in this investigation the Chon et al. expression for conductivity and the Nguyen et al. experimental data for viscosity which take into account the dependence of these properties on temperature and nanoparticle volume fraction. The results showed that for Rayleigh number $Ra \geq 10^4$, the average Nusselt number was reduced by increasing the volume fraction of nanoparticles. Accordingly, the average Nusselt number increased by increasing the volume fraction of nanoparticles for $Ra = 10^3$. The results revealed that for $Ra \geq 10^4$ and $\phi > 5\%$, the average Nusselt number is reduced by increasing the volume fraction of nanoparticles.

10. Rheological behavior of nanofluids

Nanofluids are expected to be used under flow conditions and the flow of suspension which are sometimes drastically different from that of most common heat transfer fluids that have Newtonian characteristics, so it is essential to have the rheological properties of nanofluid to use practically. Rheological properties can provide the knowledge on the microstructure under both static and dynamic conditions, which are important to understand the mechanism of heat transfer enhancement using nanofluids. Chen et al. [174] performed an experimental work and theoretical analyses on the rheological behavior of nanofluids containing rod-like nanoparticles. Ethylene glycol (EG) and titanate nanotubes (TNT) are used as the base liquid and nanoparticles, respectively, to formulate the nanofluids. The effects of particle concentration (0.5 wt%, 1.0 wt%, 2.0 wt%, 4.0 wt% and 8.0 wt%) and temperature (20 °C, 30 °C, 40 °C, 50 °C and 60 °C) were examined. The results show that a very strong shear thinning behavior of the TNT nanofluids and big influences of particle concentration and temperature on the zero shear viscosity (ZSV) and high shear viscosity (HSV). Therefore, a higher particle concentration gives a stronger shear thinning, a higher zero shear viscosity (ZSV) and a higher high shear viscosity (HSV). The results presented also that the temperature has a strong effect on the rheological behaviur of the EG–TNT nanofluids. However the higher shear viscosity increment is independent of the temperature.

Tseng and Lin [175] investigated the rheological behavior and suspension structure of anatase titanium dioxide (TiO_2) nanoparticles dispersed in pure water over a range of volumetric solids concentrations ($\phi = 0.05$–0.12) and shear rates ($\gamma = 10^1$–10^3 s^{-1}). The suspensions of nanoparticle generally exhibited a pseudoplastic flow behavior, indicating an existence of particle aggregations in the liquid medium. The suspensions became clearly thixotropic as ϕ was increased above 0.1. The results also revealed a pronounced increase in the degree of particle interactions as the volumetric concentration increased. Fractal dimension (D_f) was estimated from the suspension yield-stress and ϕ dependence, and was determined as $D_f \approx /1.46 - /1.78$ for the flocculated nanoparticle suspensions.

Chen et al. [176] presented experimental work and theoretical analyses with aims of more fundamental understanding of the rheological behavior of nanofluids and interpretation of the discrepancy in the reported rheological behavior of nanofluids in the recent literature. The experiments were carried out on EG-based TiO_2 nanofluids containing 0.5%, 1.0%, 2.0%, 4.0% and 8.0% by weight spherical nanoparticles at 20–60 °C. The theoretical analyses were carried out on the high shear viscosity, shear thinning behavior and temperature dependence. The results revealed to that the EG-based nanofluids showed Newtonian behavior under

the conditions of this work with shear viscosity as a strong function of temperature and particle concentration. Furthermore, the relative viscosity depends on particle concentration in a nonlinear manner but is independent of temperature. The Krieger–Dougherty equation can be use to predict the high shear viscosity if the solids volume fraction is replaced by the volume fraction of nanoparticle aggregates. The results showed that for the spherical nanoparticles, an aggregate size of approximately 3 times the primary nanoparticle size gives the best prediction of the experimental data.

Chen et al. [177] presented experimental work on the rheological behavior of ethylene glycol based nanofluids containing titanate nanotubes over 20–60 °C and a particle mass concentration of 0–8%. The results revealed to that EG-TNT nanofluids are non-Newtonian exhibiting shear-thinning behavior over 20–60 °C and a particle mass concentration range of 0–8%, in contrast to the Newtonian behavior for EG–TiO_2 nanofluids containing spherical particles. Furthermore, the non-Newtonian shear-thinning behavior becomes stronger at higher temperatures or higher concentrations. The results showed for a given particle concentration, there exists a certain shear rate below which the viscosity increases with increasing temperature, whereas the opposite occurs above such a shear rate. The results also presented that the normalized high-shear viscosity is independent of temperature.

11. Challenges of using nanofluids to enhance the heat transfer for MT and MC

The use of nanofluids seems attractive in a broad range of applications as reported in the previous sections. But the development in the area of nanofluid application is hindered by different reasons like the lack of agreement of results obtained by different researchers; the poor characterization of suspensions, and the lack of theoretical understanding of the mechanisms responsible for changes in properties. This review concludes several important issues that should receive greater attention in the near future such as the thermal conductivity, Brownian motion of particles, particle migration, and thermophysical property change with temperature [190]. However, recent studies indicate particle aggregation and deposition in MT and MC. Further study is required in these areas to identify the reasons for and the effects of particle deposition. Finally, there appears to be hardly any research in the use of nanofluids as working fluids. Nanoparticle dispersions in two-phase heat transfer applications can be studied to explore the possibility of improving the heat transfer characteristics of nanofluids at different application. Applied research in nanofluids which will define their future in the field of heat transfer is expected to grow faster in the near future [191,192]. The challenges of using the nanofluids are presented as follow:

11.1. long term stability of nanoparticles dispersion

Long term physical and chemical stability of nanofluids is an important practical issue because the nanoparticles always form aggregates due to very strong van der Waals interactions, so the preparation of homogeneous suspension remains a technical challenge. To get stable nanofluids, physical or chemical treatment have been conducted such as (i) an addition of surfactant; (ii) surface modification of the suspended particles; (iii) applying strong force on the clusters of the suspended particles. Generally, long term stability of nanoparticles dispersion is one of the basic requirements of nanofluids applications. Stability of nanofluids have good corresponding relationship with the enhancement of thermal conductivity where the better dispersion behavior, the higher thermal conductivity of nanofluids [194]. However the dispersion behavior of the nanoparticles could be influenced by period of time. As a result, thermal conductivity of nanofluids is eventually affected. Eastman et al. [195] reported that, thermal conductivity of ethylene glycol based nanofluids containing 0.3% copper nanoparticles is decreased with time. In their study, the thermal conductivity of nanofluids was measured twice: first was within 2 days and second was two months after the preparation. It was found that fresh nanofluids exhibited slightly higher thermal conductivities than nanofluids that were stored up to two months. This might due to reduced dispersion stability of nanoparticles with respect to time. Nanoparticles may tend to agglomerate when kept for long period of time. Lee and Mudawar [196] compared the Al_2O_3 nanofluids stability visually over time span. The results revealed that nanofluids kept for 30 days exhibit some settlement and concentration gradient compared to fresh nanofluids. It indicated long term degradation in thermal performance of nanofluids could be happened. Particles settling must be examined carefully since it may lead to clogging of coolant passages. Choi et al. [197] reported that the excess quantity of surfactant has a harmful effect on viscosity, thermal property, chemical stability, and thus it is strongly recommended to control the addition of the surfactant with great care. However, the addition of surfactant would make the particle surface coated, thereby resulting in the screening effect on the heat transfer performance of nanoparticles.

11.2. Increased pressure drop and pumping power

Pressure drop development and required pumping power during the flow of coolant determines the efficiency of nanofluids application. It is expected that coolants with higher density and viscosity leads to higher pressure drop and pumping power. However, several literatures showing significant increase of nanofluids pressure drop compared to base fluid, Lee et al. [129] investigated viscosity of Al_2O_3–water nanofluids and ZnO–ethylene glycol nanofluids. Results clearly show, viscosity of nanofluids is higher than basefluid. Vasuet al. [198] studied the thermal design of compact heat exchanger using nanofluids. In this study, it is found that pressure drop of 4% Al_2O_3–H_2O nanofluids is almost double of the basefluid. Pantzali et al. [193] reported that there was substantial increase of nanofluids pressure drop and pumping power in plate heat exchanger. About 40% increase of pumping power was observed for nanofluids compared with water. Peng et al. [199] reported that the frictional pressure drop of refrigerant-based nanofluids flow boiling inside the horizontal smooth tube is larger than that of fluid, and increases with the increase of the mass fraction of nanoparticles. The maximum enhancement of frictional pressure drop can reach 20.8% under the experimental conditions.

11.3. Thermal performance of nanofluids in turbulent flow and fully developed region

The weakness of thermal performance of nanofluids in turbulent flow and fully developed region is an important issue that must be addressed carefully. Recently, there was inconsistence of results reported by the researchers. Kim et al. [200] revealed that no convective heat transfer improvement was noticed for amorphous carbonic nanofluids in turbulent flow despite 8% improvement in laminar flow. However, Duangthongsuk and Wongwises [201] reported that heat transfer coefficient of TiO_2–water nanofluids is higher than basefluid. This property increases with the increase of Reynold numbers and particle concentrations ranging from 0.2% to 2%. Although the study revealed that 26% enhancement can be observed for nanofluids with 1% of TiO_2 nanoparticles, it showed opposing results at 2.0% volume fraction. The study indicated that heat transfer coefficient of nanofluids at this condition was 14% lower than basefluid. Pantzali et al. [193] added substitution of

conventional coolants by nanofluids seemed beneficial for laminar flow compared to turbulent flow. Moreover, Ding et al. [202] reported the weakness of thermal performance for nanofluids at fully developed region, they found that convective heat transfer coefficient of nanofluids at low Reynold number has the highest value at the entrance length of the tube, starts decreasing with axial distances and eventually reaches constant value in fully developed region.

11.4. Higher viscosity and lower specific heat

The viscosity of nanoparticle-base fluid suspensions increases in accordance with increasing particle concentration in the suspension. So, the particle mass fraction cannot be increased unlimitedly [129–134]. In addition, the ideal heat coolant fluid should possess higher value of specific heat so the fluid can exchange more heat. Previous studies revealed that the specific heat of nanofluids is lower than basefluid. Namburu et al. [203] reported that CuO–ethylene glycol nanofluids, SiO_2–ethylene glycol nanofluids and Al_2O_3–ethylene glycol nanofluids exhibit lower specific heat compared to basefluids.

11.5. High cost of nanofluids

Nanofluids can be produced by either one step or two steps methods. Both methods require advanced and sophisticated equipments. This leads to higher production cost of nanofluids which is one main reason that may hinder the application of using nanofluids in industry.

11.6. Difficulties in production process

The previous efforts to manufacture nanofluids have often employed either a single step that simultaneously makes and disperses the nanoparticles into base fluids, or a two-step approach that involves generating nanoparticles and subsequently dispersing them into a base fluid. Using either of these two approaches, nanoparticles are inherently produced from processes that involve reduction reactions or ion exchange [190]. Furthermore, the base fluids contain other ions and reaction products that are difficult or impossible to separate from the fluids. Another difficulty encountered in nanofluid manufacture is nanoparticles′ tendency to agglomerate into larger particles, which limits the benefits of the high surface area nanoparticles. To counter this tendency, particle dispersion additives are often added to the base fluid with the nanoparticles. Unfortunately, this practice can change the surface properties of the particles, and nanofluids prepared in this way may contain unacceptable levels of impurities. Most studies to date have been limited to sample sizes less than a few hundred milliliters of nanofluids. This is problematic since larger samples are needed to test many properties of nanofluids and, in particular, to assess their potential for use in new applications [204]. As an undisputed view, the nanofluids have more advantageous than disadvantegous for usage as cooling fluid. This calls for a more intensified effort in the research on nanofluids. Research needs to examine closely a variety of issues, such as synthesis, characterization, thermophysical properties, heat and mass transport, modeling. Hence, a multidisciplinary approach comprising researchers such as thermal engineers, chemical technologists, material scientists, chemists, and physicists needs to be undertaken. Only such an approach can ensure the future of nanofluids [205].

12. Conclusions

In this article, a comprehensive review of previous efforts is presented for different convective flow regimes and heat transfer through microtube (MT) and microchannel (MC). The effects of several parameters in geometry, boundary conditions, and types of fluids were extensively introduced and investigated. In addition, an extensive review for preparation, parameters, mechanisms, characteristics, convective heat transfer enhancement, applications, safety, and environmental impacts for nanofluids and challanges was also reported. It is found that nanofluids will solve many technological problems and space limitation, and will be used commercially such as other ordinary coolants in the future. It was observed from the literatures that many works have been done using conventional fluids to study the heat transfer and fluid flow characteristics in MT and MC. Thus, more work using nanofluids is needed to investigate the heat transfer enhancement in both MT and MC. The outcomes from this literature are summarized as follow:

- It has been found that SiO_2–EG nanofluid has the highest Nusselt number, followed by ZnO–EG, CuO–EG, Al_2O_3–EG, and lastly pure EG. The Nusselt number for all cases increases with the volume fraction but it decreases with the rise in the diameter of nanoparticles.
- It was also found that triangular MC has the highest thermal efficiency, the trapezoidal MC was inferior to triangular but superior to rectangular.
- Greater enhancement was observed when nanofluids were used in MT and in MC, as well as other applications.
- Theoretical and experimental research investigations are needed to comprehensively understand the heat transfer mechanism in nanofluids.
- The improved thermal, rheological, and heat transfer performances for nanofluids has been reported is some articles without correlating these performances with the specific applications.
- The production cost and nanofluids stability are the major factors that hinder the commercialization of nanofluids. Solving these challenges, it is expected that nanofluids can make substantial impact as coolant in different applications

References

[1] Zhuo Li Ya-Ling, He Gui-Hua, Tang Wen-Quan Tao. Experimental and numerical studies of liquid flow and heat transfer in microtubes. International Journal of Heat and Mass Transfer 2007;50:3447–60.

[2] Dorin Lelea Shigefumi Nishio, Kiyoshi Takano. The experimental research on microtube heat transfer and fluid flow of distilled water. International Journal of Heat and Mass Transfer 2004;47:2817–30.

[3] Yulong Ding Hajar, Alias Dongsheng, Wen Richard A Williams. Heat transfer of aqueous suspensions of carbon nanotubes (CNT nanofluids). International Journal of Heat and Mass Transfer 2006;49:240–50.

[4] Yang C-Y, Lin T-Y. Heat transfer characteristics of water flow in microtubes. Experimental Thermal and Fluid Science 2007;32:432–9.

[5] Celata GP, Cumo M, McPhail S, Zummo G. Characterization of fluid dynamic behavior and channel wall effects in microtube. International Journal of Heat and Mass Transfer 2006;27:135–43.

[6] Peng-Fei Hao Xi-Wen, Zhang Zhao-Hui, Yao Feng He. Transitional and turbulent flow in a circular microtube. Experimental Thermal and Fluid Science 2007;32:423–31.

[7] Celata GP, Cumo M, Marconi V, McPhail SJ, Zummo G. Microtube liquid single-phase heat transfer in laminar flow. International Journal of Heat and Mass Transfer 2006;49:3538–46.

[8] Sara ON, Barlay Ergu Ö, Arzutug ME, Yapıcı S. Experimental study of laminar forced convective mass transfer and pressure drop in microtubes. International Journal of Thermal Sciences 2009;48:1894–900.

[9] Zhang P, Fu X. Two-phase flow characteristics of liquid nitrogen in vertically upward 0.5 and 1.0 mm micro-tubes: visualization studies. Cryogenics 2009;49:565–75.

[10] Zhi-Gang Liu Shi-Qiang Liang. Masahiro Takei. Experimental study on forced convective heat transfer characteristics in quartz microtube. International Journal of Thermal Sciences 2007;46:139–48.

[11] Celata GP, Cumo M, McPhail SJ, Tesfagabir L, Zummo G. Experimental study on compressible flow in microtubes. International Journal of Heat and Fluid Flow 2007;28:28–36.

[12] Qi SL, Zhang P, Wang RZ, Xu. LX. Flow boiling of liquid nitrogen in micro-tubes: Part I—The onset of nucleate boiling, two-phase flow instability and two-phase flow pressure drop. International Journal of Heat and Mass Transfer 2007;50:4999–5016.

[13] Qi SL, Zhang P, Wang RZ, Xu. LX. Flow boiling of liquid nitrogen in micro-tubes: Part II—Heat transfer characteristics and critical heat flux. International Journal of Heat and Mass Transfer 2007;50:5017–30.

[14] Wen Dongsheng, Ding Yulong. Experimental investigation into convective heat transfer of nanofluids at the entrance region under laminar flow conditions. International Journal of Heat and Mass Transfer 2004;47:5181–8.

[15] Renqiang Xiong JN Chung. A new model for three-dimensional random roughness effect on friction factor and heat transfer in microtubes. International Journal of Heat and Mass Transfer 2010;53:3284–91.

[16] Sun-Xiao Zhang Ya-Ling, He Guy, Lauriat Wen-Quan Tao. Numerical studies of simultaneously developing laminar flow and heat transfer in microtubes with thick wall and constant outside wall temperature. International Journal of Heat and Mass Transfer 2010;53:3977–89.

[17] Giulio, Paola. Numerical analysis of roughness effect on microtube heat transfer. Journal of Superlattices and Microstructures 2004;35:601–16.

[18] Kamali R, Binesh AR. Numerical investigation of heat transfer enhancement using carbon nanotube-based non-Newtonian nanofluids. International Communications in Heat and Mass Transfer 2010;37:1153–7.

[19] Hong Chungpyo, Asako Yutaka. Heat transfer characteristics of gaseous flows in microtube with constant heat flux. Applied Thermal Engineering 2008;28:1375–85.

[20] Bianco V, Chiacchio F, Manca O, Nardini S. Numerical investigation of nanofluids forced convection in circular tubes. Applied Thermal Engineering 2009;29:3632–42.

[21] Nian Xiao John Elsnab, Ameel Tim. Microtube gas flows with second-order slip flow and temperature jump boundary conditions. International Journal of Thermal Sciences 2009;48:243–51.

[22] Koo J, Kleinstreuer C. Viscous dissipation effects in microtubes and micro-channels. International Journal of Heat and Mass Transfer 2004;47:3159–69.

[23] Lelea Dorin. Effects of temperature dependent thermal conductivity on *Nu* number behavior in micro-tubes. International Communications in Heat and Mass Transfer 2010;37:245–9.

[24] Lelea Dorin, Eugen Cioabla Adrian. The viscous dissipation effect on heat transfer and fluid flow in micro-tubes. International Communications in Heat and Mass Transfer 2010;37:1208–14.

[25] Ashok K Satapathy. Slip flow heat transfer in an infinite microtube with axial conduction. International Journal of Thermal Sciences 2010;49:153–60.

[26] Wang Haoli, Wang Yuan. Influence of three-dimensional wall roughness on the laminar flow in microtube. International Journal of Heat and Fluid Flow 2007;28:220–8.

[27] Aziz A, Niedbalski Nick. Thermally developing microtube gas flow with axial conduction and viscous dissipation. International Journal of Thermal Sciences 2011;50:332–40.

[28] Salman B H, Mohammed HA, SH Kherbeet A. Heat transfer enhancement of nanofluids flow in microtube with constant heat flux. International Communications in Heat and Mass Transfer 2012;39:1195–204.

[29] Jung Jung-Yeul, Oh Hoo-Suk, Kwak Ho-Young. Forced convective heat transfer of nanofluids in microchannels. International Journal of Heat and Mass Transfer 2009;52:466–72.

[30] Cheng Wang Nam-Trung Nguyen, Wong Teck Neng, Wu Zhigang, Yang Chun, Ooi Kim Tiow. Investigation of active interface control of pressure driven two-fluid flow in microchannels. Sensors and Actuators 2007;A 133:323–8.

[31] Agarwal Akhil, Bandhauer Todd M, Garimella Srinivas. Measurement and modeling of condensation heat transfer in non-circular microchannels. International Journal of Refrigeration 2010;33:1169–79.

[32] Roland Bavie´re Michel Favre-Marinet, Le Person Ste´phane. Bias effects on heat transfer measurements in microchannel flows. International Journal of Heat and Mass Transfer 2006;49:3325–37.

[33] Wu HY, Cheng Ping. An experimental study of convective heat transfer in silicon microchannels with different surface conditions. International Journal of Heat and Mass Transfer 2003;46:2547–56.

[34] Park Hee Sung, Punch Jeff. Friction factor and heat transfer in multiple microchannels with uniform flow distribution. International Journal of Heat and Mass Transfer 2008;51:4535–43.

[35] Quan Xiaojun, Dong Lining, Cheng Ping. Determination of annular condensation heat transfer coefficient of steam in microchannels with trapezoidal cross section. International Journal of Heat and Mass Transfer 2010;53:3670–6.

[36] Lee Poh-Seng, Garimella Suresh V, Liu Dong. Investigation of heat transfer in rectangular microchannels. International Journal of Heat and Mass Transfer 2005;48:1688–704.

[37] Harirchian Tannaz, Garimella Suresh V. Microchannel size effects on local flow boiling heat transfer to a dielectric fluid. International Journal of Heat and Mass Transfer 2008;51:3724–35.

[38] Barlay Ergu O, Sara ON, Yapıcı S, Arzutug ME. Pressure drop and point mass transfer in a rectangular microchannel. International Communications in Heat and Mass Transfer 2009;36:618–23.

[39] Owhaib Wahib, Martin-Callizo Claudi, Palm Bjorn. Evaporative heat transfer in vertical circular microchannels. Applied Thermal Engineering 2004;24:1241–53.

[40] Chiu Han-Chieh, Jang Jer-Huan, Yeh Hung-Wei, Wu Ming-Shan. The heat transfer characteristics of liquid cooling heatsink containing microchannels. International Journal of Heat and Mass Transfer 2011;54:34–42.

[41] Shen S, Xu JL, Zhou JJ, Chen. Y. Flow and heat transfer in microchannels with rough wall surface. Energy Conversion and Management 2006;47:1311–25.

[42] Barber Jacqueline, Sefiane Khellil, Brutin David, Tadrist Lounes. Hydrodynamics and heat transfer during flow boiling instabilities in a single microchannel. Applied Thermal Engineering 2009;29:1299–308.

[43] Lee Poh-Seng, Garimella Suresh V. Saturated flow boiling heat transfer and pressure drop in silicon microchannel arrays. International Journal of Heat and Mass Transfer 2008;51:789–806.

[44] Celata Gian Piero, Saha Sujoy Kumar, Zummo Giuseppe, Dossevi Denam. Heat transfer characteristics of flow boiling in a single horizontal microchannel. International Journal of Thermal Sciences 2010;49:1086–94.

[45] Megahed Ayman. Experimental investigation of flow boiling characteristics in a cross-linked microchannel heat sink. International Journal of Multiphase Flow 2011;37:380–93.

[46] Cortina Dı´az M, Schmidt J. Experimental investigation of transient boiling heat transfer in microchannels. International Journal of Heat and Fluid Flow 2007;28:95–102.

[47] Chen Yongping, Wua Rui, Shi Mingheng, Wua Jiafeng, Peterson GP. Visualization study of steam condensation in triangular microchannels. International Journal of Heat and Mass Transfer, 52; 5122–9.

[48] Betz Amy Rachel, Attinger Daniel. Can segmented flow enhance heat transfer in microchannel heat sinks? International Journal of Heat and Mass Transfer 2010;53:3683–91.

[49] Wojtan Leszek, Revellin Rémi, Thome John R. Investigation of saturated critical heat flux in a single, uniformly heated microchannel. Experimental Thermal and Fluid Science 2006;30:765–74.

[50] Asthana Ashish, Zinovik Igor, Weinmueller Christian, Poulikakos Dimos. Significant Nusselt number increase in microchannels with a segmented flow of two immiscible liquids: an experimental study. International Journal of Heat and Mass Transfer 2011;54:1456–64.

[51] Wang Guodong, Cheng Ping. An experimental study of flow boiling instability in a single microchannel. International Communications in Heat and Mass Transfer 2008;35:1229–34.

[52] Wu Jiafeng, Shi Mingheng, Chen Yongping, Li Xin. Visualization study of steam condensation in wide rectangular silicon microchannels. International Journal of Thermal Sciences 2010;49:922–30.

[53] Steinke Mark E, Satish G Kandlikar. Single-phase liquid friction factors in microchannels. International Journal of Thermal Sciences 2006;45:1073–83.

[54] Wu Jiafeng, Shi Mingheng, Chen Yongping, Li Xin. Visualization study of steam condensation in wide rectangular silicon microchannels. International Journal of Thermal Sciences 2010;49:922–30.

[55] Zhang TieJun, Peles Yoav, Wena John T, Tong Tao, Chang Je-Young, Prasher Ravi, Jensen Michael K. Analysis and active control of pressure-drop flow instabilities in boiling microchannel systems. International Journal of Heat and Mass Transfer 2010;53:2347–60.

[56] Kohl MJ, Abdel-Khalik SI, Jeter SM, Sadowski DL. An experimental investigation of microchannel flow with internal pressure measurements. International Journal of Heat and Mass Transfer 2005;48:1518–33.

[57] Rosengarten G, Cooper-White J, Metcalfe G. Experimental and analytical study of the effect of contact angle on liquid convective heat transfer in microchannels. International Journal of Heat and Mass Transfer 2006;49:4161–70.

[58] Tang GH, Li Zhuo, He YL, Tao WQ. Experimental study of compressibility, roughness and rarefaction influences on microchannel flow. International Journal of Heat and Mass Transfer 2007;50:2282–95.

[59] Huh Cheol, Kim Jeongbae, Kim Moo Hwan. Flow pattern transition instability during flow boiling in a single microchannel. International Journal of Heat and Mass Transfer 2007;50:1049–60.

[60] Mokrani Omar, Bourouga Brahim, Castelain Cathy, Peerhossaini Hassan. Fluid flow and convective heat transfer in flat microchannels. International Journal of Heat and Mass Transfer 2009;52:1337–52.

[61] Bertsch Stefan S, Groll Eckhard A, Garimella Suresh V. Effects of heat flux, mass flux, vapor quality, and saturation temperature on flow boiling heat transfer in microchannels. International Journal of Multiphase Flow 2009;35:142–54.

[62] Lam Ngo Tri, Kato Yasuyoshi, Nikitin Konstantin, Ishizuka Takao. Heat transfer and pressure drop correlations of microchannel heat exchangers with S-shaped and zigzag fins for carbon dioxide cycles. Experimental Thermal and Fluid Science 2007;32:560–70.

[63] Wei Xiaojin, Joshi Yogendra. Experimental and numerical study of sidewall profile effects on flow and heat transfer inside microchannels. International Journal of Heat and Mass Transfer 2007;50:4640–51.

[64] Fang Chen, David Milnes, Wang Fu-min, Goodson Kenneth E. Influence of film thickness and cross-sectional geometry on hydrophilic microchannel condensation. International Journal of Multiphase Flow 2010;36:608–19.

[65] Bogojevic D, Sefiane K, Walton AJ, Lin H, Cummins G, Kenning DBR, Karayiannis TG. Experimental investigation of non-uniform heating effect on flow boiling instabilities in a microchannel-based heat sink. International Journal of Thermal Sciences 2011;50:309–24.

[66] Wang Guodong, Cheng Ping, Bergles AE. Effects of inlet/outlet configurations on flow boiling instability in parallel microchannels. International Journal of Heat and Mass Transfer 2008;51:2267–81.

[67] García-Hernando N, Acosta-Iborra A, Ruiz-Rivas U, Izquierdo M. Experimental investigation of fluid flow and heat transfer in a single-phase liquid flow

micro-heat exchanger. International Journal of Heat and Mass Transfer 2009;52:5433–46.
[68] Yang Yue-Tzu, Lai Feng-Hsiang. Numerical study of heat transfer enhancement with the use of nanofluids in radial flow cooling system. International Journal of Heat and Mass Transfer 2010;53:5895–904.
[69] Wu Zan, Li Wei, Ye Shuang. Correlations for saturated critical heat flux in microchannels. International Journal of Heat and Mass Transfer 2011;54:379–89.
[70] Shevade Shantanu S, Rahman Muhammad M. Heat transfer in rectangular microchannels during volumetric heating of the substrate. International Communications in Heat and Mass Transfer 2007;34:661–72.
[71] Gamrat G, Favre-Marinet M, Le Person S. Modelling of roughness effects on heat transfer in thermally fully-developed laminar flows through micro-channels. International Journal of Thermal Sciences 2009;48:2203–14.
[72] Mlcak Justin D, Anand NK, Rightley Michael J. Three-dimensional laminar flow and heat transfer in a parallel array of microchannels etched on a substrate. International Journal of Heat and Mass Transfer 2008;51:5182–91.
[73] Chen Yongping, Zhang Chengbin, Shi Mingheng, Wu Jiafeng. Three-dimensional numerical simulation of heat and fluid flow in noncircular microchannel heat sinks. International Communications in Heat and Mass Transfer 2009;36:917–20.
[74] Zhu X, Liao Q. Heat transfer for laminar slip flow in a microchannel of arbitrary cross section with complex thermal boundary conditions. Applied Thermal Engineering 2006;26:1246–56.
[75] Ji Yan, Yuan Kun, Chung JN. Numerical simulation of wall roughness on gaseous flow and heat transfer in a microchannel. International Journal of Heat and Mass Transfer 2004;49:1241–53.
[76] Sui Y, Teo CJ, Lee PS, Chew YT, Shu C. Fluid flow and heat transfer in wavy microchannels. International Journal of Heat and Mass Transfer 2010;53:2760–72.
[77] Rahman Muhammad M, Shevade Shantanu S, Ojada Ejiro. Convective heat transfer in a composite trapezoidal microchannel during magnetic heating. International Communications in Heat and Mass Transfer 2010;37:1175–81.
[78] Liu Jiang-Tao, Peng Xiao-Feng, Yan Wei-Mon. Numerical study of fluid flow and heat transfer in microchannel cooling passages. International Journal of Heat and Mass Transfer 2007;50:1855–64.
[79] Renksizbulut M, Niazmand H, Tercan. G. Slip-flow and heat transfer in rectangular microchannels with constant wall temperature. International Journal of Thermal Sciences 2006;45:870–81.
[80] Niazmand Hamid, Renksizbulut Metin, Saeedi Ehsan. Developing slip-flow and heat transfer in trapezoidal microchannels. International Journal of Heat and Mass Transfer 2008;51:6126–35.
[81] Khadem MH, Shams M, Hossainpou S. Numerical simulation of roughness effects on flow and heat transfer in microchannels at slip flow regime. International Journal of Heat and Mass Transfer 2009;36:69–77.
[82] Zade Azad Qazi, Renksizbulut Metin, Friedman Jacob. Heat transfer characteristics of developing gaseous slip-flow in rectangular microchannels with variable physical properties. International Journal of Heat and Fluid Flow 2011;32:117–27.
[83] Shokouhmand H, Bigham. S. Slip-flow and heat transfer of gaseous flows in the entrance of a wavy microchannel. International Communications in Heat and Mass Transfer 2010;37:695–702.
[84] Mohammed HA, Gunnasegaran P, Shuaib NH. Influence of channel shape on the thermal and hydraulic performance of microchannel heat sink. International Communications in Heat and Mass Transfer 2011;38:474–80.
[85] Mohammed HA, Gunnasegaran P, Shuaib NH. Numerical simulation of heat transfer enhancement in wavy microchannel heat sink. International Communications in Heat and Mass Transfer 2011;38:63–8.
[86] Kosar Ali. Effect of substrate thickness and material on heat transfer in micro-channel heat sinks. International Journal of Thermal Sciences 2010;49:635–42.
[87] Mohammed HA, Bhaskaran G, Shuaib NH, Abu-Mulaweh HI. Influence of nanofluids on parallel flow square microchannel heat exchanger performance. International Communications in Heat and Mass Transfer 2011;38:1–9.
[88] Mohammed HA, Bhaskaran G, Shuaib NH, Saidur R. Numerical study of heat transfer enhancement of counter flow of nanofluids in rectangular micro-channel heat exchanger. Superlattices and Microstructures 2011;50 (3):215–33.
[89] Revellin Remi, Thome John R. A theoretical model for the prediction of the critical heat flux in heated microchannels. International Journal of Heat and Mass Transfer 2008;51:1216–25.
[90] Revellin Rémi, Mishima Kaichiro, Thome John R. Status of prediction methods for critical heat fluxes in mini and microchannels. International Journal of Heat and Fluid Flow 2009;30:983–92.
[91] Rosa P, Karayiannis TG, Collins MW. Single-phase heat transfer in micro-channels: the importance of scaling effects. Applied Thermal Engineering 2009;29:3447–68.
[92] Hwang Y, Lee JK, Lee JKu, Jeong YM, Cheong SI, Ahn YC. Production and dispersion stability of nanoparticles in nanofluids. Powder Technology 2008;186:145–53.
[93] Chopkar M, Das P, Manna I. Synthesis and characterization of nanofluid for advanced heat transfer applications. Scripta Materialia 2006;55:549–52.
[94] Li C, Williams W, Buongiorno J, Hu L, Peterson. G. Transient and steady-state experimental comparison study of effective thermal conductivity of AlO/water nanofluids. International Journal of Heat and Mass Transfer 2008 042407.
[95] Zhang X, Gu H, Fujii M. Effective thermal conductivity and thermal diffusivity of nanofluids containing spherical and cylindrical nanoparticles. Experimental Thermal and Fluid Science 2007;31:593–9.
[96] Murshed S, Leong K, Yang C. Enhanced thermal conductivity of TiO_2–water based nanofluids. Int. J. Thermal Sciences 2005;44:367–73.
[97] Murshed S, Leong K, Yang C. Investigations of thermal conductivity and viscosity of nanofluids. International Journal of Thermal Sciences 2008;47:560–8.
[98] Oh D, Jain A, Eaton J, Goodson K, Lee J. Thermal conductivity measurement and sedimentation detection of aluminum oxide nanofluids by using the 3 [omega] method. International Journal of Heat and Fluid Flow 2008;29:1456–61.
[99] Patel, H, Sundararajan, T, Das, S.. An experimental investigation into the thermal conductivity enhancement in oxide and metallic nanofluids. Journal of Nanoparticle Research 12:1015–1031.
[100] Xie H, Wang J, Xi T, Liu Y. Thermal conductivity of suspensions containing nanosized SiC particles. International Journal of Thermophysics 2002;23:571–80.
[101] Sharma, P, Baek, I, Cho, T, Park, S, Lee, K. Enhancement of thermal conductivity of ethylene glycol based silver nanofluids. Powder Technology.
[102] Wong K, Kurma T. Transport properties of alumina nanofluids. Nanotechnology 2008;19:345702.
[103] Turgut A, Tavman I, Chirtoc M, Schuchmann H, Sauter C, Tavman. S. Thermal conductivity and viscosity measurements of water-based TiO_2 nanofluids. International Journal of Thermophysics 2009;30:1213–26.
[104] Chandrasekar, M, Suresh, S. Limits for thermal conductivity of nanofluids. Thermal Science 14:65–71.
[105] Chen H, Witharana S, Jin Y, Kim C, Ding Y. Predicting thermal conductivity of liquid suspensions of nanoparticles (nanofluids) based on rheology. Particuology 2009;7:151–7.
[106] Hong T, Yang H, Choi C. Study of the enhanced thermal conductivity of Fe nanofluids. Journal of Applied Physics 2009;97:064311.
[107] Liu M, Lin M, Tsai C, Wang C. Enhancement of thermal conductivity with Cu for nanofluids using chemical reduction method. International Journal of Heat and Mass Transfer 2006;49:3028–33.
[108] Yu W, Xie H, Chen L, Li Y. Investigation of thermal conductivity and viscosity of ethylene glycol based ZnO nanofluid. Thermochimica Acta 2009;491:92–6.
[109] Xie H, Yu W, Li Y. Thermal performance enhancement in nanofluids containing diamond nanoparticles. Journal of Physics D: Applied Physics 2009;42:095413.
[110] Jiménez-Pérez J, Cruz-Orea A, Sánchez-Ramírez J, Sánchez-Sinencio F, Martínez-Pérez L, López Muñoz. G. Thermal characterization of nanofluids with different solvents. International Journal of Thermophysics 2009;30:1227–33.
[111] Patel, H, Sundararajan, T, Das, S. An experimental investigation into the thermal conductivity enhancement in oxide and metallic nanofluids. Journal of Nanoparticle Research 12:1015–1031.
[112] E Timofeeva, D Smith, W Yu, D France, D Singh, J Routbort. Particle size and interfacial effects on thermo-physical and heat transfer characteristics of water-based –SiC nanofluids. Nanotechnology 21:215703.
[113] Anoop K, Sundararajan T, Das S. Effect of particle size on the convective heat transfer in nanofluid in the developing region. International Journal of Heat and Mass Transfer 2009;52:2189–95.
[114] Beck M, Yuan Y, Warrier P, Teja. A. The effect of particle size on the thermal conductivity of alumina nanofluids. Journal of Nanoparticle Research 2009;11:1129–36.
[115] Chopkar M, Sudarshan S, Das P, Manna I. Effect of particle size on thermal conductivity of nanofluid. Metallurgical and Materials Transactions 2008;39:1535–42.
[116] Ding Y, Wen D. Particle migration in a flow of nanoparticle suspensions. Powder Technology 2005;149:84–92.
[117] Xian-Ju W, Xin-Fang L. Influence of pH on nanofluids′ viscosity and thermal conductivity. Chinese Physics Letters 2009;26:056601.
[118] Wang X, Zhu D. Investigation of pH and SDBS on enhancement of thermal conductivity in nanofluids. Chemical Physics Letters 2009;470:107–11.
[119] Nguyen C, Roy G, Gauthier C, Galanis N. Heat transfer enhancement using Al_2O_3–water nanofluid for an electronic liquid cooling system. Applied Thermal Engineering 2007;27:1501–6.
[120] Mintsa H, Roy G, Nguyen C, Doucet D. New temperature dependent thermal conductivity data for water-based nanofluids. International Journal of Thermal Sciences 2009;48:363–71.
[121] Yu-Hua L, Wei Q, Jian-Chao. F. Temperature dependence of thermal conductivity of nanofluids. Chinese Physics Letters 2008;25:3319.
[122] Nguyen C, Desgranges F, Roy G, Galanis N, Mare T, Boucher S, Angue Mintsa. H. Temperature and particle-size dependent viscosity data for water-based nanofluids-hysteresis phenomenon. International Journal of Heat and Fluid Flow 2007;28:1492–506.
[123] Hosseini, S, Ahmadi, A. Effect of temperature increasing on nanofluid structure. In: International conference on computer engineering and technology; 2010; 5:527-530.
[124] Xie H, Wang J, Xi T, Liu Y, Ai F. Dependence of the thermal conductivity of nanoparticle-fluid mixture on the base fluid. Journal of Materials Science Letters 2002;21:1469–71.
[125] Li C, Peterson G. Mixing effect on the enhancement of the effective thermal conductivity of nanoparticle suspensions (nanofluids). International Journal of Heat and Mass Transfer 2007;50:4668–77.
[126] Xie H, Wang J, Xi T, Liu Y, Ai F, Wu Q. Thermal conductivity enhancement of suspensions containing nanosized alumina particles. Journal of Applied Physics 2002;91:4568.
[127] Maïga S, Nguyen C, Galanis N, Roy G. Heat transfer behaviours of nanofluids in a uniformly heated tube. Superlattices and Microstructures 2004;35:543–57.
[128] Shin D, Banerjee D. Enhanced specific heat of silica nanofluid. Journal of Heat Transfer 2010;133(2) (024501-024501).

[129] Lee J, Hwang K, Jang S, Lee B, Kim J, Choi S, Choi C. Effective viscosities and thermal conductivities of aqueous nanofluids containing low volume concentrations of Al_2O_3 nanoparticles. International Journal of Heat and Mass Transfer 2008;51:2651–6.
[130] Kole M, Dey T. Thermal conductivity and viscosity of Al_2O_3 nanofluid based on car engine coolant. Journal of Physics D: Applied Physics 2010;43:315501.
[131] Masoumi N, Sohrabi N, Behzadmehr. A. A new model for calculating the effective viscosity of nanofluids. Journal of Physics D: Applied Physics 2009;42:055501.
[132] Abu-Nada E, Chamkha A. Effect of nanofluid variable properties on natural convection in enclosures filled with a CuO–EG–water nanofluid. International Journal of Thermal Sciences 2010;49:2339–52.
[133] Nguyen C, Desgranges F, Galanis N, Roy G, Mare T, Boucher S, Mintsa H Angue. Viscosity data for Al_2O_3–water nanofluid–hysteresis: is heat transfer enhancement using nanofluids reliable? International Journal of Thermal Sciences 2008;47:103–11.
[134] Jia-Fei Z, Zhong-Yang L, Ming-Jiang N, Ke-Fa C. Dependence of nanofluid viscosity on particle size and pH value. Chinese Physics Letters 2009;26:066202.
[135] Feng Y, Yu B, Xu P, Zou. M. The effective thermal conductivity of nanofluids based on the nanolayer and the aggregation of nanoparticles. Journal of Physics D: Applied Physics 2007;40:3164.
[136] Tillman P, Hill J. Modelling the Thermal Conductivity of Nanofluids 2007:105–18.
[137] Wang B, Zhou L, Peng. X. A fractal model for predicting the effective thermal conductivity of liquid with suspension of nanoparticles. International Journal of Heat and Mass Transfer 2003;46:2665–72.
[138] Xue Q, Xu. W. A model of thermal conductivity of nanofluids with interfacial shells. Materials Chemistry and Physics 2005;90:298–301.
[139] Leong K, Yang C, Murshed. S. A model for the thermal conductivity of nanofluids—the effect of interfacial layer. Journal of Nanoparticle Research 2006;8:245–54.
[140] Koo J, Kleinstreuer. C. A new thermal conductivity model for nanofluids. Journal of Nanoparticle Research 2004;6:577–88.
[141] Yu W, Choi. S. The role of interfacial layers in the enhanced thermal conductivity of nanofluids: a renovated Hamilton–Crosser model. Journal of Nanoparticle Research 2004;6:355–61.
[142] Moghadassi A, Masoud Hosseini S, Henneke D, Elkamel A. A model of nanofluids effective thermal conductivity based on dimensionless groups. Journal of Thermal Analysis and Calorimetry 2009;96:81–4.
[143] Nan C, Shi Z, Lin. Y. A simple model for thermal conductivity of carbon nanotube-based composites. Chemical Physics Letters 2003;375:666–9.
[144] Patel H, Anoop K, Sundararajan T, Das S. Model for thermal conductivity of CNT-nanofluids. Bulletin of Materials Science 2008;31:387–90.
[145] Xue Q. Model for effective thermal conductivity of nanofluids. Physics Letters A 2003;307:313–7.
[146] Xu J, Yu. B. A new model for heat conduction of nanofluids based on fractal distributions of nanoparticles. Journal of Physics D: Applied Physics 2008;41:139801.
[147] Mirmasoumi S, Behzadmehr A. Effect of nanoparticles mean diameter on mixed convection heat transfer of a nanofluid in a horizontal tube. International Journal of Heat and Fluid Flow 2008;29:557–66.
[148] Behzadmehr A, Saffar-Avval M, Galanis N. Prediction of turbulent forced convection of a nanofluid in a tube with uniform heat flux using a two phase approach. International Journal of Heat and Fluid Flow 2007;28:211–9.
[149] Ben-Abdallah P. Heat transfer through near-field interactions in nanofluids. Applied Physics Letters 2006;89:113117.
[150] Pérez-Madrid A, Rubí J, Lapas L. Heat transfer between nanoparticles: thermal conductance for near-field interactions. Physical Review B: Condensed Matter 2008;77:155417.
[151] Putnam S, Cahill D, Braun P, Ge Z, Shimmin R. Thermal conductivity of nanoparticle suspensions. Journal of Applied Physics 2006;99:084308.
[152] Eapen J, Rusconi R, Piazza R, Yip. S. The classical nature of thermal conduction in nanofluids. Journal of Heat Transfer 2010;132:102402–1-102402-1-14.
[153] Moghaddami M, Mohammadzade A, Esfehani S. Second law analysis of nanofluid flow. Energy Conversion and Management 2011;52:1397–405.
[154] Liu D, Yu. L. Single-phase thermal transport of nanofluids in a minichannel. Journal of Heat Transfer 2010;133(3):031009.
[155] Kumar S, Prasad S, Banerjee J. Analysis of flow and thermal field in nanofluid using a single phase thermal dispersion model. Applied Mathematical Modelling 2010;34:573–92.
[156] Keblinski P, Prasher R, Eapen J. Thermal conductance of nanofluids: is the controversy over? Journal of Nanoparticle Research 2008;10:1089–97.
[157] Keblinski. P. Thermal conductivity of nano fluids. Thermal Nanosystems and Nanomaterials 2009;118:213–21.
[158] Xuan Y, Li Q, Hu W. Aggregation structure and thermal conductivity of nanofluids. AIChE Journal 2003;49:1038–43.
[159] Evans W, Fish J, Keblinski P. Role of Brownian motion hydrodynamics on nanofluid thermal conductivity. Applied Physics Letters 2009;88:093116.
[160] Nie C, Marlow W, Hassan Y. Discussion of proposed mechanisms of thermal conductivity enhancement in nanofluids. International Journal of Heat and Mass Transfer 2008;51:1342–8.
[161] Buongiorno J. Convective transport in nanofluids. Journal of Heat Transfer 2006;128:240.
[162] Keblinski P, Phillpot S, Choi S, Eastman J. Mechanisms of heat flow in suspensions of nano-sized particles (nanofluids). International Journal of Heat and Mass Transfer 2002;45:855–63.
[163] Yu W, Choi. S. The role of interfacial layers in the enhanced thermal conductivity of nanofluids: a renovated Maxwell model. Journal of Nanoparticle Research 2003;5:167–71.
[164] Xie H, Fujii M, Zhang X. Effect of interfacial nanolayer on the effective thermal conductivity of nanoparticle-fluid mixture. International Journal of Heat and Mass Transfer 2005;48:2926–32.
[165] Xue L, Keblinski P, Phillpot S, Choi S, Eastman J. Effect of liquid layering at the liquid–solid interface on thermal transport. International Journal of Heat and Mass Transfer 2004;47:4277–84.
[166] Tillman P, Hill J. Determination of nanolayer thickness for a nanofluid. International Communications in Heat and Mass Transfer 2007;34:399–407.
[167] Karthikeyan N, Philip J, Raj B. Effect of clustering on the thermal conductivity of nanofluids. Materials Chemistry and Physics 2008;109:50–5.
[168] Evans W, Prasher R, Fish J, Meakin P, Phelan P, Keblinski P. Effect of aggregation and interfacial thermal resistance on thermal conductivity of nanocomposites and colloidal nanofluids. International Journal of Heat and Mass Transfer 2008;51:1431–8.
[169] Sommers A, Yerkes K. Experimental investigation into the convective heat transfer and system-level effects of Al_2O_3–propanol nanofluid. Journal of Nanoparticle Research 2010;12:1003–14.
[170] Mansour R, Galanis N, Nguyen C. Effect of uncertainties in physical properties on forced convection heat transfer with nanofluids. Applied Thermal Engineering 2007;27:240–9.
[171] Guo S, Li Y, Jiang J, Xie. H. Nanofluids containing $-Fe_2O_3$ nanoparticles and their heat transfer enhancements. Nanoscale Research Letters 2010;5:1222–7.
[172] Mosavian M, Heris S, Etemad S, Esfahany M. Heat transfer enhancement by application of nano-powder. Journal of Nanoparticle Research 2010;12:2611–9.
[173] Abu-Nada E. Effects of variable viscosity and thermal conductivity of Al_2O_3–water nanofluid on heat transfer enhancement in natural convection. International Journal of Heat and Fluid Flow 2009;30:679–90.
[174] Chen H, Ding Y, Lapkin A. Rheological behaviour of nanofluids containing tube/rod-like nanoparticles. Powder Technology 2009;194:132–41.
[175] Tseng W, Lin K. Rheology and colloidal structure of aqueous TiO_2 nanoparticle suspensions. Materials Science and Engineering A 2003;355:186–92.
[176] Chen H, Ding Y, Tan C. Rheological behaviour of nanofluids. New Journal of Physics 2007;9:367.
[177] Chen H, Ding Y, Lapkin A, Fan X. Rheological behaviour of ethylene glycol-titanate nanotube nanofluids. Journal of Nanoparticle Research 2009;11:1513–20.
[178] Chon S U S, Kihm Chan Hee, Lee Kenneth D, Choi Shin Pyo. Empirical correlation finding the role of temperature and particle size for nanofluid (Al_2O_3) thermal conductivity enhancement. Applied Physics Letters 2005;87 (153107-153107).
[179] Vajjha RS, Das DK. Experimental determination of thermal conductivity of three nanofluids and development of new correlations. International Journal of Heat and Mass Transfer 2009;52:4675–82.
[180] Corcione M. Heat transfer features of buoyancy-driven nanofluids inside rectangular enclosures differentially heated at the sidewalls. International Journal of Thermal Sciences 2010;49:1536–46.
[181] Seyf H R, Feizbakhshi M. Computational analysis of nanofluid effects on convective heat transfer enhancement of micro-pin-fin heat sinks. International Journal of Thermal Sciences 2012;58:168–79.
[182] Koo J, Kleinstreuer C. Impact analysis of nanoparticle motion mechanisms on the thermal conductivity of nanofluids. International Communications in Heat and Mass Transfer 2005;32:1111–8.
[183] Vajjha RS, Das DK, Kulkarni DP. Development of new correlations for convective heat transfer and friction factor in turbulent regime for nanofluids. International Journal of Heat and Mass Transfer 2010;53:4607–18.
[184] Mahbubul IM, Saidur R, Amalina MA. Latest developments on the viscosity of nanofluids. International Journal of Heat and Mass Transfer 2012;55:874–85.
[185] Tseng WJ, Chen CN. Effect of polymeric dispersant on rheological behavior of nickel–terpineol suspensions. Materials Science and Engineering A 2003;347: 145–53.
[186] Cheng, NS, Law, AWK. Exponential formula for computing effective viscosity. Powder Technology 2003; 129:156–160.
[187] Kulkarni DP, Das DK, Chukwu GA. Temperature dependent rheological property of copper oxide nanoparticles suspension (nanofluid). Journal of Nanoscience and Nanotechnology 2006;6:1150–4.
[188] Namburu P, Kulkarni D, Misra D, Das D. Viscosity of copper oxide nanoparticles dispersed in ethylene glycol and water mixture. Experimental Thermal and Fluid Science 2007;32:397–402.
[189] Masoud Hosseini S, Moghadassi AR, Henneke. DE. A new dimensionless group model for determining the viscosity of nanofluids. Journal of Thermal Analysis and Calorimetry 2010;100:873–7.
[190] Saidur R, Leong KY, Mohammad. HA. A review on applications and challenges of nanofluids. Renewable and Sustainable Energy Reviews 2011;15:1646–68.
[191] Godson L, Raja Mohan Lal D, Wongwises S. Enhancement of heat transfer using nanofluids—an overview. Renewable and Sustainable Energy Reviews 2010;14:629–41.
[192] Hwang Y, Park HS, Lee JK, Jung WH. Thermal conductivity and lubrication characteristics of nanofluids. Current Applied Physics 2006;6:67–71.
[193] Pantzali MN, Mouza AA, Paras SV. Investigating the efficacy of nanofluids as coolants in plate heat exchangers (PHE). Chemical Engineering Science 2009;64:3290–300.

[194] Wen D, Lin G, Zhang Vafaei S. Review of nanofluids for heat transfer applications. Particuology 2009;7:141–50.
[195] Eastman JA, Choi SUS, Li S, Yu W, Thompson LJ. Anomalously increased effective thermal conductivities of ethylene glycol-based nanofluids containing copper nanoparticles. Applied Physics Letters 2001;78(6):718–20.
[196] Lee J, Mudawar I. Assessment of the effectiveness of nanofluids for single-phase and two-phase heat transfer in micro-channels. International Journal of Heat and Mass Transfer 2007;50(3–4):452–63.
[197] Choi C, Yoo HS, Oh JM. Preparation and heat transfer properties of nanoparticle-in-transformer oil dispersions as advanced energy-efficient coolants. Current Applied Physics 2008;8:710–2.
[198] Vasu V, Rama Krishna K, Kumar ACS. Heat transfer with nanofluids for electronic cooling. International Journal of Materials and Product Technology 2009;34:158–71.
[199] Peng H, Ding G, Jiang W, Hu H, Gao Y. Measurement and correlation of frictional pressure drop of refrigerant-based nanofluid flow boiling inside a horizontal smooth tube. International Journal of Refrigeration 2009;32:1756–64.
[200] Kim J, Kang YT, Choi CK. Soret and Dufour effects on convective instabilities in binary nanofluids for absorption application. International Journal of Refrigeration 2007;30(2):323–8.
[201] Duangthongsuk W, Wongwises S. An experimental study on the heat transfer performance and pressure drop of TiO_2–water nanofluids flowing under a turbulent flow regime. International Journal of Heat and Mass Transfer 2010;53(1–3):334–44.
[202] Ding G, Peng H, Jiang W. The migration characteristics of nanoparticles in the pool boiling process of nanorefrigerant and nanorefrigerant–oil mixture. International Journal of Refrigeration 2009;32(1):114–23.
[203] Namburu PK, Das DK, Tanguturi KM, Vajjha RS. Numerical study of turbulent flow and heat transfer characteristics of nanofluids considering variable properties. International Journal of Thermal Sciences 2009;48:290–302.
[204] NETL. www.netl.doe.gov; 2009 [12.10.09].
[205] Sarit K. Das nanofluids—the cooling medium of the future. Heat Transfer Engineering 2006;27(10):1–2.